Numerical analysis of rebar pull-out behaviour in concrete using cohesive zone modelling

van den Bulck, S.

Award date:
2015

Technische Universiteit
Eindhoven
University of Technology

Department of Architecture, Building and Planning
Unit Structural Design

Numerical analysis of rebar pull-out behaviour in concrete using cohesive zone modelling

Master Thesis

Sven van den Bulck
A-2015.111

Supervisors:
Prof. Dr. Ir. A.S.J. (Akke) Suiker
Prof. Dr. Ir. T.A.M. (Theo) Salet
Prof. Dr. Ir. S.N.M. (Simon) Wijte

Final Version

Eindhoven, September 2015

PREFACE

This report considers the results of my master thesis and literature survey at the Eindhoven University of Technology.

In this report a numerical model of rebar pull- out of concrete is presented. A Finite element model using cohesive zone modelling should be able to predict the initial phase of pull-out for different geometries and material characteristics. In addition, literature study should give more clarity in the formation of several national standards and performed experimental, analytical and numerical research in history.

I would like to thank Theo Salet, Simon Wijte, friends and family for supporting me during this project. A special thanks goes out to Akke Suiker for his time and perseverance during the programming and testing of the UMAT.

Sven van den Bulck
14 September 2015

PART I:
PAPER

Numerical analysis of rebar pull-out behaviour in concrete using cohesive zone modelling

Sven van den Bulck
Eindhoven University of Technology
s.v.d.bulck@student.tue.nl

14 September 2015

Abstract

In the literature experimental research has been reported for obtaining a better understanding of the behaviour of anchorage length and lap splices in concrete. Mechanical interaction between concrete and steel is of importance for the failure behaviour of rebar pull-out of concrete. However, these experiments show a large variation in results due to variations in boundary conditions and material composition of concrete. Therefore, a numerical model of rebar pull-out of concrete is presented in this study in addition to experimental research. This may provide more clarity of mechanical interaction between the rebar and concrete. In order to achieve this, a cohesive zone model with an interface damage law formulation is used to simulate concrete cracking. The simulated results show good agreement for the initial phase of pull-out.

Keywords: Rebar, Concrete, Pull-out, Cohesive zone modelling, Traction separation, Friction, Dilatancy, Finite element analysis, Experiment

1. Introduction

As generally known, the tensile strength of concrete is relatively low with respect to the compressive strength. Therefore, reinforced concrete is common in the world of structural design in order to cope with such tensile stresses in concrete elements after cracks have developed. However, the interaction and cooperation between concrete and steel is a complex behaviour. Boundary conditions and material characteristics (concrete class, steel strength, transverse pressure, concrete cover, rebar geometry and transverse reinforcement) have a major influence on the failure mechanism. The national/European standards provide simple design rules in order to obtain a safe value for the anchorage length and lap splice, these formulas are based on experimental databases. Over the past decades, the number of experimental researches has increased, with the consequence of increasing variation in results. Hereby, the safe lower limit for design rules should be renewed to meet the experimental databases.

Since the introduction of Eurocode 2 concrete structures (NEN-EN 1992-1-1), that replaces TGB concrete structures (NEN 6720), there are changes regarding the design rules of anchorage length and lap splice. These prescribed values have increased significantly compared to the old Dutch standard. The explanation is revealed in Figure 1; the experimental database of EC 2 (Stuttgart, FIB TIG4.5) show larger deviation compared to the TGB database (VBC, CUR23). In order to achieve a safe assumption, the prescribed anchorage length and lap splice should be enhanced to meet the Stuttgart database.

Consequently, the recent design rules of Eurocode 2 (which are based on Model code 1990) prescribe significantly larger values for the lap splice and anchorage length. The following renewed EC 2 will be based upon Model code 2010; however, as shown in figure 1, the prescribed values of MC 10 are located close to EC 2, nevertheless on the negative side.

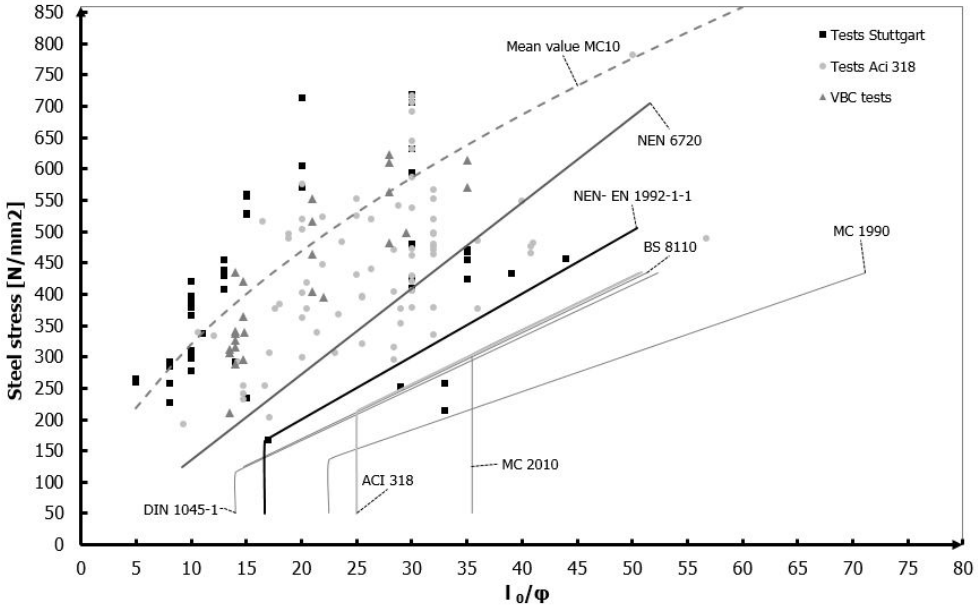

Figure 1: *Steel stress as a function of the lap splice as multiple of the rebar diameter for good bond conditions.*

These standards assume that pull-out behaviour is governing instead of splitting failure. Splitting failure is brittle due to the abrupt crack development of radial cracks in the concrete cover (*Tepfers and Lorenzis, 2003*). In practice, abrupt failure is undesirable in structural elements; therefore, minimum values for boundary conditions and specimen characteristics are prescribed for all of these standards to avoid brittle failure. Tassios (*1979*) described the possible stages for rebar pull-out, see figure 2. Depending on several boundary conditions and specimen characteristics, a bond- stress slip relationships can be obtained.

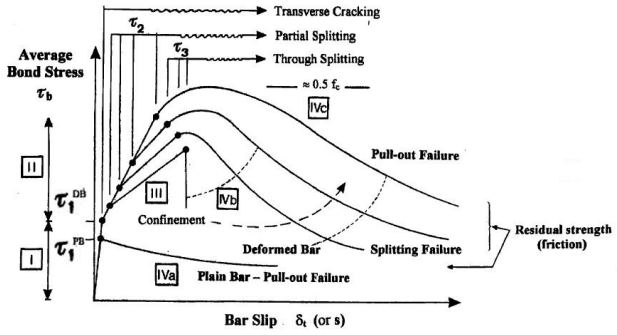

Figure 2: *Different stages for rebar pull-out depending on the boundary conditions and specimen characteristics (Tassios, 1979)*

First the linear elastic relationship in stage I up to τ_1^{PB} (Figure 2), the strain of concrete and steel is equal (*Bruggeling, 1980*). The bond of interaction is caused by chemical adhesion (*Fib bulletin 10, 2000*) and slip is the measured displacement at the top of the rebar. Herewith, the maximum bond stress is reached for plain rebars. Subsequently, the rebar is debonded and only friction of the steel- concrete interface is able to transfer shear stresses in stage IVa. In case of a deformed bar, the maximum bond stress is not reached after stage I due to the presence of the lugs. These lugs induce large bearing stresses caused by the interlocking of steel and concrete in stage II; the rebar remains confined.

Subsequently, boundary conditions and specimen characteristics of the concrete element are of main importance for the sequel of the bond- slip relationship in stage III. Hoop stresses (*Tepfers, 1973)* could cause radial cracks through the concrete cover resulting in splitting failure (stage IVb). Conversely, heavy confinement of the rebar ensures pull-out failure (stage IVc) with transverse cracks and longitudinal cracks between the lugs. However, a compromise between these two extremes is also possible when radial cracks are not able to penetrate the entire concrete cover.

2. Experiments

Two experimental studies will be discussed here, namely pull-out of a smooth and deformed rebar. Deformed rebars have been frequently investigated with respect to various parameters (rebar diameter, bar geometry, rebar strength, concrete strength, transverse pressure and reinforcement, concrete cover). As a reference for this numerical research, experiments have been conducted at Eindhoven University of Technology by Marinus (2015). The smooth rebar is not common in structural elements due to the relatively low ultimate strength for pull out. However, these experiments can be useful to gain insight into the interaction between steel and concrete, see also Fabbrocino et al. (2005).

2.1. Pull out of smooth rebar

The smooth rebar is considered to be a starting point for the numerical investigation of anchorage length. This is an attempt to observe the interaction behaviour between steel and concrete. Subsequently, a numerical model is created to simulate the pull-out behaviour of a smooth rebar in a concrete matrix. However, experimental reference research is required to obtain interaction properties as input for the numerical calculation. Therefore, the experimental results of Fabbrocino et al. (2005) have been used in this numerical investigation of a smooth rebar. Three pull-out tests of Ø12 mm rebars carried out.

2.1.1 Material properties

The experimental specimen consisted of a hot rolled smooth rebar classified as Feb22k embedded 10*Ø= 120 mm in the center of a concrete cube. Tensile tests carried out on the 12 mm rebars have shown a mean yielding stress $\sigma_{s,y} = 320N/mm^2$. Furthermore, initial hardening occurs at a strain $\epsilon_{s,h} = 3\%$, the ultimate stress $\sigma_{s,u} = 440N/mm^2$ and the ultimate strain $\epsilon_{s,u} = 23\%$. The stress- strain plots are revealed in figure 3.

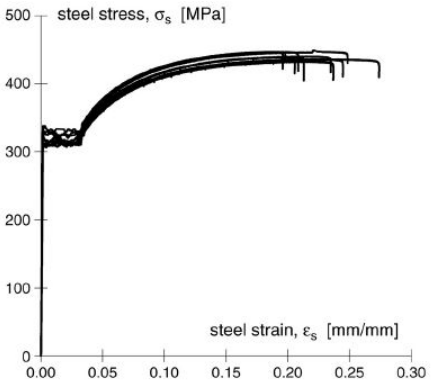

Figure 3: *Steel stress smooth rebar Ø12 mm*

The concrete mixture for pull-out specimens have been prepared according to table 1. Cubes of 150 mm wide were used as testing specimen to define the mean concrete strength. The specimens and cubes have been cast together and cured under the same open air environmental conditions. After 28 days, both pull-out and compressive tests have been carried out. The concrete specimens exhibited a mean cubic compressive strength of 29.34 MPa as shown in figure 4.

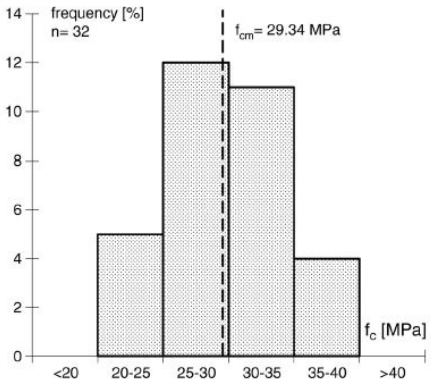

Figure 4: *Compressive strength of the pull-out specimens*

Component		Units
Water/cement ratio	0.45	
Aggregate size (0-4mm)	10.14	kN/m^3
Aggregate size (4-10mm)	3.13	kN/m^3
Aggregate size (10-20mm)	5.16	kN/m^3

Table 1: Concrete mix design

2.1.2 Experimental setup

The experimental setup that has been applied in the research of Fabbrocino et al (2005) is revealed in figure 5. A concrete specimen of 300 mm wide was used with an embedded rebar Ø12 mm in the center of the cube. At the bottom side, a plastic sleeve had been casted in order to ensure the condition of an embedded zone of 10 times the rebar diameter. Before testing, the concrete cube had been positioned in a bolted steel envelope with threaded rebars on both surfaces that restrained displacements. It is worth noting that special care had been devoted to avoid tensile stresses in the threaded rebars to keep the specimen unconfined and free of lateral compression stresses during pull-out. Both loaded and unloaded ends have been measured and the test were carried out under displacement control at the top of the rebar to follow the softening branch after passing the maximum bond stress.

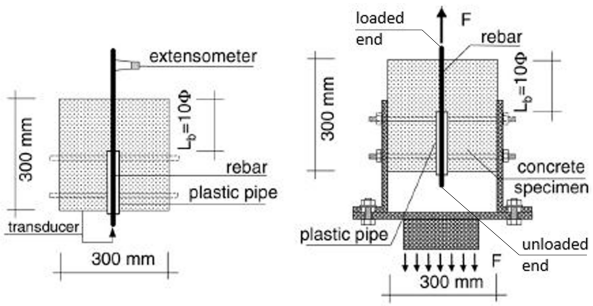

Figure 5: *Experimental pull-out setup for smooth rebar according to Fabbrocino et al. (2005)*

2.1.3 Results and discussion

The results obtained from the pull out tests are revealed in steel stress- slip of figure 6 plot and bond stress- slip plot of figure 7. The differences between the loaded and unloaded ends are negligibly small due to the relatively low steel stress, about 65 to 95 N/mm^2, and the small strains (figure 3). For the smooth rebar, the chemical adhesion warrants the transfer of forces before reaching the maximum bond stress (Tassios, 1979). Hereafter, force transfer is provided by friction and is strongly affected by interface wear and transverse pressure (Fib Bulletin 10, 2000).

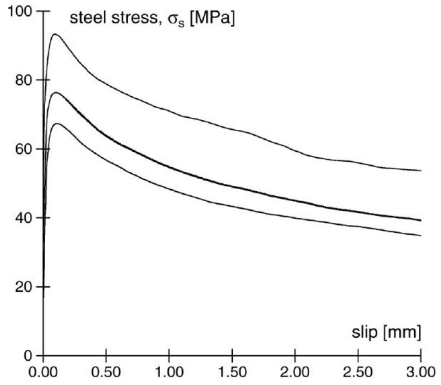

Figure 6: *Steel stress- slip diagram of pull-out of smooth rebar of unloaded end (Fabbrocino et al, 2005)*

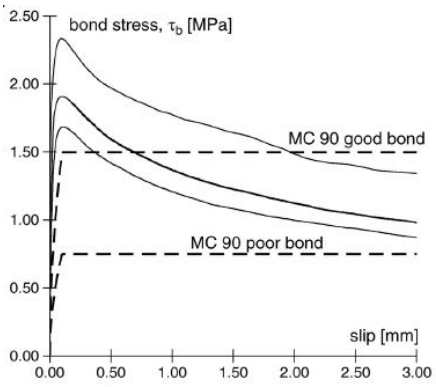

Figure 7: *Bond stress- slip diagram of pull-out of smooth rebar of unloaded end (Fabbrocino et al, 2005)*

Specimen	Slip (mm)	τ_{bmax} (MPa)
1	0.14	2.3
2	0.14	1.9
3	0.15	1.67
Mean value	0.14	1.96

Table 2: Results for pull-out test specimens

Due to the geometry of the specimen and rebar, splitting failure did not occur; the concrete cubes were not damaged microscopically after testing. Furthermore, the bond stress- slip plot can be subdivided into three stages.

Adhesion :
The first stage is elastic and is caused by bonding between concrete and steel, which is formed during curing. The connection is relatively weak and brittle. When the stiffness decreases in the bond stress- slip relationship, the debonding stage starts.

Debonding :
The second stage is debonding; this is the transition between chemical adhesion and friction (stage three). Due to the non- uniform stress distribution over the height of the rebar, the debonding occurs gradually from the top to the bottom.

Friction :
The third stage, friction, is caused by shear resistance between concrete and steel. However, in order to achieve frictional stresses, normal stresses are required (Coulomb's friction law $\tau = \sigma_n \cdot \mu$). Normal stresses on the rebar could be caused by both curing shrinkage and imperfections during pull-out or casting. As an assumption for the numerical model, imperfections are assumed to be negligibly small and curing shrinkage is governing for normal stress development along the rebar.

More detailed information about the descending branch of a smooth rebar will be given in section 5.

2.2. Pull-out of deformed rebar

From a practical point of view, smooth rebars are not applicable in structural elements. The improvement with respect to plain concrete loaded in tension is relatively small. Therefore, deformed rebars are commonly used in reinforced concrete. The lugs of the steel bar are able to transfer high stresses into the concrete specimen. Marinus (2015) conducted pull-out experiments on 8 mm and 16 mm rebars according to RILEM RC-6, which is described in annex D of NEN-EN10080. These force- slip relationships can be used as reference for the axissymmetric numerical models. Noteworthy however, is that deformed rebars do not have an ideally axissymetrical shape. Nevertheless, it will be assumed this has a negligible effect on the force- slip relationship.

2.2.1 Material properties

The experimental specimens consisted of a steel rebar FeB 500 HKN Ø8 or FeB 500 HWL Ø16 mm and a concrete C20/25 cube of 200 mm wide. Dimensions of both rebars have been measured in a 2D plane perpendicular to the rebar to gain insight in the geometry for the axissymmetric numerical model.

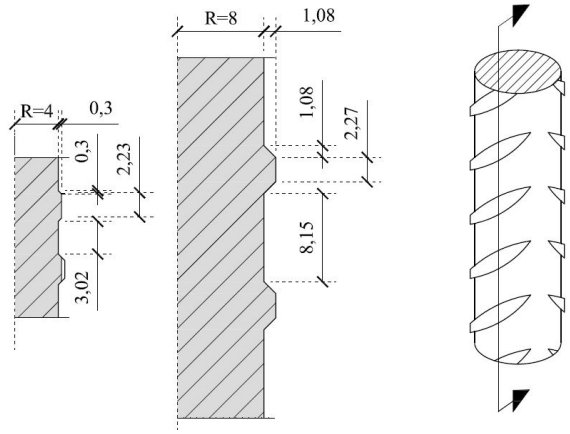

Figure 8: *Geometry of Ø8 and Ø16 mm in 2D*

The rebars of the experimental specimens are depicted in figures 9 and 10.

Figure 9: *Geometry of Ø8 mm*

Figure 10: *Geometry of Ø16 mm*

The concrete mixture that was applied in these specimens is standard C20/25 with a maximum grain size of 16 mm. The specimens for pull-out and compression tests were casted together. After 28 days of curing in an indoor environment (20^oC), covered with wet cloths, the specimens were tested.

Concrete C20/25		Units
Cement:CEM III/B 42.5 N		-
Water/cement ratio	0.55	-
Maximum grain size	16	mm
Consistency class	S3	-
Environmental class	XC2	-

Table 3: Concrete mix design

First, the data obtained by the compressive tests is shown in table 4, which result in a mean value of 35.4 MPa with a standard deviation of 0.57 MPa.

Concrete specimen	Compressive strength (MPa)
UB/01	34.49
UB/02	35.70
UB/03	36.15
UB/04	35.72
UB/05	35.52
UB/06	34.80
Mean value	35.40

Table 4: Results for pull-out test specimens

2.2.2 Setup

The pull-out experiments were conducted using a 250 kN hydraulic test bench. The test- setup was prepared in accordance with RILEM RC-6 (figure 11 and 12). Both types of rebars were casted in the center of the concrete cubes with an aluminum sleeve for the free pre- length. The embedded zone of Ø8 is 40 mm and Ø16 is 80 mm, which is equal to 5 times diameter. The specimens were casted sideways to ensure that the casted side does not affect the rebar during pull-out and thus the results. Furthermore, the sealing between sleeve and rebar of number seven in figure 11 should be watertight to prevent leakage. Otherwise, the prescribed embedded zone would no longer be valid.

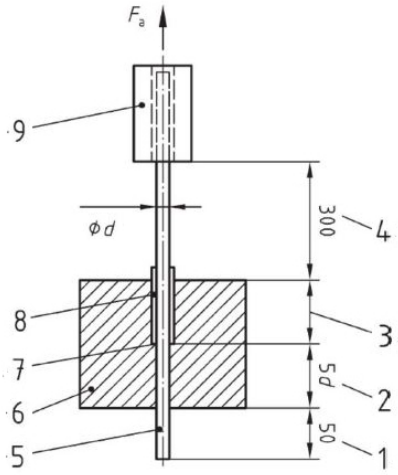

Figure 11: *Experimental setup for rebar pull out prescribed by EN10080;2005.*
1. Extra length for the measuring device 2. Bond length 3. Free pre- length 5d, min 200 mm-5d 4. Part of the bar to the point of application of the tensile force 5. Rebar 6. Concrete 7. Plugging 8. Aluminum sleeve 9. Grip of the testing machine

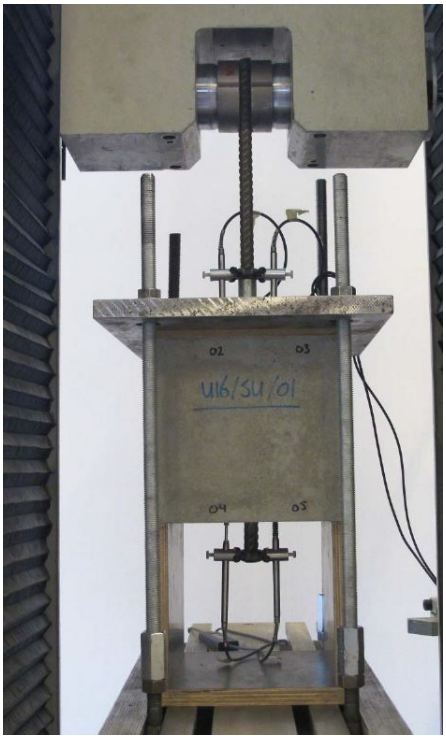

Figure 12: *Setup according to RILEM RC-6*

In the setup, the specimen is placed on a U- shaped platform to create space for the measuring device, namely two LVDT's with a range of 5 mm at the unloaded end as shown in figure 12. Furthermore, a steel plate with threaded rebars is set at the top of the specimen to restrain displacements of the concrete cube during pull-out. Finally, the rebar is clamped in a hydraulic grip to avoid slip at the fixed end. The displacement of the loaded end has been measured by two LVDT's. All experiments were performed displacement controlled at a rate of 0.5 mm/min. The slip was measured up to 5 mm due to the maximum range of the LVDT's. Next, the entire rebar was pulled out to observe the failure mechanism in more detail.

2.2.3 Results and discussion

The force- slip relationships of both Ø8 and Ø16 mm are revealed in figures 13 and 14. The initial stiffness is equal for both types of rebars. Hereafter, the stiffness decreases, which indicates that failure is initiated. Observation of the tested specimens shows that no macroscopic damage occurs, e.g. hoop stresses cause no radial cracking during pull out. The relatively large concrete cover is able to capture the confining stresses and thus splitting failure is prevented.

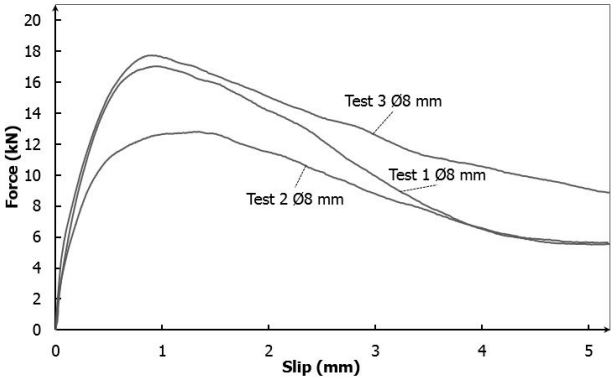

Figure 13: *Force- slip relationship of Pull-out Ø8 mm*

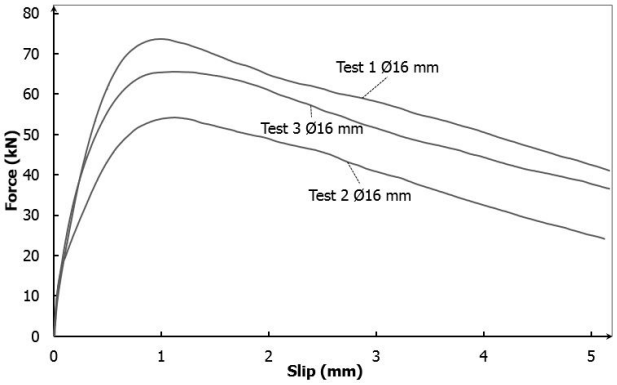

Figure 14: *Force- slip relationship of Pull-out Ø16 mm*

In order to develop a numerical model, the nature of failure should be known. The literature (Fib bulletin 10, 2000) indicates that transverse cracking due to the wedging action of the lugs occurs as caused by tensile stresses right behind the lugs. Simultaneously, longitudinal cracks between the lugs will develop gradually from top to bottom. Since differences between data of the loaded and unloaded end are relatively small, it is assumed that the longitudinal crack is fully developed at the top of the force- slip curve. Hereafter, residual stresses are generated due to frictional resistance between cracked concrete surfaces. More detailed information about the failure mechanisms and force- slip relationship will be given in section 5.

The assumption of longitudinal cracks between the lugs is supported by observation of the pulled rebars in figure 15 and 16. The concrete between the lugs is almost undamaged.

Figure 15: *Pull-out Ø8 mm*

Figure 16: *Pull-out Ø16 mm*

3. Numerical modelling

This section presents the theory of the Cohesive zone Modelling, which is used for the simulations in Abaqus 6.12-3 (2012) as a UMAT for pull out behaviour in concrete.

3.1. Geometry

In order to clarify the theory that is described in this section, a simple two element test of figure 17 has been used. It consists of two continuum elements with linear elastic behaviour and an interface (cohesive) element to model damage (cracking) between both continuum elements. Both loading in Mode I (tension) and Mode II (shearing, figure 17) will be described.

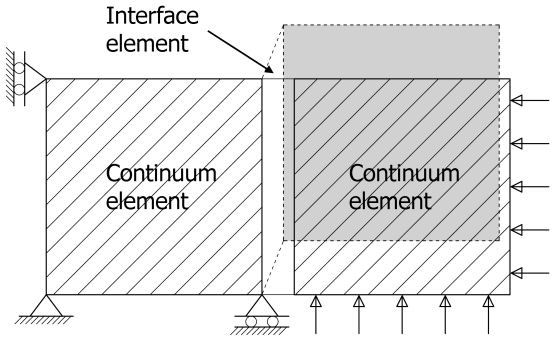

Figure 17: *Two element model as testing simulation in Mode II for UMAT*

3.2. Interface damage model

The formulation of the cohesive zone model follows the description in Cid Alfaro et al (2009). According to the traction-separation law in figure 18, the inelastic fracture behaviour can be captured by cohesive elements. The governing equations of the cohesive zone model will be presented for a 2D configuration. In principle, the effective relative displacement v is related to the effective traction t in the cohesive element. First, elastic behaviour is described until $t^u = Kv^o$. Subsequently, damage (d) is initiated. During the development of damage, the stiffness K decreases with $(1-d)K$.

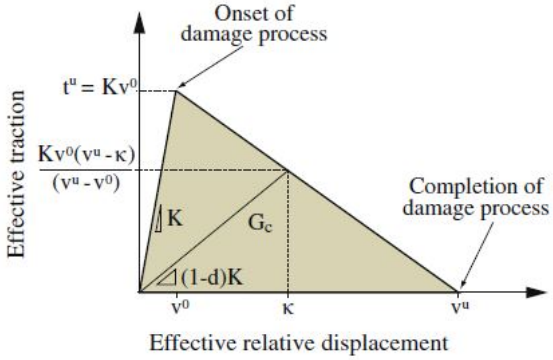

Figure 18: *Traction separation law according to Cid Alfaro et al (2009)*

The constitutive equation, which relates the traction to the relative displacement, has the form:

$$t_i = (1-d)C_{ij}v_j - dC_{ij}\delta_{1j}\langle -v_1\rangle \quad (\text{where} \quad i,j \in 1,2) \tag{1}$$

where d is the damage between 0 and 1 , K the stiffness parameter, δ_{ij} the Kronecker delta symbol, indices 1 and 2 indicate the normal and tangential directions on a crack plane, respectively, of the traction t_i and separation v_i and C_{ij} is the elastic stiffness tensor:

$$C_{ij} = K\delta_{ij} \tag{2}$$

Notice in the last term of equation 1, that crack penetration of two opposite faces is prevented due to the Macauley brackets $\langle\rangle$. A negative separation in normal direction (compression) causes contact of two faces with the elastic behaviour being equal to K.

The evolution of the damage parameter as a function of the relative separation is formulated through a rate-dependent kinetic law.

$$\dot{d} = \begin{cases} \frac{\hat{F}(\lambda,\kappa)}{\eta} & for \quad \lambda \geq \kappa \quad and \quad v^0 \leq \kappa < v^u, \\ 0 & for \quad 0 \leq \lambda < \kappa \quad or \quad \kappa = v^u, \end{cases} \tag{3}$$

where η is a relaxation parameter with the dimension of time, κ is the history parameter, $\hat{F}(\lambda,k)$ is the damage loading function, and λ is the effective separation. The effective separation λ is taken here

as the Euclidean norm of the vector of relative crack face displacements i.e., $\lambda = \|\nu\| = \sqrt{\nu_1^2 + \nu_2^2}$. Furthermore, the history variable κ is determined as the maximum value of the effective separation attained during the previous steps. The lower expression of equation 3 indicates the domain of κ where the damage rate is equal to zero and the upper expression sets the damage rate equal to the loading function with linear softening, as described by

$$\hat{F}(\lambda,\kappa) = \hat{f}(\lambda) - \hat{d}(\kappa) = \frac{\nu^u(\lambda-\nu^0)}{\lambda(\nu^u-\nu^0)} - \frac{\nu^u(\kappa-\nu^0)}{\kappa(\nu^u-\nu^0)} \tag{4}$$

In order to model the combination of Mode I and mode II (i.e. mixed mode) fracture, a mode-mixity parameter β is introduced:

$$\beta = \frac{\nu_2}{\nu_2 + \langle\nu_1\rangle} \tag{5}$$

In this expression, pure mode I loading ($\nu_2 = 0$) shows that $\beta = 0$ while pure shear loading leads to ($\nu_1 = 0$) and $\beta = 1$. Furthermore, the functions $\nu^0 = \hat{\nu^0}(\beta)$ and $\nu^u = \hat{\nu^u}(\beta)$ are based upon a common expression for characteristics mixed mode toughness data.

$$\frac{G_I}{G_{I,c}} + \frac{G_{II}}{G_{II,c}} = 1 \tag{6}$$

where G_I and G_{II} are the energy release rates in respectively Mode I en II and $G_{I,c}$ and $G_{II,c}$ the fracture toughnesses under pure mode I and II loading conditions. Accordingly, the relative displacement at damage initiation and damage completion can be elaborated into (Cid Alfaro et al., 2009)

$$\nu^0 = \hat{\nu^0}(\beta) = \nu_1^0\nu_2^0\sqrt{\frac{1+2\beta^2-2\beta}{(\beta\nu_1^0)^2 + ((1-\beta)\nu_2^0)}}, \tag{7}$$

and

$$\nu^u = \hat{\nu^u}(\beta) = \frac{2(1+2\beta^2-2\beta}{K\nu^0}\left[\left(\frac{(1-\beta)^2}{G_{I,c}}\left(\frac{\beta^2}{G_{II,c}}\right)\right]^{-1}\right. \tag{8}$$

Notice from equations 7 and 8 that the mode-mixity β is the only variable in both expressions. The other parameters can be extracted from interfacial fracture data. For more detailed information on the interface damage model the reader is referred to Cid Alfaro et al (2009).

3.3. Addition of friction

For an adequate description of rebar pull-out, the fracture model of Cid Alfaro et al. (2009) is extended with the effect of frictional sliding, for which the well-known Coulomb's law is taken as a basis. Accordingly, during slip of two opposite crack faces, the tangential traction t_2 reaches a critical value given by

$$t_2^{cr} = \mu\,\langle -t_1\rangle\,\frac{\dot{v}_2}{|\dot{v}_2|}, \tag{9}$$

where μ is the friction coefficient characterizing the roughness of the crack faces. The Macauly brackets $\langle x\rangle = (x+|x|)/2$ warrant that slip only becomes active under a negative normal traction t_1, whereby the two opposite crack faces are in contact. Note that the last term in the right-hand side of equation 9 ensures that the direction of the critical tangential traction equals the direction of the tangential velocity $\dot{v}_2$.

The transition from fully sticking crack faces to sliding crack faces occurs when the "magnitude of the elastic tangential traction", $|t_2^e| = K|v_2|$, becomes larger than the critical frictional resistance, $\mu\,\langle -t_1\rangle$. This transition can be incorporated in equation 9 by introducing the following Heaviside function:

$$H_{v_2^m}(|v_2|) = H(|v_2| - v_2^m) \quad \text{with} \quad v_2^m = \frac{\mu\,\langle -t_1\rangle}{K}, \tag{10}$$

where v_2^m is the minimal tangential displacement required for frictional sliding to occur. Furthermore, $H_c(x) = 0$ for $x < c$ and $H(x) = 1$ for $x \geq c$. Combining equation 9 with equation 10 turns the critical tangential traction during frictional sliding into

$$t_2^{cr} = \mu\,\langle -t_1\rangle\,\frac{\dot{v}_2}{|\dot{v}_2|}\,H_{v_2^m}(|v_2|). \tag{11}$$

The friction model given by equation 11 suffices when the roughness of the crack faces is moderate to small, such that the additional normal crack opening resulting from interactions of microscale asperities at opposite crack faces, known as dilation, is negligible. Although this assumption is reasonable for relatively smooth crack surfaces appearing in steels and polymers, in concrete the roughness of crack faces may be substantial, which requires the effect of dilation on the frictional resistance to be taken incorporated in the model. For this purpose, the additional normal crack opening v_1^p, as generated by rough crack surfaces subjected to frictional sliding, is described in rate form as

$$\dot{v}_1^p = \psi |\dot{v}_2| \,, \tag{12}$$

with ψ the dilatancy coefficient. The superindex p refers to "plasticity", since dilation commonly is interpreted as a plasticity effect. For consistency, the tangential velocity appearing in the right-hand side of equation 12 should have been reflected by its plastic component as well. However, in order to keep the numerical implementation of the model relatively simple and without iterations, the total tangential velocity $\dot{v}_2$ is used here instead. It is emphasized that this formulation is able to realistically account for dilatancy effects during frictional sliding, though with a slightly alternative kinematic interpretation for the dilatancy coefficient ψ, namely as the proportionality factor between the *plastic* normal velocity and the *total* tangential velocity (instead of the *plastic* tangential velocity).

Using equation 12, the plastic normal crack opening, v_1^p, straightforwardly follows from integration with respect to the time t reflecting the duration of the cracking process,

$$v_1^p = \int \dot{v}_1^p dt = \int \psi |\dot{v}_2| dt. \tag{13}$$

In accordance with the additive decomposition of deformation used in the theory of plasticity, the plastic normal crack opening v_1^p may be related to the total normal crack opening v_1 and the elastic normal crack opening v_1^e as

$$v_1 = v_1^e + v_1^p. \tag{14}$$

During frictional sliding the crack faces are kept in contact by means of a negative normal traction t_1, whereby the elastic normal displacement simply follows as $v_1^e = t_1/K$. Combining this expression with equation 13 and inserting the result into equation 11 gives

$$t_2^{cr} = \mu \left\langle -K\left(v_1 - v_1^p\right)\right\rangle \frac{\dot{v}_2}{|\dot{v}_2|} H_{v_2^m}(|v_2|) \qquad \text{with} \quad v_2^m = \mu \left\langle -\left(v_1 - v_1^p\right)\right\rangle . \tag{15}$$

Finally, for reasons of numerical robustness, the effect of an abrupt reverse in the sign of the critical tangential traction under a changing direction of the tangential velocity $\dot{v}_2$ is slightly smoothened by extending the velocity term in the right-hand side of equation 15 with a regularization parameter δ (Wriggers, 2002), i.e.,

$$t_2^{cr} = \mu \left\langle -K\left(v_1 - v_1^p\right)\right\rangle \frac{\dot{v}_2}{\sqrt{\dot{v}_2{}^2 + \delta^2}} H_{v_2^m}(|v_2|) \qquad \text{with} \quad v_2^m = \mu \left\langle -\left(v_1 - v_1^p\right)\right\rangle . \tag{16}$$

The constitutive formulation describing the combined effects of fracture and friction can now be obtained by adding the above friction model to equation 1 for the fracture behaviour. This leads to the following constitutive expressions for the normal and tangential tractions in the crack:

$$t_1 = (1-d)K\left(v_1 - v_1^p\right) - dK\left\langle -\left(v_1 - v_1^p\right)\right\rangle ,$$

$$t_2 = (1-d)Kv_2 + \mu \left\langle -K\left(v_1 - v_1^p\right)\right\rangle \frac{\dot{v}_2}{\sqrt{\dot{v}_2{}^2 + \delta^2}} H_{v_2^m}(|v_2|) \qquad \text{with} \quad v_2^m = \mu \left\langle -\left(v_1 - v_1^p\right)\right\rangle , \tag{17}$$

in which the elastic stiffness represented by equation 2 has been included. Note that in the expression for the normal traction component t_1, the dependency on the normal displacement v_1 given by equation 1 has been replaced by a dependency on the elastic normal displacement $v_1 - v_1^p$, in accordance with the decomposition given by Eq.(14). The

two constitutive expressions represented by Eq.(17) can be conveniently captured in tensorial form as

$$t_i = (1-d)\,K\left(v_i - v_1^p\delta_{1i}\right) - dK\delta_{1i}\left\langle -\left(v_1 - v_1^p\right)\right\rangle + \delta_{2i}\,\mu\left\langle -K\left(v_1 - v_1^p\right)\right\rangle \frac{\dot{v}_2}{\sqrt{\dot{v}_2{}^2+\delta^2}} H_{v_2^m}(|v_2|),$$

$$\text{with} \qquad v_2^m = \mu\left\langle -\left(v_1 - v_1^p\right)\right\rangle \tag{18}$$

In order to monitor the influence of δ on the traction-separation law, a similar two element test as figure 17 is performed. Figure 19 reveals the influence of various values. In order to not underestimate the friction, a value of 10^{-3} is necessary.

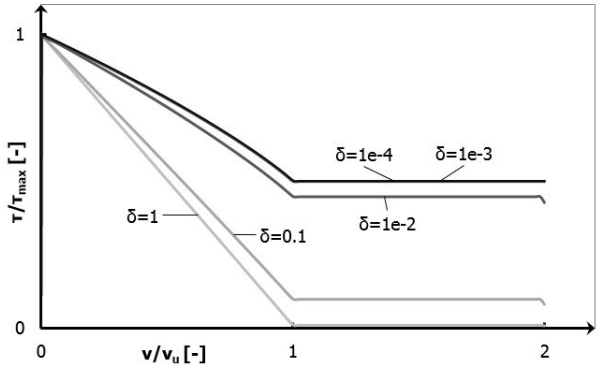

Figure 19: *Regularisation parameter*

The roughness of the crack faces may evolve during fracture and sliding, due to the continuous breakage, flattening and grinding of micro asperities. Consequently, the values of the friction coefficient μ and dilatancy coefficient ψ change with deformation. Initially the friction coefficient increases monotonically, starting from a zero value at the onset of fracture (where $\kappa = v_0$, see figure 20) and ending at a maximum value μ_{max} at completion of fracture (where $\kappa = v_u$, see figure 20). This stage is known as frictional hardening. Under a further increase of the tangential deformation, at a specific value $v_2 = v_{2,s}$ the friction coefficient may start to monotonically decrease from μ_{max} towards a residual value μ_{res}. This behaviour can be characterised as frictional softening. The hardening and softening phases are, respectively, described by following functions

$$\mu = \hat{\mu}(\kappa) = \mu_{max}\left(1 - \left(1 - \frac{\kappa - v_0}{v_u - v_0}\right)^n\right) \quad \text{for} \quad v_0 \le \kappa \le v_u,$$
$$\mu = \hat{\mu}(v_2) = \mu_{max} + (\mu_{res} - \mu_{max})\left(1 - \exp\left(-\gamma\left(|v_2| - v_{2,s}\right)\right)\right) \quad \text{for} \quad v_2 \ge v_{2,s}\,(\ge v_u), \tag{19}$$

where n and γ represent calibration parameters. The figures 20 and 21 visualize the influence of both parameters on the curves for the hardening and softening phase. Note that $v_{2,s}$ is set as zero for the curves of figure 21.

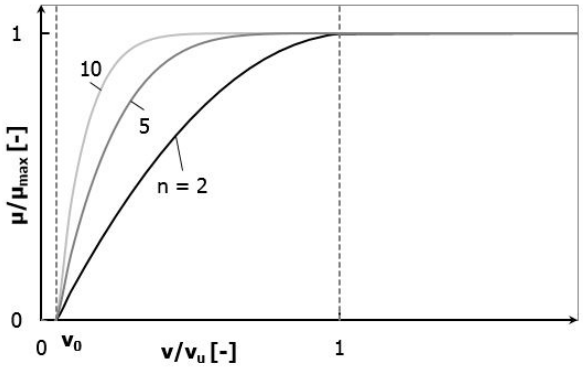

Figure 20: *Infuence of n for the development of friction hardening*

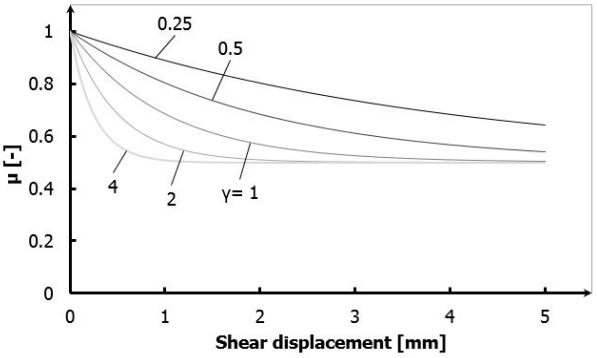

Figure 21: *Frictional softening law dependent on the value γ*

Previous equations can be summarized in a graph with the simulation of the two element test. Figure 22 reveals the curve where cohesive failure, friction and softening are incorporated.

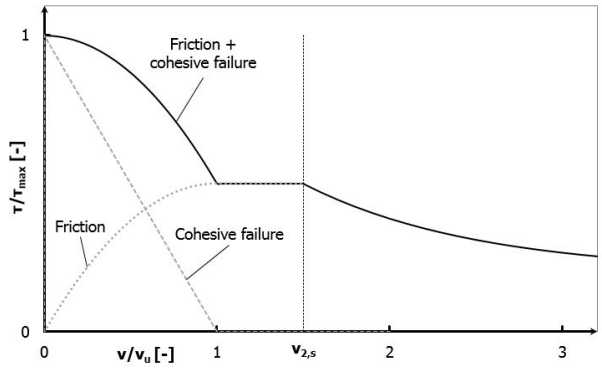

Figure 22: *Curve with due consideration of cohesive failure, friction and softening*

The evolution of the dilatancy coefficient is directly coupled to the evolution of the friction coefficient by means of a factor α, in accordance with

$$\begin{aligned} \psi = \hat{\psi}(\kappa) = \alpha\hat{\mu}(\kappa) \qquad & \text{for} \qquad v_0 \leq \kappa < v_u, \\ \psi = \hat{\psi}(v_2) = \alpha\hat{\mu}(v_2)\exp\left(-\gamma\left(|v_2| - v_{2,s}\right)\right) \qquad & \\ \text{for} \qquad v_2 \geq v_{2,s}\,(\geq v_u)\,. & \end{aligned} \tag{20}$$

with $\hat{\mu}(\kappa)$ and $\hat{\mu}(v_2)$ thus given by equation 19. Note from equation 20_2 that under progressive softening the dilatancy coefficient ψ asymptotically approaches to zero in the limit of $v_2 \to \infty$.

4. Simulations

The material model formulated in the previous section can be applied for simulating rebar pull-out of concrete. The simulations were performed displacement controlled with the Newton Raphson method to describe softening during fracture and frictional sliding.

4.1. Geometry and mesh

The geometry considered is modelled axissymmetrical, see figure 23. The constraint of the smooth rebar is positioned at the bottom side to restrict displacements in vertical direction comparable to the experimental setup. The deformed rebar specimen is restrained at the top side to suggest the threaded steel plate. Finally, a displacement of 3 or 5 mm is applied at the top of the rebar to simulate pull-out.

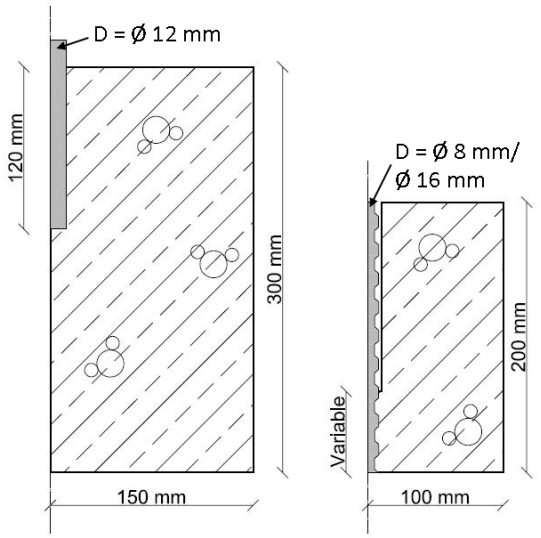

Figure 23: *Geometry of axisymmetric numerical model of smooth rebar and deformed rebar respectively.*

The basic geometry for the model is taken from the experiments; furthermore, the material characteristics of concrete are assigned tot the interface elements and continuum elements. The continuum elements behave elastically and the interface elements represent the inelastic behaviour, e.g. cracking and frictional sliding.

The principle of the applied cohesive zone model is revealed in figure 24. This detail is taken at the steel- concrete interface.

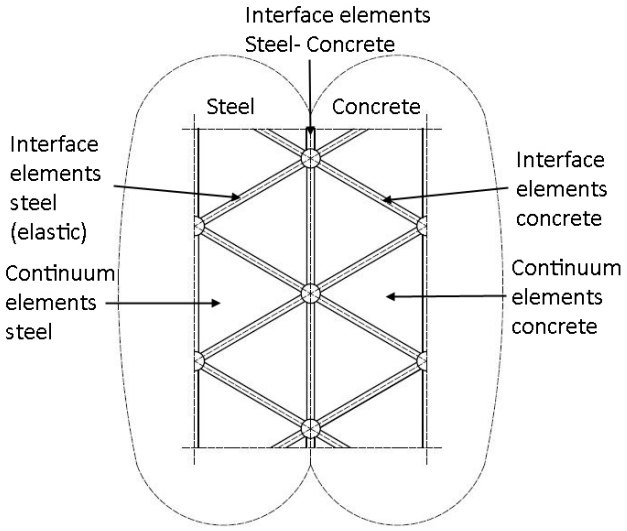

Figure 24: *Principle of meshing with interface elements located at rebar- concrete interface.*

A mesh of triangular elements was generated. By means of a Python script, interface elements were placed between the continuum elements. The interface elements have a certain thickness, thus the size of the continuum elements will be reduced 1% to create area. The mesh size meets the requirement in accordance with Cid Alfaro et al. (2009), where the size of the interface elements:

$$\frac{\Delta}{v^u} \approx \qquad 1.5 \quad to \quad 2.5 \qquad (21)$$

where δ represents the mesh size and v^u is the separation in which damage is fully developed in the interface elements.

4.2. Material properties

The finite element model simulates three materials, namely steel, concrete and the steel- concrete interface. This paragraph will give an overview of the chosen material parameters.

4.2.1 Steel rebar behaviour

The steel behaviour is assumed as elastic for both the smooth and deformed rebars. During pull-out, the steel stress is relatively low, which is maximally 95 N/mm^2 for smooth rebars and maximally 370 N/mm^2 for deformed rebars. Since steel grade FeB 500 was used, no yielding occurs. Therefore, the following parameters were used.

Parameter		Units
Youngs modulus	$2.1 \cdot 10^5$	N/mm^2
Poisson ratio	0.3	-

Table 5: Material parameters for steel rebar

Due to the generation method of the mesh, interface elements were placed in the concrete and steel sections. However, interface elements in the steel section are unnecessary. Instead of cohesive behaviour for the interface elements, the elements were chosen to behave elastically similar to the continuum elements. Yielding is disregarded.

4.2.2 Concrete behaviour

The continuum elements modelling the concrete have the following parameters of table 6. Shrinkage of the continuum elements was applied in the radial direction before pull-out. This results in a compressive stress on the rebar.

Parameter		Units
Youngs modulus	$3 \cdot 10^4$	N/mm^2
Poisson ratio	0.2	-
Shrinkage strain	$1.5 \cdot 10^4$	-

Table 6: Material parameters for concrete section

Furthermore, the parameters for the interface elements are determined with values reported in the literature and the fitting on experimental data, see table 7.

More detailed information about the geometrical constraints and material parameters of concrete section will be given in section 4.4.

Material parameters		Units
K mode I/II	10^6	N/mm^3
t_1/ t_2	7	N/mm^2
G_1/ G_2	1	N/mm^2
ϵ	10^{-12}	-
η	0.01	-
μ_{max}	1	-
n	100	-
δ	0.001	-
α	0.005	-
μ_{res}	0.5	-
γ	1	-
$\nu_{2,s}$	0.1	-

Table 7: Concrete in UMAT

4.2.3 Concrete-steel behaviour

Finally, the material parameters for the interface elements between both materials are obtained by fitting on experimental data.

Material parameters		Units
K mode I/II	10^6	N/mm^3
t_1/ t_2	1	N/mm^2
G_1/ G_2	0.05	N/mm^2
ϵ	10^{-12}	-
η	0.0001	-
μ_{max}	0.9	-
n	2	-
δ	0.001	-
α	0	-
μ_{res}	0.35	-
γ	1.4	-
$\nu_{2,s}$	0.1	-

Table 8: Concrete- steel interface in UMAT

All material parameters were discussed in the previous section, except η. The value of this parameter reflects the viscosity on the strain rate. The convergence behaviour of the simulation improves for a higher value of the viscosity. However, a significant overshoot of t_1/t_2 should be avoided when calibrating this parameter.

4.3. Results smooth rebar

The geometry of the rebar embedded in the concrete matrix has been implemented in Abaqus. The failure behaviour at the steel- concrete interface is simulated with a UMAT presented in Appendix B as Fortran script. Information about the mesh is shown in table 9 and mesh refinement is applied around the rebar as depicted in figure 25.

	Type	*Number*
Continuum elements	CPS3	15636
Interface elements	C0H2D	23210

Table 9: *Information about element types in the mesh for smooth rebar*

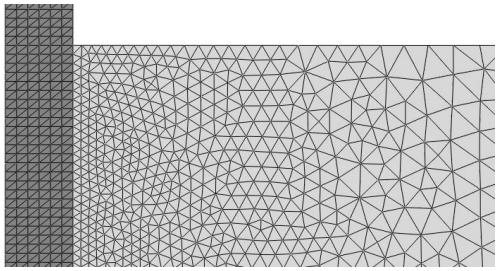

Figure 25: *Mesh of the smooth rebar*

Running the simulation of the smooth rebar gives the bond stress- slip relationship depicted in figure 26. Due to the implementation of frictional softening in the UMAT, the softening branch can be described in detail.

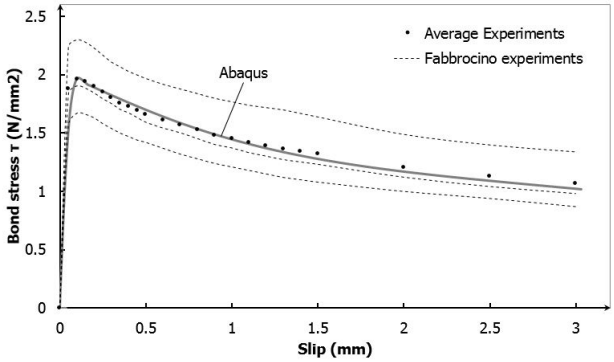

Figure 26: *Bonds stress- slip relationship for smooth rebar compared to experiments of Fabbrocino (2005)*

In order to fit the numerical model to the experimental data, the parameters t_i, G_i, μ_{max}, n, μ_{res}, γ and $\nu_{2,s}$ are calibrated. The height of the maximum bond stress is dependent on t_i, G_i and μ_{max} and shifts horizontally based on the fracture energy G_i. Furthermore, the descending branch can be adjusted by μ_{res} (residual stress), γ (exponential parameter) and $\nu_{2,s}$ (starting point for softening). More information about the variation of values will be given in next paragraph.

The failure behaviour in terms of crack pattern is depicted in figure 27 and more detailed in Appendix A. During pull out, the rebar gradually breaks the chemical adhesion and develops frictional resistance. Tensile stresses in concrete are sufficiently low to avoid transverse cracking of the concrete matrix.

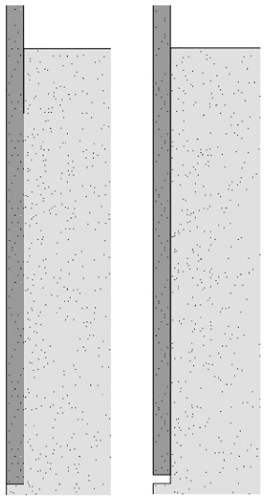

Figure 27: *Crack pattern of the smooth rebar Ø12 mm at 0.05 mm and 3 mm pull out*

Note that the chosen fracture values for mode I en II in table 8 are taken equal for reasons of numerical stability.

4.4. Results deformed rebar

The concrete section in the previous analysis is completely undamaged due to the relatively low tensile stresses generated during pull-out. In contrast, in case of the deformed rebar, failure in concrete section is governing. According to previous studies, shearing failure is the main mechanism for pull-out if the lateral confining stress is sufficiently high. Information about both meshes is given in tables 10 and 11. Furthermore, the meshes are depicted in figures 28 and 29.

	Type	*Number*
Continuum elements	CPS3	10542
Interface elements	C0H2D	13058

Table 10: Element types of Ø8 mm rebar

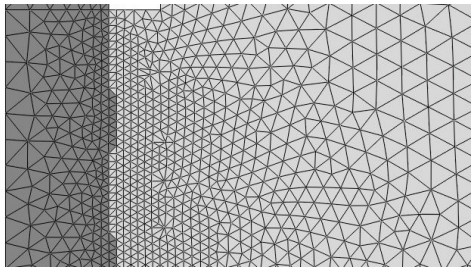

Figure 28: *Mesh for deformed rebar Ø8 mm*

	Type	*Number*
Continuum elements	CPS3	18095
Interface elements	C0H2D	26947

Table 11: Element types of Ø16 mm rebar

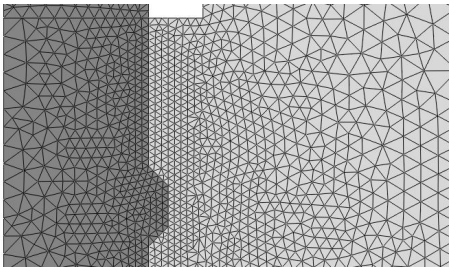

Figure 29: *Mesh for deformed rebar Ø16 mm*

4.4.1 Homogeneous bulk material

Simulations of both meshes can be performed resulting in a force- slip relationship of figure 30.

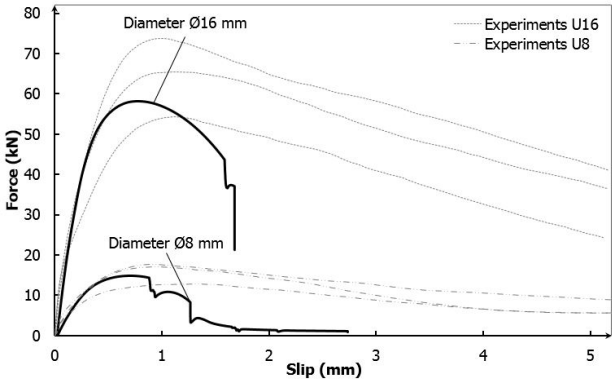

Figure 30: *Force- slip relationship for Ø8 and Ø16 mm*

The numerical results of figure 30 deviate from the experimental results for slip larger than 1 mm. Analyzing the deformation in the mesh, the following issue is observed. As shown in figure 31, cracks initiate in the vertical and diagonal interface elements.

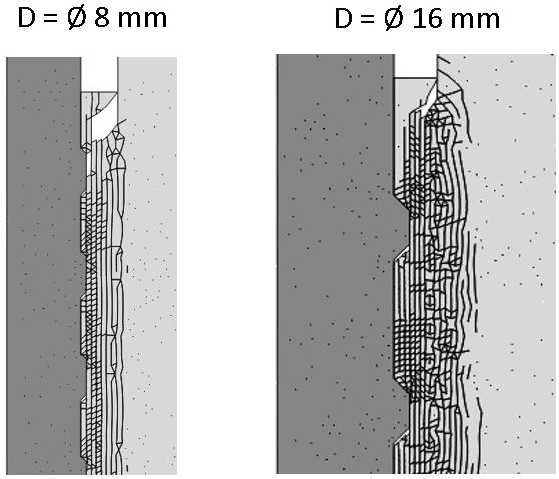

Figure 31: *Crack pattern for rebars after 1,8 mm pull-out*

Elements will rotate relative to each other for larger shear displacements. Figure 32 shows this effect, as visualized by the dotted line. Due to the rotation, compression in normal direction changed into

tension. As a result, the necessary dilatancy and friction does not contribute to the residual strength. Only the traction separation law of Alfaro et al. (2009) will be followed. This effect is reflected in the force slip relationships of both Ø8 an Ø16 mm. The abrupt turning point from compression to tension results in a drop and relative low residual strength for larger displacements.

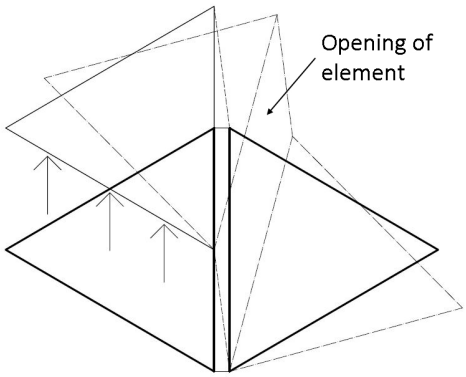

Figure 32: *Rotation of elements during pull out*

4.4.2 Addition of elastic zones

In order to reduce the previously described issue, the diagonal interface elements above the lugs have been assigned an elastic behaviour, as shown in figure 33. As a result, shearing mode II is possible. However, elements have been forced to follow the shear plane and remain free of rotations.

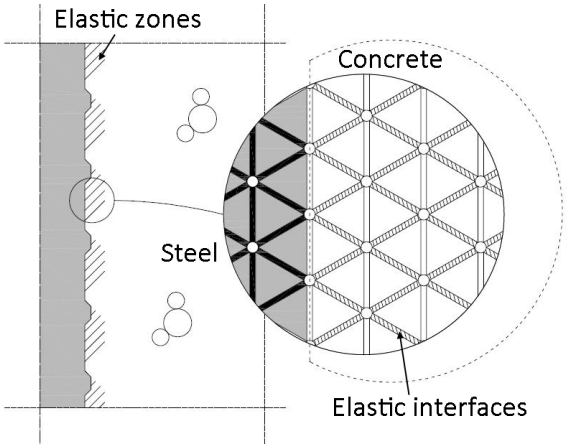

Figure 33: *Addition of elastic zones by means of elastic interface elements to avoid large rotations*

The UMAT of Appendix B and the parameters of table 7 and 8 were used for running simulations with Abaqus. Plots of the results are shown in figure 34.

The numerical analysis shows good agreement in the initial phase of pull-out. Substantially, the numerical simulation became sensitive to divergence problems. which is related to stiffness parameter K and will be discussed more in detail in paragraph 5.2.

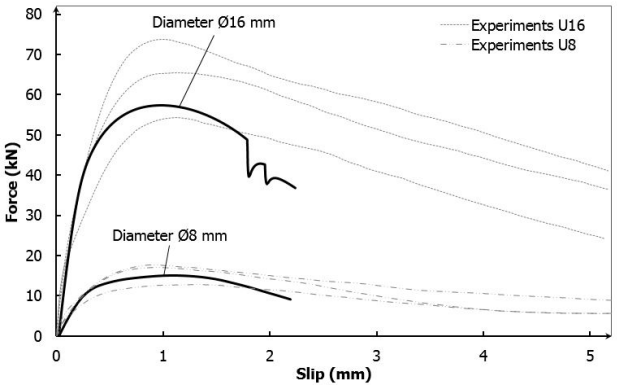

Figure 34: *Force- slip relationship for Ø8 and Ø16 mm*

In order to gain insight in the numerical response, the influence of the model parameters has been investigated by varying their values.

Influence of stiffness K :
K is the fictive stiffness, and thus not equal to the youngs modulus (E) of the material. However, according to Turon et al. (2007), the value of K can be estimated by dividing E by the thickness of interface element. The interface thickness close to the rebar is approximately 0.006 mm, in combination with E of 30000 N/mm^2, K should be $5 * 10^6$ N/mm ^{3} or larger. Due to divergence problems, the value is not attainable and therefore chosen as 10^6N/mm^3.

Influcence of traction t_1/t_2 :
As described before, values for mode I and II have been assumed equal. Therefore, the shear strength of concrete is derived from literature. According to Rots (1988) a value of 7 N/mm^2 is realistic for the shear strength of concrete.

Influcence of Fracture Energy G :
Due to the activation of normal traction caused by dilatancy, friction is mobilized. This effect is dominating the energy dissipation instead of the fracture energy of mode II, which is shown in figure 35. The value of G for mode II fracture in concrete is not widely reported in literature (Carpenteri et al., 1992), and therefore assumed as 1 N/mm.

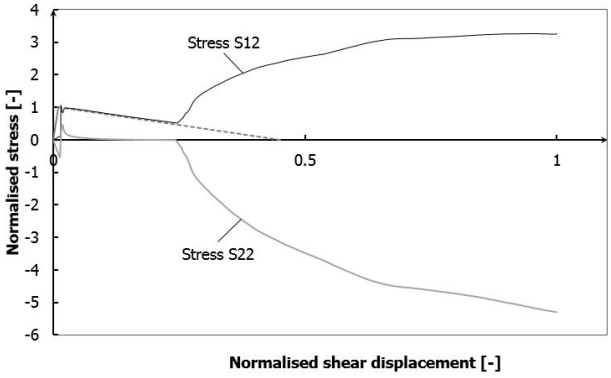

Figure 35: *Stress displacement relationship of an interface element in shear plane respecting dilatancy. (The dotted line is the standard traction separation law including the fracture energy G.)*

Influence of η :
The rate for pull-out is set to 1.5 mm/min, with a value of 0.01 seconds for η, the numerical simulation for the deformed rebar runs fairly smoothly. Furthermore, the traction overshoot is limited in the most interface elements.

Influence of μ :
The value of μ is obtained from the literature. According to Wriggers (2002), the friction coefficient for concrete- concrete surface may vary between 0.5 and 1.0 depending on the roughness. Therefore, μ_{max} is chosen as 1.0 and μ_{final} as 0.5 to incorporate softening due to sliding and grinding of the crack surfaces.

Influence of n :
The POWER parameter determines the amount of energy dissipation for friction during crack evolution. Figure 36 and 37 reveals the influence for varying values. As can be concluded, the dissipation during crack initiation is significant, the evolution of friction is substantially instantaneous for the best fitted value of 100.

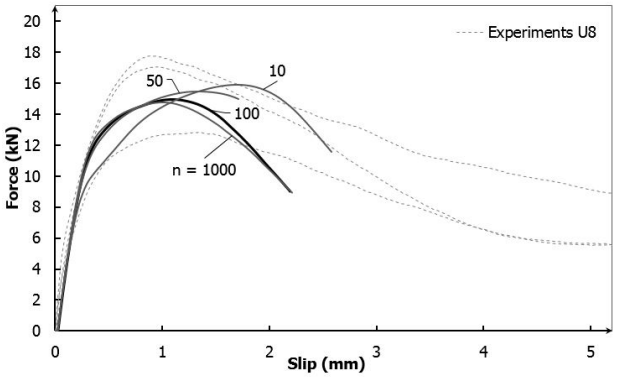

Figure 36: *Force- slip relationship for deformed rebar Ø8 mm*

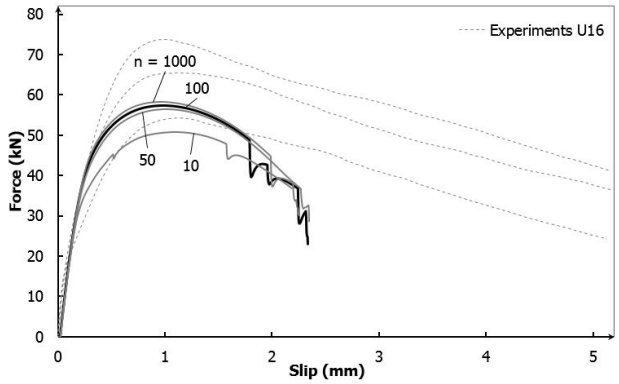

Figure 37: *Force- slip relationship for deformed rebar Ø16 mm*

Influence of δ :
In order to not underestimate the friction, the value is set to 0.001, based on two-element test.

Influence of DILATANCY, α :
Dilatancy could be of major influence for granular materials as concrete. The confinement of the concrete rebar ensures a high level of interlocking. This effect is captured in the numerical model by a volume expansion in normal direction. This increases the normal force in the interface elements and thus the frictional resistance.

The α parameter for dilatancy was varied as 0.003, 0.005 and 0.01 to investigate the effect for Ø8 and Ø16 mm. The results are revealed in figure 38 and 39. An increase of confinement provides higher strength and larger dissipation of energy during pull out.

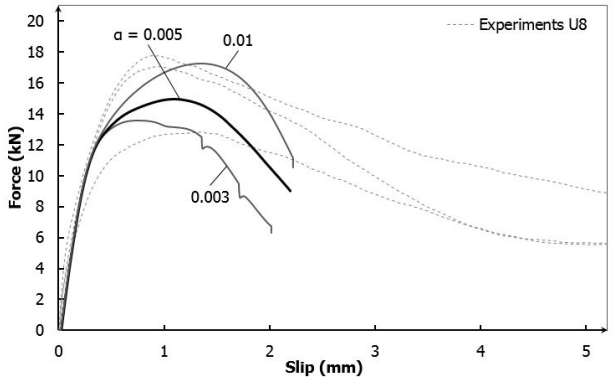

Figure 38: *Force- slip relationship for deformed rebar Ø8 mm dependent on α*

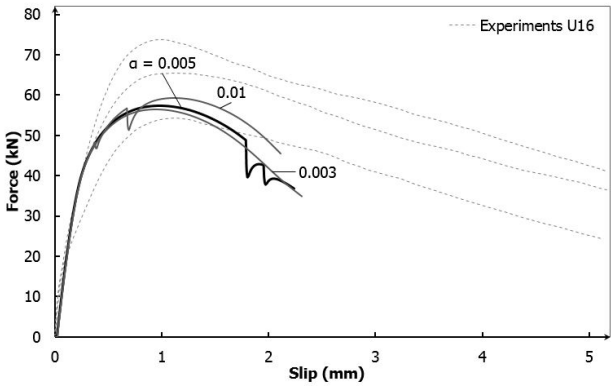

Figure 39: *Force- slip relationship for deformed rebar Ø16 mm dependent on α*

Obviously, the increase for Ø8 is higher than the Ø16 mm due to the rebar geometry. However, the absolute raise in pull-out force is comparable when increasing the dilatancy from 0.005 to 0.01.

A similar conclusion can be obtained from the crack pattern of figure 40 and 41 derived from these simulations. Increasing the dilatancy for Ø8 mm results in significant growth of cracks, this is less visible for Ø16 mm rebar pull-out. More detailed crack patterns are given in appendix A.

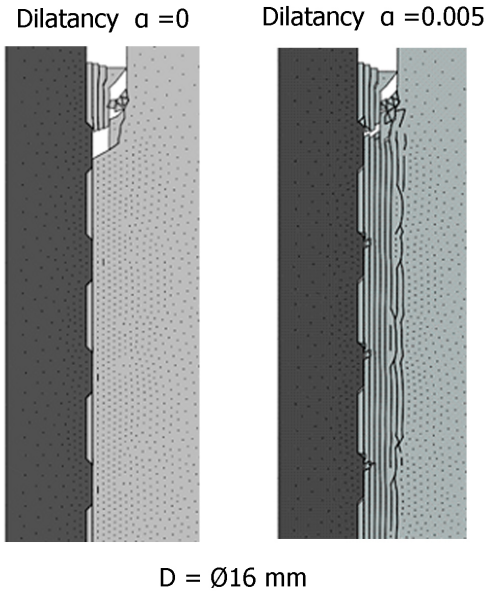

Figure 40: *Crack pattern of Ø8 mm with and without dilatancy after 2 mm pull-out*

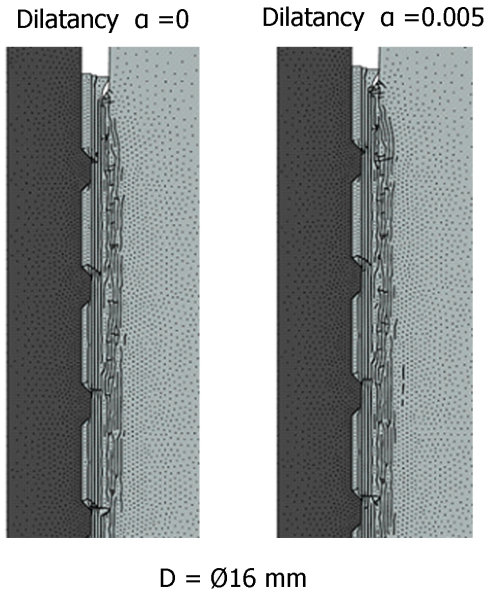

Figure 41: *Crack pattern of Ø16 mm with and without dilatancy after 2 mm pull-out*

Influence of γ :
The shape of the softening branch is dependent on the γ parameter. This exponential parameter is responsible for the course of the reduction of friction and dilatancy. As shown in figures 42 and 43, the energy dissipation during softening can be varied with this parameter. However, due to divergence problems for larger displacements, the dissipation is limited. Slow softening leads to convergence issues as revealed by the curves for γ = 0.5 and 0.25 for Ø8 mm. Similar to parameter α, the influence for Ø16 mm is smaller. Due to the fact that the material is fully damaged during frictional softening, only normal stresses provide residual shear stress through friction.

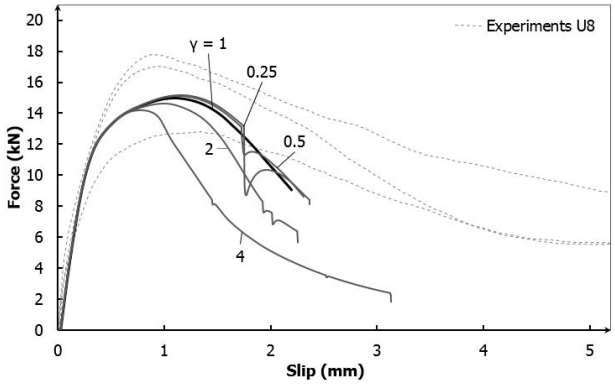

Figure 42: *Force- slip relationship for deformed rebar Ø8 mm dependent on γ*

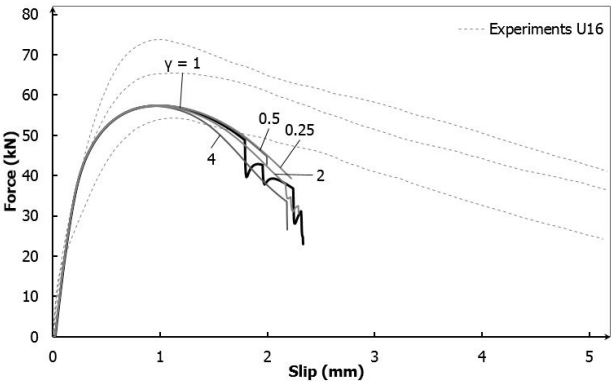

Figure 43: *Force- slip relationship for deformed rebar Ø16 mm dependent on γ*

Influence of $v_{2,s}$:
Finally, the parameter $v_{2,s}$ has been varied as depicted in figures 44 and 45. The influence is insignificant for the chosen values. The chosen values of 0.05, 0.1, 0.2 and 0.3 mm. Their effect on the force-slip plots of both rebars Ø8 and Ø16 mm is small.

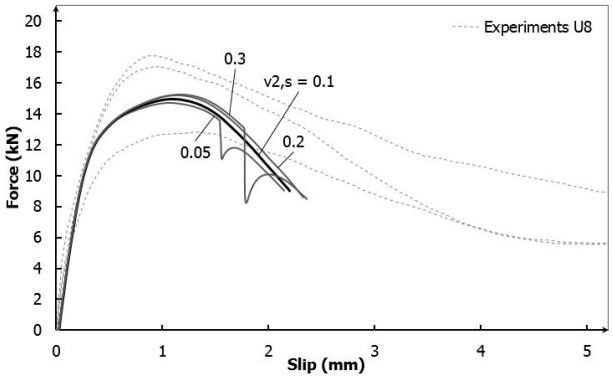

Figure 44: *Force- slip relationship for deformed rebar Ø8 mm dependent on $v_{2,s}$*

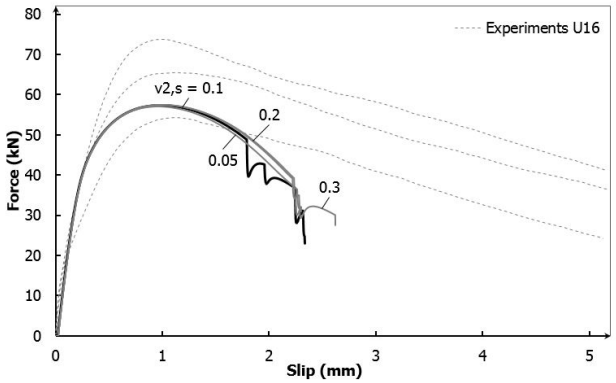

Figure 45: *Force- slip relationship for deformed rebar Ø16 mm dependent on $v_{2,s}$*

4.4.3 Influence of lug geometry

Furthermore, the dimensions of the lugs were increased in addition to the parameter study. It is assumed that the numerical model is capable to simulate the initial phase of pull-out with the universal parameters. Therefore, variation in lug dimensions can also be simulated. Figure 46 shows the renewed dimensions of the rebars.

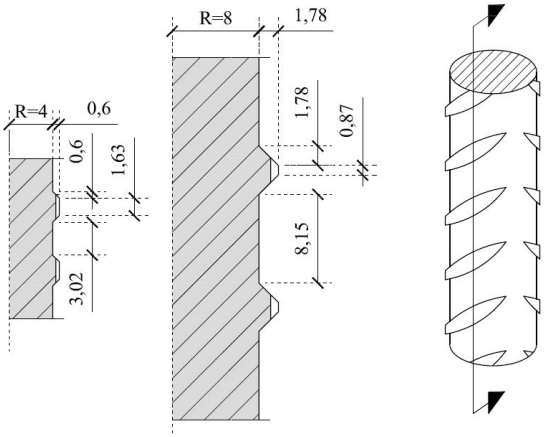

Figure 46: *Rebar geometry for increasing lug dimensions*

The force- slip relationships obtained from these simulations are depicted in figure 47. The increase in lug dimensions result in a higher ultimate pull-out strength for both rebars. Remarkable is the improvement of convergence for Ø8 mm; conversely, the divergence problems for Ø16 mm occur at an earlier stage. It can be concluded that larger lugs have a positive effect on the strength.

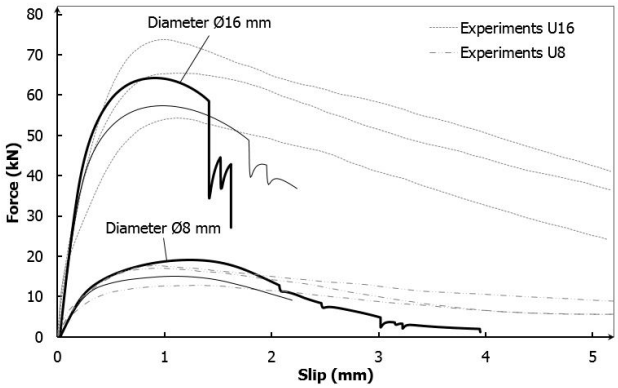

Figure 47: *Force- slip relationship for increasing lug dimensions*

5. Discussion of results

5.1. Smooth rebar pull out

The pull-out of a smooth rebar involves a softening branch. Possible explanations for this softening behaviour are outlined below.

5.1.1 Absence of frictional softening

In case of a constant frictional coefficient, the bond stress- slip relationship has the form as depicted in figure 48. After reaching the maximum bond stress, the residual bond stress remains approximately constant. This relationship does not correspond with the experimental results. Three phenomena could be responsible for the softening effect.

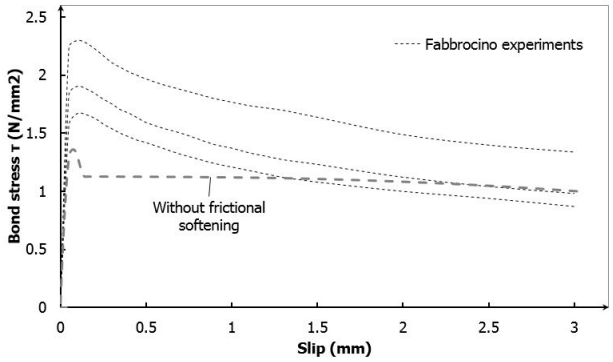

Figure 48: *Bonds stress- slip relationship without frictional softening*

5.1.2 Emperical explanation

Transverse cracking :
A possible explanation for softening is transverse cracking of the concrete section close to the rebar, as shown in figure 49. This causes a discontinuous concrete surface and thus a non-constant friction coefficient. The damaged concrete provides stacking of the smooth rebar. After a certain displacement slip weakening occurs due to interface wear. However, the numerical model shows that the tensile stresses in concrete have a maximum of approximately $1 N/mm^2$. Smooth rebars induce relatively low tensile stresses in concrete. As a result, no crack initiation is able to arise during pull out.

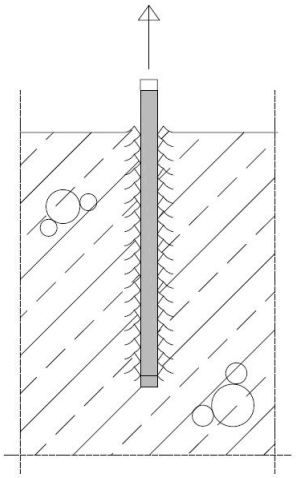

Figure 49: *Toothmechanism caused by transverse cracking in the concrete section*

Radial cracking :
A subsequent option is radial cracking due to hoop (radial) stresses (Tepfers, 1973) as revealed in figure 50. These cracks reduce the confinement and transverse pressure and therefore induce a reduction in residual strength. However, according to Fabbrocino et al. (2005): "Due to the nature of the reinforcement and the geometry of the specimen, splitting phenomena did not occur, so concrete blocks were not damaged macroscopically during the test". As a result the smooth rebar remains confined and the reduction in normal stresses by this effect is negligibly small.

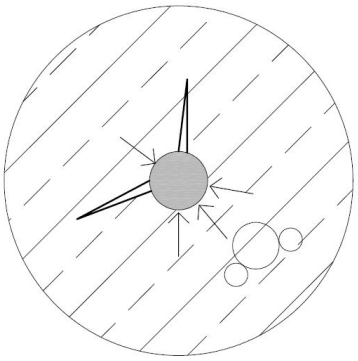

Figure 50: *Radial cracking caused by Hoop stresses*

Damage at microlevel :
The third option is slip weakening due to local damage of the concrete- steel interface. Concrete is not damaged macroscopically. However, small particles of the matrix could constrain the rebar during the first stage of pull out. As a result, the rebar with the concrete is heterogeneous along the rebar length as revealed in figure 52. These particles start grinding and rolling when slip occurs. This affects the friction between concrete and steel negatively. After a certain displacement, this effect occurs along the entire length of the rebar, resulting in a constant friction coefficient. A frictional softening law has been implemented to account for this effect.

5.1.3 Analytical validation

The assumption of slip weakening is supported by Palmer and Rice (1973). Although, the study considers soils, granular materials as concrete have related material behaviour. An analytical method has been developed to describe the softening branch for shear failure. Therefore the following has been assumed, a distribution of τ with distance from the tip of the shear band, a distribution which contains the end-region length ω as a parameter, and calculating from elasticity theory the implied τ, σ curve as revealed in figure 51.

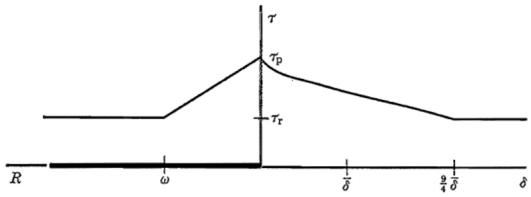

Figure 51: *Assumed distribution of shear stress on band within end zone and implied relation between shear stress and relative displacement across band (Palmer and Rice, 1973)*

.

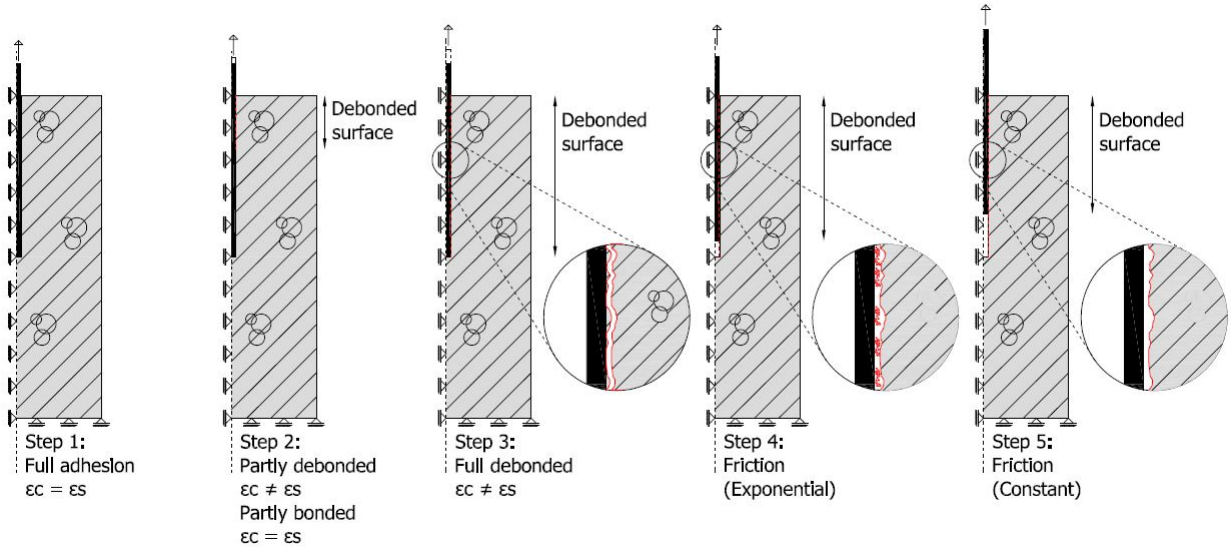

Figure 52: *Possible explanation for slip weakening during pull out of a smooth rebar. Step 1: First stage of bond stress-slip diagram before the chemical adhesion is broken (ultimate bond stress); Step 2: After reaching the ultimate bond stress, debonding of the concrete- steel interface occurs at the loaded end; Step 3: Further debonding over the entire rebar; however, small particles could stick to the rebar. Simultaneously, step 4 starts at the loaded end; Step 4: The increased displacement causes grinding and rolling of the particles; Step 5: Due to interface wear the resistance is reduced and attained a constant value for friction.*

The expressions associated with figure 51 have been described by Palmer and Rice (1973). The shear stress τ as function of of the end- region length ω and R can be written as:

$$\tau - \tau_r = (\tau_p - \tau_r)\left(1 - \frac{R}{\omega}\right) \quad (0 < R < \omega) \quad (22)$$

where ω can be estimated by

$$\omega \cong 125\frac{\tau_p}{\tau_p - \tau_r}\overline{\delta} \quad (23)$$

Finally, calculations of crack elasticity can be done using the slip displacement implied by expression 22 for $\tau - \tau_r$.

$$\delta = \frac{9}{8}\overline{\delta}\left[\left(1 + \frac{R}{\omega}\right)\sqrt{\frac{R}{\omega}} - \frac{1}{2}\left(1 - \frac{R}{\omega}\right)^2 \ln\frac{1 + \sqrt{\frac{R}{\omega}}}{1 - \sqrt{\frac{R}{\omega}}}\right] \quad (24)$$

For more detailed information about the analtyical derivation of these equations is referred to Palmer and Rice (1973) and Rice (1968).

Using the previously discussed expressions, a shear stress- displacement relationship can be obtained. Therefore, input parameters from experimental data are necessary, e.g. $\tau_p = 1.97N/mm^2$, $\tau_r = 0.97N/mm^2$ and $\frac{9}{4}\overline{\delta} = 3mm$. Implementing these parameters in expressions 22, 23 and 24, a relationship can be obtained by increasing R from 0 to ω as depicted in figure 53.

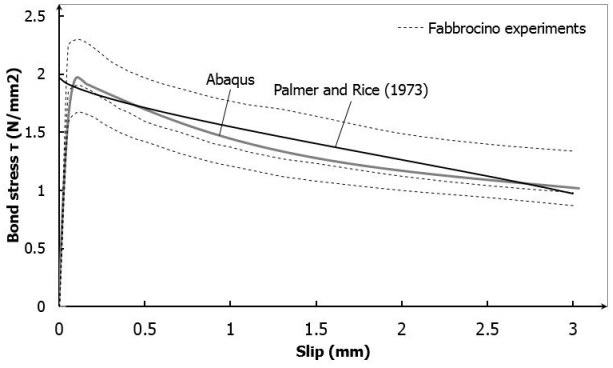

Figure 53: *Bond stress- slip relationship for experimental, analytical and numerical results.*

The curve is consistent with the numerical model and experimental data. The assumption of slip weakening seems to be reasonable based on the experimental observations and additional analytical models.

5.2. Deformed rebar pull out

Finally, the issues of friction, dilatancy, stiffness and divergence for deformed rebar are discussed in more detail.

5.2.1 Absence of friction

Initially, friction was not incorporated in the UMAT. As a result, residual stress can not be captured. Running the simulations gave the curves of figure 54. These are not consistent with the experiments. However, no divergence problems occur, pull-out up to 5mm is possible.

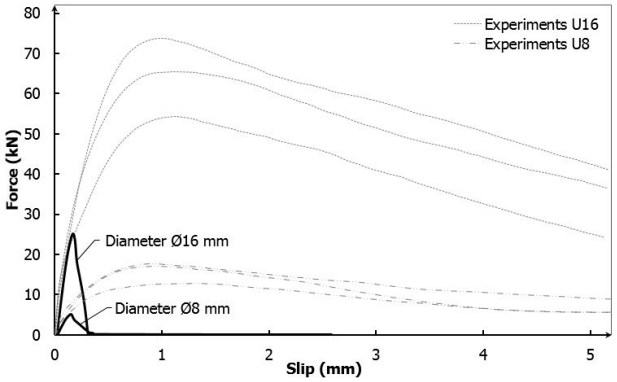

Figure 54: *Force- slip relationship without coulomb friction law*

5.2.2 Absence of dilatancy

In the first simulations of section 4 the dilatancy is set to zero, see figure 55. As a result, the residual pull- out force for both rebars are relatively low. As discussed in section 4, shrinkage is applied to the concrete section. However, these strains cause normal stresses which are not comparable with the induced residual stresses. Figure 55 reveals the plots of the numerical simulations without dilatancy and with the insufficient shrinkage stress.

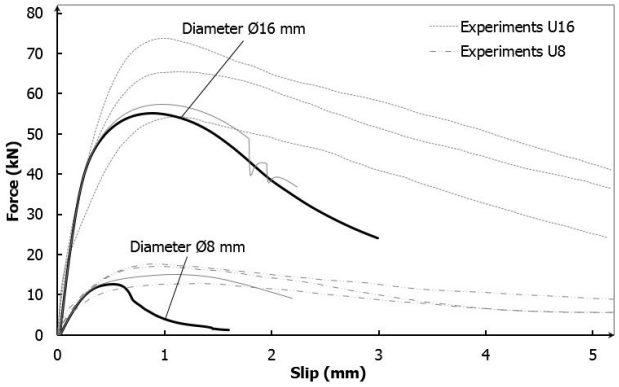

Figure 55: *Force- slip relationship without dilatancy*

5.2.3 Phenomenon dilatancy

During frictional failure of granular materials, the dilatancy represents a volume expansion due to a shear displacement, as discussed by Pereira et al. (1993) and Feenstra et al. (1991). For instance, the dilatancy angle for steel is zero since the evolution of a shear crack is parallel to the force. A shear crack in concrete has rough surfaces as shown in figure 56. Due to aggregate interlock, the load carrying capacity is considerable after cracking. Both surfaces should move relative to each other in normal direction to allow shear displacement. In addition, shearing failure of the teeth is a possible mechanism as discussed by Pereira et al. (1993).

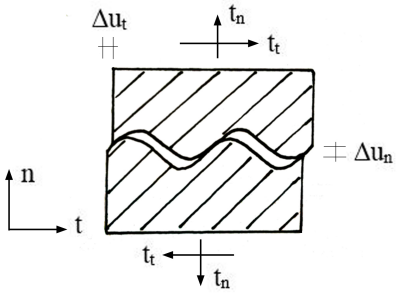

Figure 56: *Principle of dilatancy in a shear crack (Feenstra et al. 1991)*

Due to the confinement of the deformed rebar, the restriction on dilatant deformations induces significant normal stresses along the frictional plane. Correspondingly, the residual force increases significantly.

5.2.4 Stiffness

In figure 54, the pull- out of the smooth rebar is performed for three different stiffnesses of the interface elements. The pull-out displacement is set to 20mm.

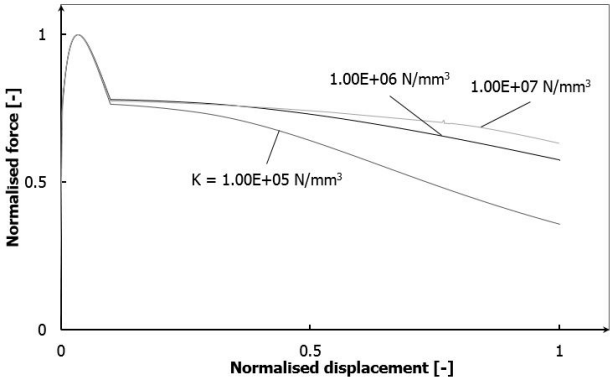

Figure 57: *Influence of the stiffness on shear resistance*

The higher the stiffness, the better the representation of friction at failure under increasing displacement. It can be expected that a stiffness value close to 10^7 N/mm^3 is reasonable for keeping the reduction of stress under continuous stress limited. However, when using a relatively high value of K = $5 * 10^6$ N/mm^3 for the model of the deformed rebar, the simulation experiences convergence problems as shown in figure 58. Hence, in the numerical variation studies presented in the previous section a value of 10^6 N/mm^3 was used.

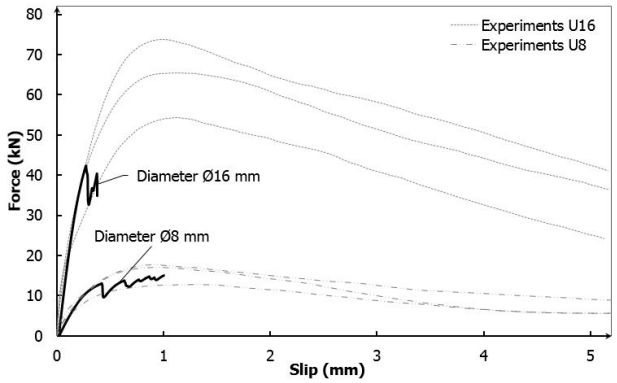

Figure 58: *Curves for $K = 5 * 10^6$ N/mm^3*

6. Conclusion

This report has discussed the pull-out behaviour of smooth and deformed rebars in experimental and numerical simulations. The experimental results were obtained from the literature and from lab tests performed at the Eindhoven University of Technology. The assumption has been made that differences between actual rebar geometry and the axissymmetric rebar geometry used in the numerical simulations are negligibly small in terms of failure behaviour and the force- slip relationship. Accordingly, only the pull-out mechanism has been considered, and splitting or cone failure was disregarded.

The attempt to simulate pull-out was performed by means of cohesive zone modeling to capture the crack pattern during failure. The traction separation behaviour of Cid Alfaro et al. (2009) is listed in a UMAT as input for the interface elements in ABAQUS. The ability to simulate cracking of concrete loaded in tension has been reported in Cox (2015). However, the present research mainly considers shear as the governing loading mode.

Coulomb's friction law is used to capture the effect of frictional resistance. Regarding the smooth rebar, the addition of friction to the cohesive law can adequately to simulate the bond stress- slip relationship.

The addition of a volume expansion in normal direction due to shear displacement models the effect of dilatancy. Results show good agreement for the initial phase of pull-out. Subsequently, elements starts to rotate due to moment equilibrium, which affects the stability of the numerical simulations. Incorporating elastic zones prevents this mechanism. Nevertheless, for significant shear displacements, the convergence behaviour of the simulation can not be warranted. Nevertheless, the numerical models are able to predict the maximum strength of the deformed rebar pull-out for Ø8 and Ø16 mm.

Recommendation for further research concerning rebar pull-out is to rewrite the script from UMAT to VUMAT and perform explicit numerical simulations. These simulations should be less sensitive for divergence problems. Additionally, it is recommended to expand the axissymmetric model to a 3D configuration. For an explicit calculation, the computing time can be kept within reasonable bounds. This 3D configuration provides an actual representation of the geometry and is able to simulate multiple mechanisms, e.g. splitting and cone failure.

Additionally, experiments can be conducted for smooth and deformed rebars embedded in heterogeneous concrete that induces aggregates. According to Cox (2015), heterogeneity of numerical concrete can be investigated. Different grain sizes can be implemented in the numerical model and in the experimental specimens. Hitherto, concrete is considered homogeneous for matters of simplicity.

References

ACI 408, Bond test database; may be obtained from: http://fibtg45.dii.unile.it/files%20scaricabili/Database %2010-2001.xls

BRUGGELING, A.S.J., DE BRUIJN, W.A., Theorie en praktijk van het gewapend beton, deel 1, Den Bosch: Vereniging Nederlandse Cementindustrie, 1986.

CAIRNS, J., "Bond and anchorage of embedded steel reinforcement of the fib model code 2010", *Structural concrete*, vol 16, No 1, pp. 45-55, 2014.

CARPENTERI, A., VALENTE, S., FERRARA, G., MELCHIORRI, G., "Is mode II fracture property a real property?", *Composites and Structures* Vol. 48, No 3, pp. 397-413, 1992.

CEB TASK GROUP BOND MODELS, Bulletin 10, Bond of reinforcement in concrete, *State of art report*, Lausanne, Switzerland, 2000.

CID ALFARO, M.V., SUIKER, A.S.J., DE BORST, R., REMMERS, J.J.C., "Analysis of fracture and delamination in laminates using 3D numerical modelling", *Engineering fracture mechanics*, vol. 76, pp. 761-780, 2009.

COX, S.B., "The Influence of Concrete Heterogeneity on the Pull-out Behaviour of Steel Fibres", Master Thesis: Eindhoven University of Technology, 2015.

CUR RAPPORT 23, Onderzoek naar de samenwerking van geprofileerd staal met beton, commissie voor de uitvoering van research ingesteld door de betonvereniging: Den Haag, 1963.

FABBROCINO, G., VERDERAME G.M., MANFREDI M., "Experimental behaviour of anchored smooth rebars in old type reinforced concrete buildings", *Engineering structures* Vol. 27, pp. 1575âĂŞ1585, 2005.

FEENSTRA, P.H., DE BORST, R., ROTS, J.G., "Numerical study on crack dilatancy. I: Models and stability analysis", textitJournal of Engineering Mechanics Vol. 117, No 4, 1991.

FIB MODEL CODE 2010, Bulletin 65, Ernst and Sohn: Berlin, Germany, 2013.

FIB TIG4.5, Bond test database; may be obtained from: http://fibtg45.dii.unile.it/files%20*scaricabili/Database_ splicetest*%20*Stuttgart*%20*sept*%202005.*xl*

MARINUS, P.C.P., "Ultra lightweight concrete for monolith facade structures", Master thesis: Eindhoven University of Technology, 2015.

PALMER, A.C., RICE, J.R., "The growth of slip surfaces in the progressive failure of over- consolidated clay" Proc. Roy. Soc. Lond. A. 332, 527-548, 1973

PEREIRA, J.P., DE FREITAS, M.H., "Mechanisms of shear failure in artificial fractures of sandstone and their implication for models for hydromechanical coupling", *Rock mechanics and rock engineering*, Vol. 26, pp. 195-214, 1993.

RICE, J.R., "In fracture: an advanced treatise (ed. H. Liebowitz)", Academic Press No.2, 191-311, 1968.

ROTS, J.G., Computational modelling of concrete fracture, PhD thesis: Delft University of Technology, p.99, 1988.

TASSIOS, T.P., "Properties of bond between concrete and steel under load cycles idealizing seismic actions", *CEB Bulletin* No. 131, pp. 67-122, 1979.

TEPFERS, R., DE LORENZIS, L., "Bond of FRP reinforcement in concrete", *Mechanics of Composite Materials*, Vol. 39, No 4, pp. 510-526, 2003.

TEPFERS, R., A theory of bond applied to overlapped tensile reinforcement splices for deformed bars, PhD thesis: Chalmers University of Technology, 1973.

TURON, A., DÁVILLA, C. G., CAMANHO, P. P., COSTA, J., "An Engineering Solution for Mesh Size Effects in the Simulation of Delamination Using Cohesive Zone Models", *Engineering Fracture Mechanics*, Vol. 74, No. 10, pp. 1665-1682, 2007.

WRIGGERS, P., Computational contact mechanics, Hannover: Springer, 2002.

APPENDIX A: Detailed crack pattern smooth rebar Ø12mm and deformed rebar Ø8 and Ø16 mm

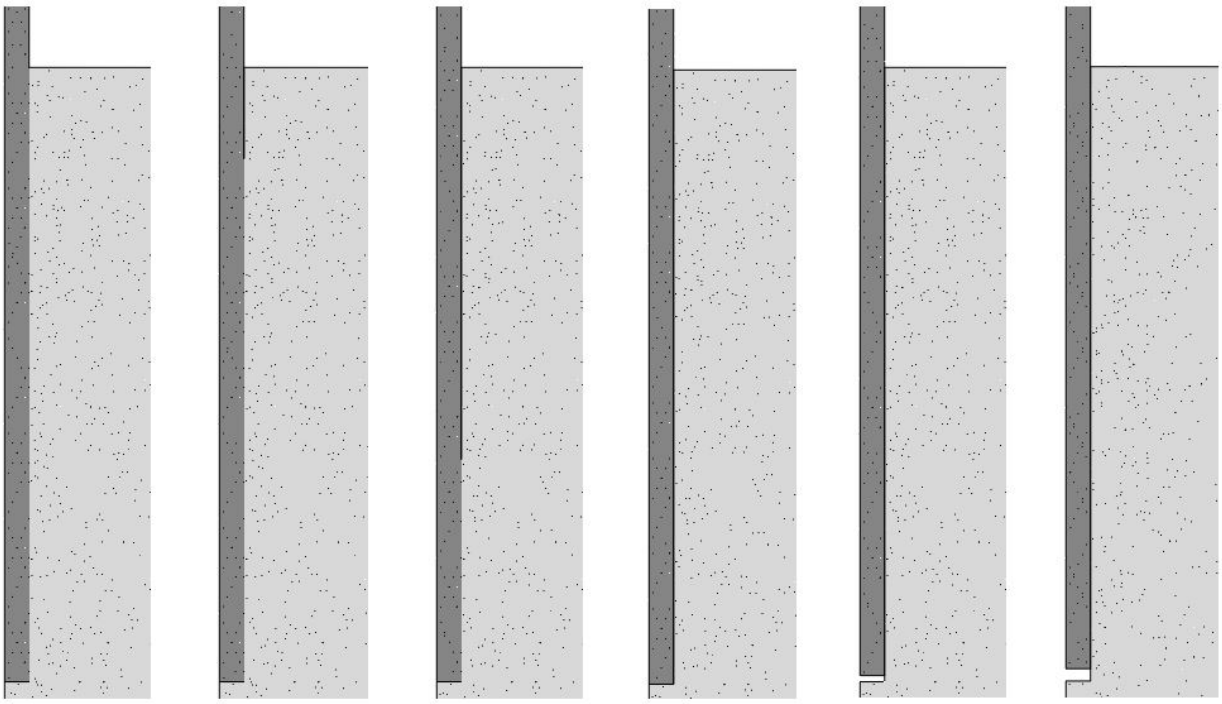

Figure 59: Crack pattern of Ø12 mm for respectively 0, 0.05, 0.075, 0.1, 1.5 and 3.0 mm pull-out

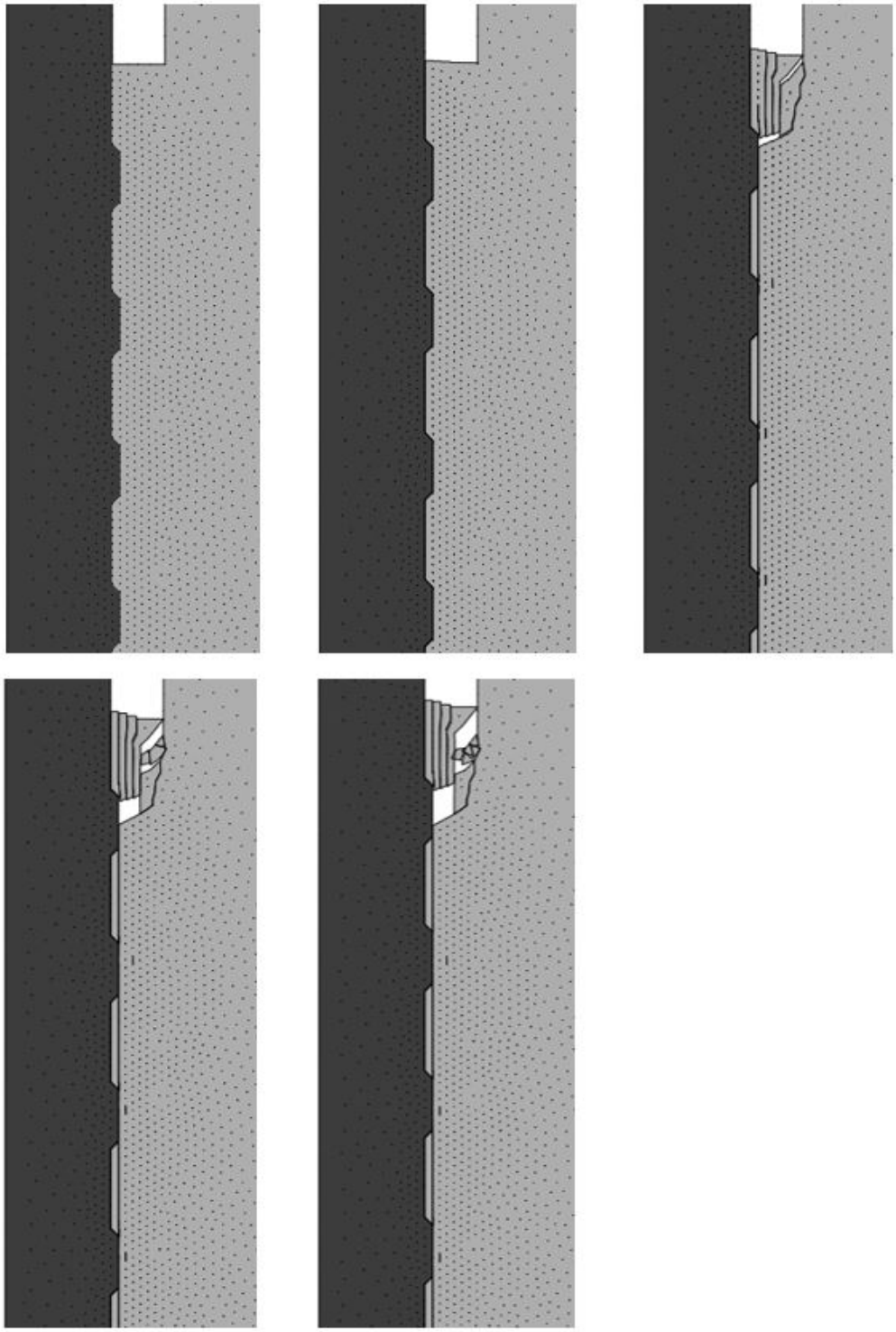

Figure 60: Crack pattern of Ø8 mm without dilatancy for respectively 0, 0.4, 0.8, 1.2 and 1.6 mm pull-out

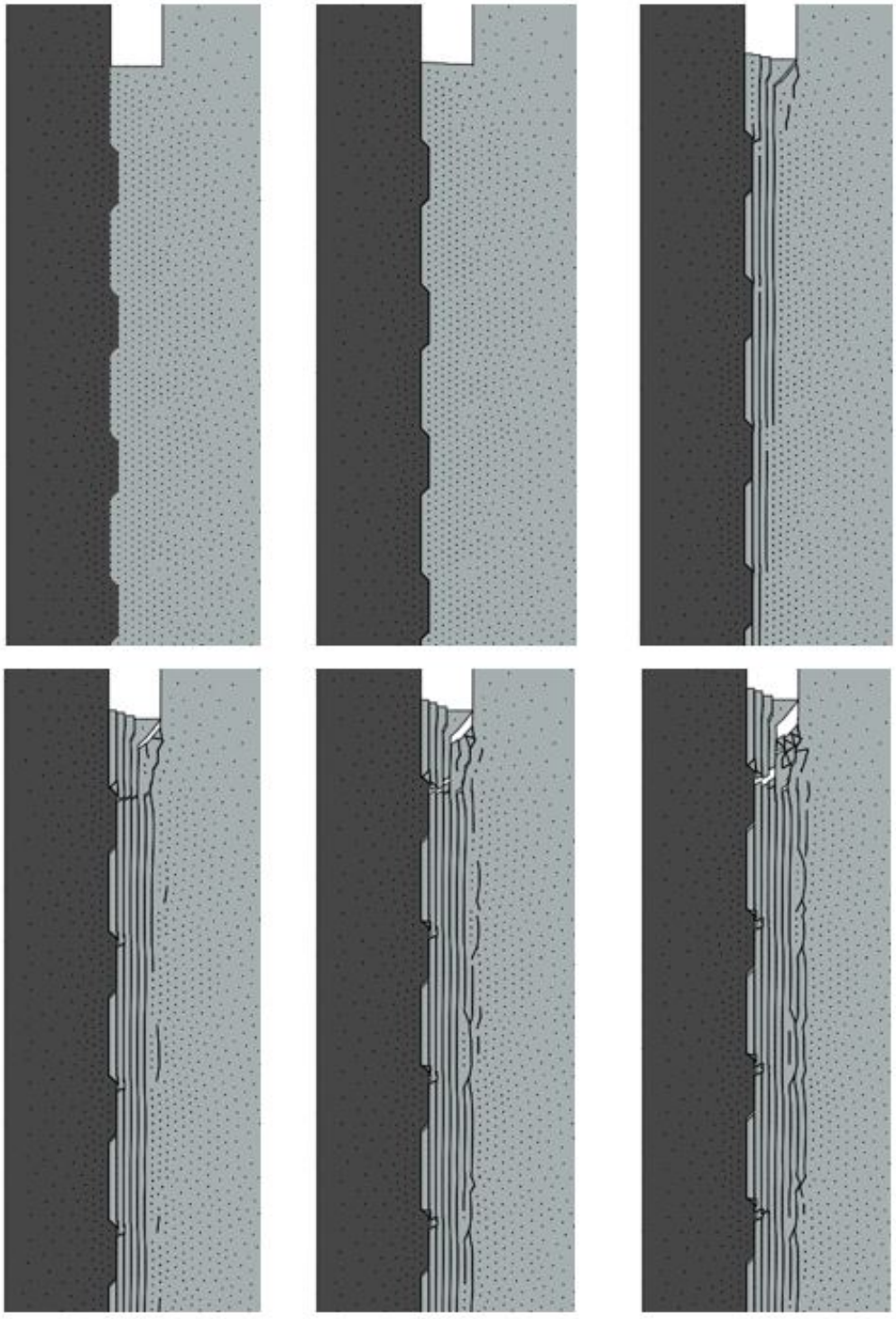

Figure 61: Crack pattern of Ø8 mm with dilatancy for respectively 0, 0.4, 0.8, 1.2, 1.6 and 2.0 mm pull-out

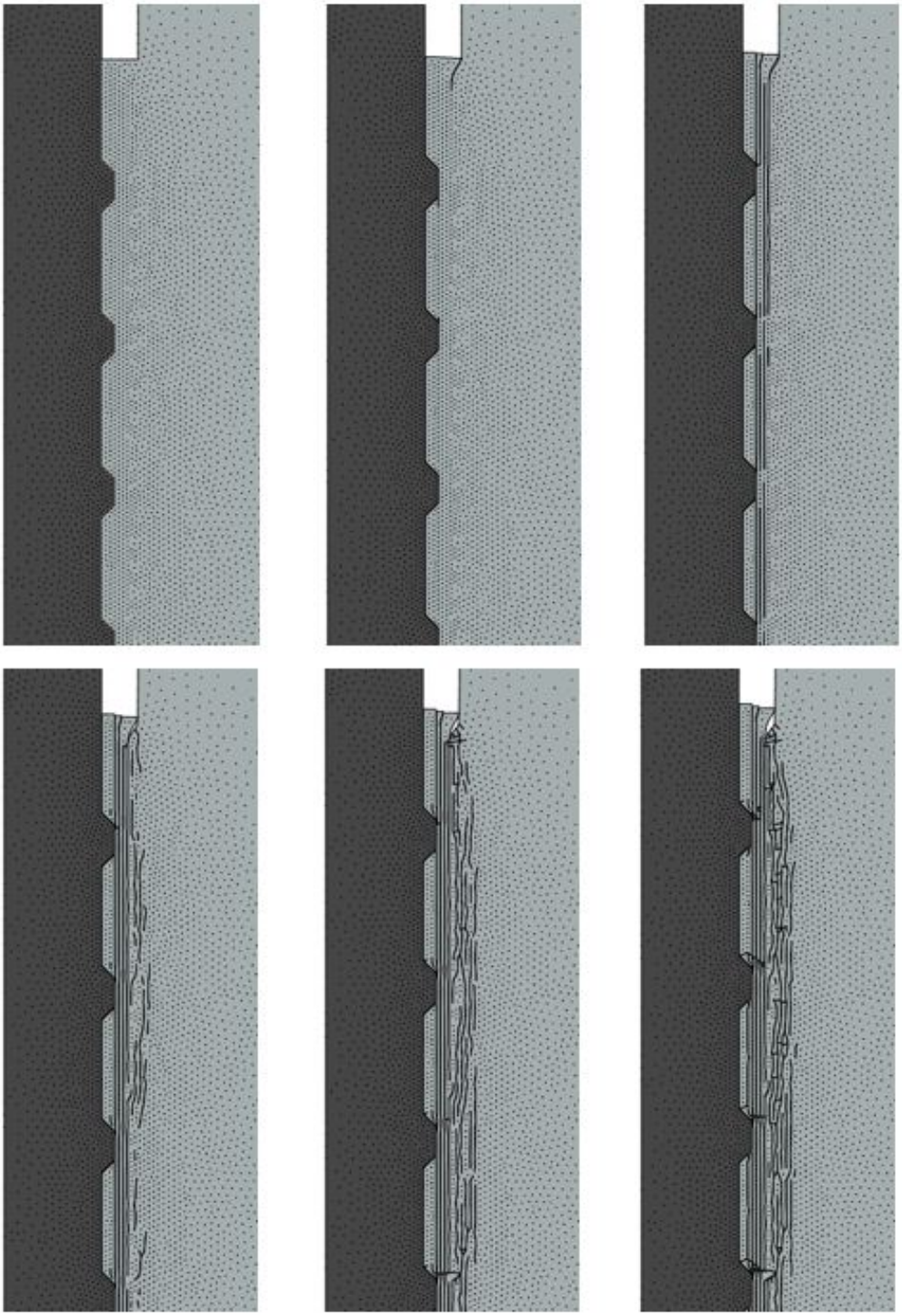

Figure 62: Crack pattern of Ø16 mm without dilatancy for respectively 0, 0.4, 0.8, 1.2, 1.6 and 2.0 mm pull-out

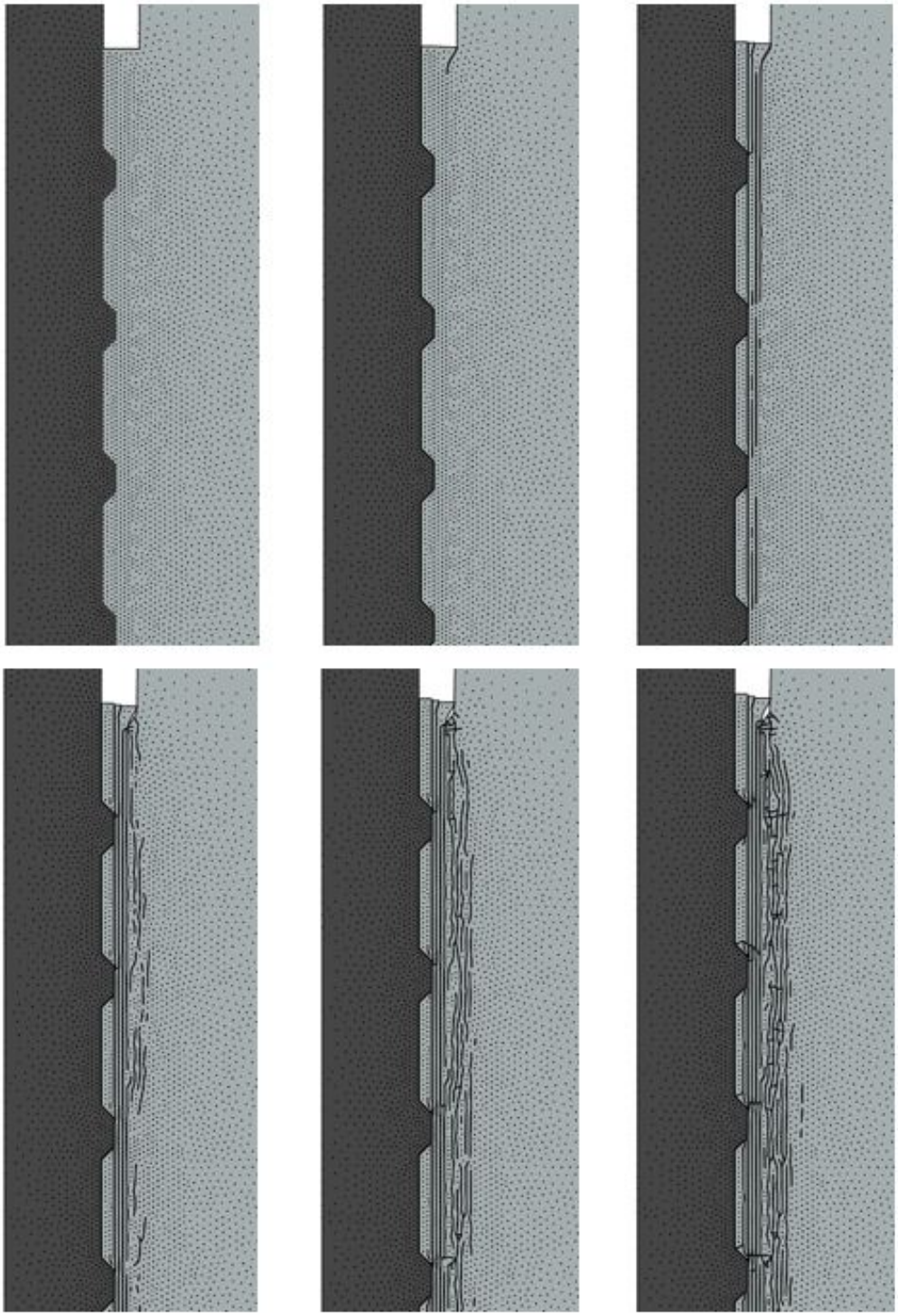

Figure 63: Crack pattern of Ø16 mm with dilatancy for respectively 0, 0.4, 0.8, 1.2, 1.6 and 2.0 mm pull-out

APPENDIX B: UMAT

```
      SUBROUTINE UMAT(STRESS,STATEV,DDSDDE,SSE,SPD,SCD,
     1 RPL,DDSDDT,DRPLDE,DRPLDT,
     2 STRAN,DSTRAN,TIME,DTIME,TEMP,DTEMP,PREDEF,DPRED,CMNAME,
     3 NDI,NSHR,NTENS,NSTATV,PROPS,NPROPS,COORDS,DROT,PNEWDT,
     4 CELENT,DFGRD0,DFGRD1,NOEL,NPT,LAYER,KSPT,KSTEP,KINC)

      INCLUDE 'ABA_PARAM.INC'

      CHARACTER*80 CMNAME

      DIMENSION STRESS(NTENS),STATEV(NSTATV),
     1 DDSDDE(NTENS,NTENS),
     2 DDSDDT(NTENS),DRPLDE(NTENS),
     2 STRAN(NTENS),DSTRAN(NTENS),TIME(2),PREDEF(1),DPRED(1),
     3 PROPS(NPROPS),COORDS(3),DROT(3,3),DFGRD0(3,3),DFGRD1(3,3)

      PARAMETER (M=3,N=3,ID=3,ZERO=0.D0,ONE=1.D0,TWO=2.D0,THREE=3.D0,
     & PI=3.14159265358979323846D-20,H=1.D-08)

      INTEGER I,J
      DOUBLE PRECISION STIFFN(4),DSTRANP(2),STRESSP(2),GAMMA,GAMMA_P,GAMMAN,
     & D,D_P,DN,TIN,TSHN,VIN_DIL,VI_DIL,VI_DIL_P,MU,DIL

C # ------------------------------------------------------------ #
C # SAVING PREVIOUSLY CALCULATED KAPPA AND DAMAGE (STATEV 1 AND 2) #
C #           FOR USE IN RETURN MAPPING CALCULATIONS               #
C # ------------------------------------------------------------ #
      GAMMA_P=STATEV(1)           ! KAPPA FROM PREVIOUS CALCULATION KAPPA_N
      D_P=STATEV(2)               ! DAMAGE FROM PREVIOUS CALCULATION DAMAGE_N
      VI_DIL_P=STATEV(3)
      MU=STATEV(4)
      DIL=STATEV(5)
C # ---------------------------------- #
C # STARTING FIRST CALCULATION USING TSL #
C # ---------------------------------- #
      CALL TSL(PROPS,STRAN,DSTRAN,STATEV,DTIME,STRESS,NPROPS,NTENS,
     & NSTATV)

      GAMMAN = STATEV(1)
      DN = STATEV(2)
      VIN_DIL = STATEV(3)
      MU=STATEV(4)
      DIL=STATEV(5)
C
      TIN = STRESS(1)
      TSHN = STRESS(2)

      DO 200, I=1, NTENS

        DO 150, J=1, NTENS
          DSTRANP(J) = DSTRAN(J)

150     CONTINUE

        DSTRANP(I) = DSTRANP(I) + H
        STATEV(1) = GAMMA_P
        STATEV(2) = D_P
        STATEV(3) = VI_DIL_P
        STATEV(4) = MU
        STATEV(5) = DIL

        CALL TSL(PROPS,STRAN,DSTRANP,STATEV,DTIME,STRESS,NPROPS,NTENS,
     &  NSTATV)

        STIFFN(2*(I-1) +1) = (STRESS(1) - TIN )/H
        STIFFN(2*(I-1) +2) = (STRESS(2) - TSHN )/H

200   CONTINUE

      STATEV(1)=GAMMAN
      STATEV(2)=DN
      STATEV(3)=VIN_DIL
      STATEV(4) = MU
      STATEV(5) = DIL
C
```

```
      STRESS(1)=TIN
      STRESS(2)=TSHN

      DDSDDE(1,1)= STIFFN(1)
      DDSDDE(1,2)= STIFFN(2)
      DDSDDE(2,1)= STIFFN(3)
      DDSDDE(2,2)= STIFFN(4)

      END

C -------------------------------------------------------------------
C # SUBROUTING - CULATING VALUES FOR TRACTION-SEPARATION DIAGRAM #
C -------------------------------------------------------------------


      SUBROUTINE TSL(PROPS,STRAN,DSTRAN,STATEV,DTIME,STRESS,NPROPS,
     & NTENS,NSTATV)

      PARAMETER (ZERO=0.D0,ONE=1.D0,TWO=2.D0,THREE=3.D0)

      DOUBLE PRECISION PROPS(NPROPS),STRAN(NTENS),DSTRAN(NTENS),
     & STATEV(NSTATV),STRESS(NTENS),DTIME,D,GAMMA,ENN,ESS,TIMAX,TSHMAX,
     & GSH,EPSILON,ETA,MUMAX,MU,POW,VI0,VIMAX,VSH0,VSHMAX,VI,VSH,DVSH,
     & VIN,VSHN,VINM,VINMN,ALFA,EMM,BETA,V0,VU,F,DI,DN,GAMMAN,TIN,EPSV,
     & GI, FACT, DIL, VIN_DIL, VINMN_DIL,
     & VI_DIL,MUFINAL,RATE,VSHSOFT

      INTEGER NTENS,NPROPS

          ENN=PROPS(1)
          ESS=PROPS(2)
          TIMAX=PROPS(3)
          TSHMAX=PROPS(4)
          GI=PROPS(5)
          GSH=PROPS(6)
          EPSILON=PROPS(7)
          ETA=PROPS(8)
          MUMAX=PROPS(9)
          POW=PROPS(10)
          EPSV=PROPS(11)
          FACT=PROPS(12)
          MUFINAL=PROPS(13)
          RATE=PROPS(14)
          VSHSOFT=PROPS(15)
C
          VI0=TIMAX/ENN
          VIMAX=TWO*GI/TIMAX
          VSH0=TSHMAX/ESS
          VSHMAX=TWO*GSH/TSHMAX
C -------------------------------------------------
C # PRESCRIBING PARAMTERS FOR USE IN CALCULATIONS #
C -------------------------------------------------

           VI=STRAN(1)
           VSH=STRAN(2)
           DVI=DSTRAN(1)
           DVSH=DSTRAN(2)
           VIN=STRAN(1)+DSTRAN(1)
           VSHN=STRAN(2)+DSTRAN(2)

C     OTHER VALUES USED IN CALCULATIONS:
           VINM=(VIN+ABS(VIN))/TWO
           VINMN=(-VIN+ABS(-VIN))/TWO
           ALFA=SQRT(VIN**TWO+VSHN**TWO)
           EMM=ENN
           GAMMA=STATEV(1)
           D=STATEV(2)
           VI_DIL=STATEV(3)
           MU=STATEV(4)
           DIL=STATEV(5)

C -----------------------------------------------------------
C # CALCULATING MODE-MIXITY PARAMETER BETA_n+1, FORMULA (7) #
C -----------------------------------------------------------
```

```
            IF (VINM.EQ.ZERO) THEN
              BETA=ONE
            ELSE IF (VSHN.EQ.ZERO) THEN
              BETA=ZERO
            ELSE
              BETA=VSHN/(VSHN+VINM)
            END IF

C -------------------------------------------------------
C # CALCULATING V0_n+1 AND VU_n+1 FORMULAS (13) AND (14) #
C -------------------------------------------------------

            V0=VI0*VSH0*SQRT((ONE+(TWO*(BETA**TWO))-(TWO*BETA))/
     &        (((BETA*VI0)**TWO)+((ONE-BETA)*VSH0)**TWO))
            VU=(TWO*(ONE+(TWO*(BETA**TWO))-(TWO*BETA)))/
     &        (EMM*V0)*((((ONE-BETA)**TWO)/GI)+((BETA**TWO)/GSH))**(-ONE)

C -----------------------------------------------
C # CALCULATING F_n+1 ACCORDING TO FORMULA (16)  #
C -----------------------------------------------

            IF ((ALFA.EQ.ZERO) .OR. ((VU-V0).EQ.ZERO)) THEN
                F=ZERO
            ELSE
                F=(VU*(ALFA-V0))/(ALFA*(VU-V0))
            END IF

C ---------------------------------------------------------------
C # CALCULATING DI_n+1 (DAMAGE INCREMENT) ACCORDING TO FORMULA (15) #
C ---------------------------------------------------------------

            IF (ALFA.LE.GAMMA) THEN
              DI=ZERO
            ELSE
              DI=(F-D)*DTIME/(ETA+DTIME)
            END IF

C ---------------------------------------------------------------------------------------------
    ---------
C # CALCULATING NEW DAMAGE VARIABLE D_n+1 ACCORDING TO FORMULA (17) AND UPDATING D_n TO
    D_n+1 (DN) #
C ---------------------------------------------------------------------------------------------
    ---------

            IF ((D+DI).LE.ZERO) THEN
              DN=ZERO
            ELSE
              DN=MIN(D+DI,ONE-EPSILON)
            END IF

            STATEV(2)=DN
C -----------------------------------------------
C # UPDATING GAMMA_n+1 ACCORING TO FORMULA(19) #
C -----------------------------------------------

            GAMMAN=(V0*VU)/(VU-((VU-V0)*DN))
            STATEV(1)=GAMMAN
C -------------------------------------------------------
C # CALCULATING NEW STRESSES ACCORDING TO FORMULA (18) #
C -------------------------------------------------------
            IF (GAMMAN .GT. V0) THEN
               MU=MUMAX*(ONE-(ONE-(GAMMAN-V0)/(VU-V0))**POW)
            ELSE
               MU = 0.0D0
            END IF
C
C           SOFTENING UNTIL THE VALUE MUFINAL IS REACHED.
C           NOTE THAT THE INPUT VALUE OF VSHSOFT NEEDS TO BE EQUAL OR LARGER THAN THE
C           INPUT VALUE OF VU
C
            IF (ABS(VSHN) .GT. VSHSOFT) THEN
               MU=MUMAX+(MUFINAL-MUMAX)*(1.0D0-EXP(-1.0D0*RATE*
     &                                          (ABS(VSHN)-VSHSOFT)))
            END IF
C
C
```

```
      DIL=FACT*MU
      IF (ABS(VSHN) .GT. VSHSOFT) THEN
         DIL=FACT*MU*EXP(-1.0D0*RATE*(ABS(VSHN)-VSHSOFT))
      END IF
C
      VIN_DIL = VI_DIL + DIL*ABS(DVSH)
      STATEV(3) = VIN_DIL
      STATEV(4) = MU
      STATEV(5) = DIL
C
      VINMN_DIL=(-(VIN-VIN_DIL)+ABS(-(VIN-VIN_DIL)))/TWO
c
      TIN =(ONE-DN)*EMM*(VIN-VIN_DIL)-(DN*EMM*VINMN_DIL)
c
      STRESS(1)=TIN
c
      IF (( (VI-VI_DIL) .LT. ZERO) .AND.
     &              (ABS(VSH) .GT. MU*ABS(VI-VI_DIL))) THEN
          STRESS(2)=(ONE-DN)*EMM*VSHN+MU*ABS(EMM*(VI-VI_DIL))
     &     *(DVSH/(SQRT(DVSH**TWO+EPSV**TWO)))
      ELSE
          STRESS(2)=(ONE-DN)*EMM*VSHN
      END IF

    RETURN
    END
```

PART II:
LITERATURE SURVEY

LITERATURE SURVEY

OVERLAP SPLICES OF REBARS IN CONCRETE STRUCTURES

14 September 2015
Sven van den Bulck
0725345

Eindhoven University of Technology
Architecture Building and Planning
Unit Structural Design

Colophon

Subject

Preperation for master graduation project
Literature survey
7P545

Authors

S. van den Bulck
s.v.d.bulck@student.tue.nl
0725345

Program

Architecture, building and planning
Unit Structural Design

Eindhoven University of Technology
Den Dolech 2
5600 MB Eindoven, Netherlands

Supervisors

Prof. Dr. Ir. A.S.J. (Akke) Suiker
Applied Mechanics and Design

Prof. Dr. Ir. T.A.M. (Theo) Salet
Material related Structural Design
- Concrete Structures

Prof. Dr. Ir. S.N.M. (Simon) Wijte
Sustainment of Concrete Structures

Ir. G.W. (Gijs) Schalkwijk
B-invented

Date

Eindhoven, 14 September 2015

Abstract

Since the introduction of the Eurocode 2 concrete structures (NEN-EN 1992-1-1), that replaces TGB concrete structures (NEN 6720), there are changes regarding the design rules. In particular, the calculation method concerning anchorage length and lap splice. The design rules in NEN 6720 art. 9.6 are very straightforward; this is in contrast to NEN-EN 1992-1-1 art. 8.4/ 8.7. However, more important are the results obtained from these formulas. Many construction companies considered significant difference between both outcomes. The length for anchorage or lap splice prescribed by NEN 6720 is shorter than Eurocode 2. Suddenly, since the introduction, the amount of steel in a concrete section is increased. In order to assess the differences, the origin of several standards and the (mechanical) behaviour of bond for a steel- concrete interface should be investigated in this study.

Table of contents

I. Introduction 5
II. Anchorage (development)- and overlap length of rebars in concrete 6
1. Analytical 6
1.1. Bar- concrete interaction 6
1.2. Bond mechanics for macroscopically uncracked concrete 9
1.3. Bond mechanics for transversely- cracked concrete 12
1.5. Splitting of concrete cover 15
1.6. Lap vs Anchorage length 20
1.7. Lap splices in bending 20
2. Experiments 21
2.1. Experimental setups 21
2.2. Experimental research 23
3. Numerical 25
3.1. Layer model 25
3.2. Interaction between surfaces 26
3.3. Damage model 26
3.4. Detailed model 27
III. Backgrounds to Standards 28
4. NEN 6720: article 9.6 28
4.1. CUR 23 28
4.2. CUR 94-13 30
5. NEN- EN 1992-1-1: article 8.4/8.7 32
5.1. Model code 1990 33
5.2. Model code 2010 33
6. DIN 1045-1: article 12,5/12.6 36
7. BS 8110: article 3.12.8 37
8. ACI 318: article 12.2 and 12.15 38
8.1. ACI committee report 408R 38
9. Comparison 41
9.1. Parameters of the databases 41
9.2. Results of the standards 42
IV. Conclusion 45
References 46

I. Introduction

Steel-to-concrete bond is an essential aspect in reinforced concrete structures. This interface allows longitudinal forces to be transferred from the reinforcement to the surrounding concrete and vice versa. Considerable researches were performed on the interaction between both materials to get a better understanding of the behaviour. An additional difficulty for reinforced concrete is lap splices of rebars. Due to the limited dimensions and shapes of reinforcement, lap splices are necessary in concrete sections. However, the minimum lap splice to prevent failure in the Ultimate Limit State for certain structural elements is still unclear from mechanical point of view. In the past, experimental, analytical and numerical research was performed to investigate the behaviour of lap splices.

Based on the experimental research, standards prescribe simple calculation methods to design structural elements. The origin of several standards is often indistinct. Investigation of the background should give a better understanding of the formation. Furthermore, it is interesting to compare how standards are related to each other and in particular to experimental research. The main question enclosed; are the standards an accurate reflection of the actual situation with due consideration of safety?

II. Anchorage (development)- and overlap length of rebars in concrete

1. Analytical

1.1. Bar- concrete interaction

The interaction between steel and concrete is of importance in order to investigate the behaviour of lap splices in a concrete section. The local bond- slip law for rebar pull-out can be described by Tassios (1979), the derived bond stress – slip relationships are revealed in figure 1.1.

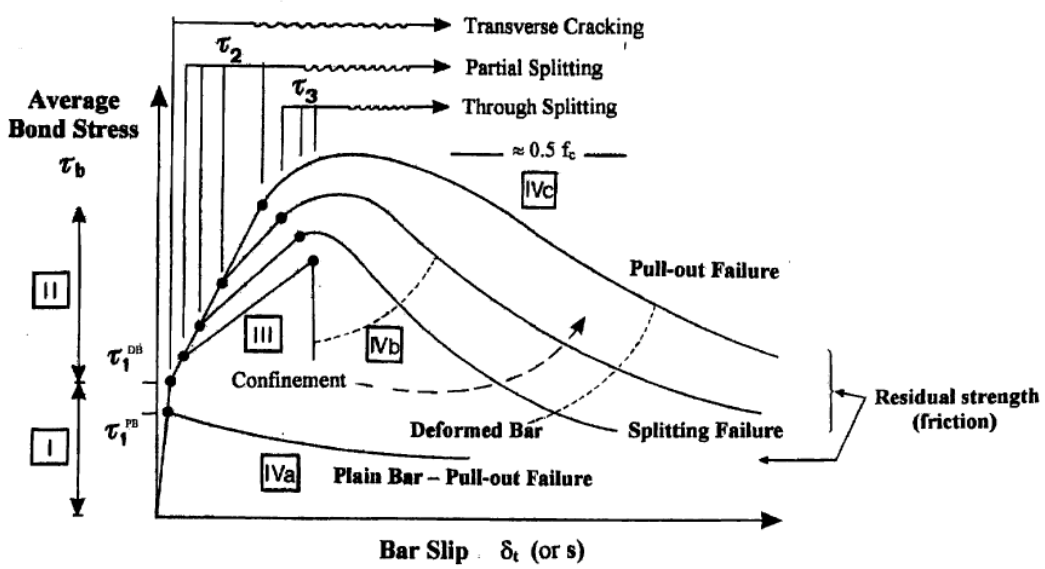

Figure 1.1: Local bond- slip relationship according to Tassios (1979). Where the bond stress is the maximum steel force divided by circumference times the embedded length of the rebar and the slip is the displacement of the loaded or unloaded end of the rebar with respect to the concrete specimen.

The interaction of rebar and concrete during pull-out can be subdivided into four stages.

Stage I: In this stage, the relationship between bond stress and slip is linear. The strain of concrete and steel is equal (Bruggeling, 1980), consequently displacement is caused by elastic strain of concrete and steel. The bond of the interaction is caused by chemical adhesion (Fib bulletin 10, 2000). This chemical adhesion is the only bond stress in case of a plain rebar (stage IVa). The displacement in this stage is the elastic deformation of concrete (shear deformation) and elongation of the steel rebar; this declares the high stiffness of bonding in this stage.

Stage II: If the bond stress passes τ_1^{pb}, the chemical adhesion is broken. In case of a deformed bar, the maximum bond stress is not reached due to the presence of the lugs. These lugs induce large bearing stresses into the concrete section. These compressive stresses of the lugs cause a tension force in the concrete specimen right behind the lugs parallel to the rebar, which could cause transverse cracking.

Stage III: For higher bond stresses, the longitudinal cracks spread radially due to the wedging action of the lugs (figure 1.2a). These lugs induce compressive stresses in longitudinal and transverse direction due to the angle α of the lugs (figure 1.2b). Perpendicular to these transverse stresses, tensile stresses occur in the surrounding concrete, which are called hoop stresses according to Tepfers (1973). These stresses (σ_c in figure 1.3b) could cause splitting failure (stage IVb). This failure behaviour is highly dependent on the transverse confinement. For both splitting and pull-out failure, interlocking of concrete and the deformed bar is essential to achieve a higher ultimate bond- and residual stress.

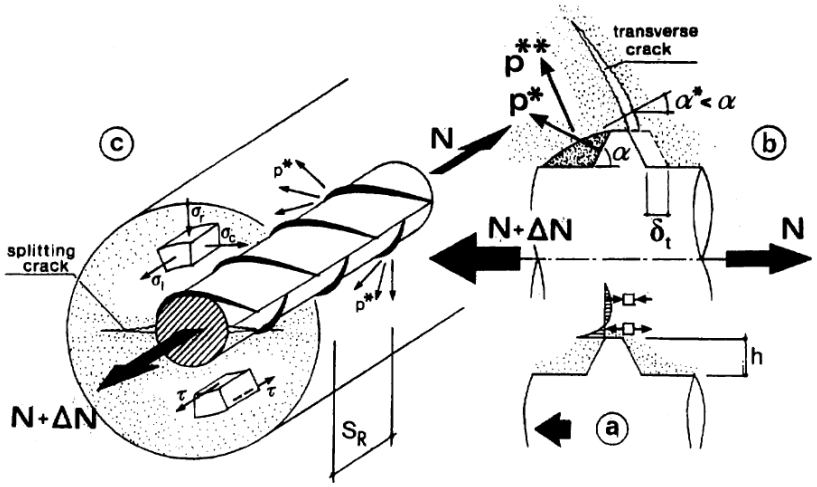

Figure 1.2: Stresses in the surrounding concrete during; a) typical peak stresses; b) wedging action of the bar; c) main parameters.

Stage IVa: As already discussed; the maximum bond strength of plain rebars is achieved by chemical adhesion of concrete and steel. Hereafter, the rebar is debonded and only friction of the steel and concrete interface is able to transfer forces. Friction is affected by the transverse pressure, which is induced by concrete shrinkage. The concrete shrinkage and roughness of the bar have positive effect for the shearing resistance. However, the radial compressive stresses are reduced due to damage of the sliding plane during pull-out. Herewith the bond stresses are reduced too resulting in softening for larger displacements. (Fib bulletin 10, 2000).

Stage IVb: In case of insignificant confinement through transverse reinforcement and concrete cover, the splitting cracks cause abrupt failure. The residual strength after passing the ultimate bond stress is relatively low. Conversely, increasing the values of these parameters, the residual strength can be enhanced. After splitting of the cover, the residual strength is provided by confinement (cover, stirrups and transverse pressure). The magnitude of the interlocking effect of the lugs with the damaged concrete is governing for the frictional resistance.

Stage IVc: At a certain point, where the transverse reinforcement is heavy and the concrete cover is large, no splitting failure occurs. Although, the hoop stresses may cause splitting cracks; the stirrups, transverse pressure and concrete cover are able to capture the tensile stresses to prevent splitting through the entire cover. The deformed rebar remains confined, failure can be carried out by pull-out.

Several modes for pull-out failure can occur. The shape of the lugs and the length of anchorage defines the mechanism of failure (figure 1.3). If the angle (α) is large, pull-out is provided by shear planes. The longitudinal bearing stresses are significant and the concrete is not able to resist the stresses and fails in shear. After shear failure, the residual strength is provided by the friction of the damaged concrete- concrete interface. This type of failure is captured by Ertzibengoa et al (2012), see figure 1.4. Another failure mode is splitting induced pull-out accompanied by crushing and/or shearing- off in the concrete below the lugs. The third possible mode is splitting accompanied by slip on the lug faces. This could occur in the case of small angle (α), the induced longitudinal stresses are relatively small compared to the transverse compressive stresses (and subsequently the tangential tensile stresses). As a result, splitting failure is governing accompanied with slip of the lug faces Cairns, 1992). Finally, in case of relative short anchorages, failure carried out by cone failure. However, this mode is disregarded in the sequel of the report due to the fact that minimum prescribed values of the anchorage length prevent this mode of failure. Only large anchorages or lap splices will be considered.

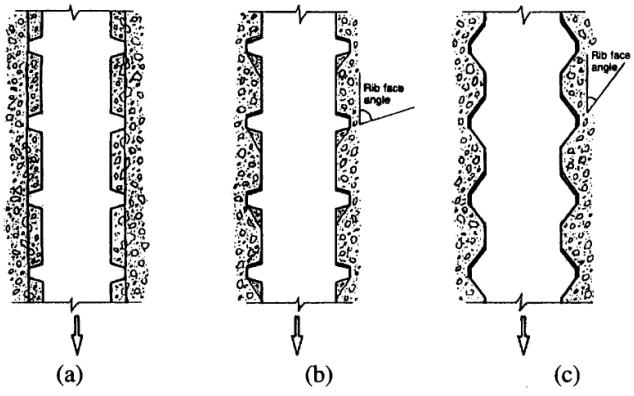

Figure 1.3: Modes of bond failure.

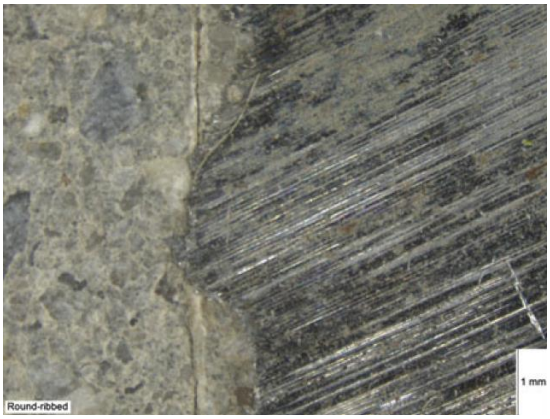

Figure 1.4: Shearing- off failure, mode (a).

In addition to the modes of bond failure for pull-out, a number of modes for splitting failure are possible. Depending on the structural setting cracks will occur at a certain location, figure 1.5 reveals the possible modes of failure. As already discussed, the failure mode is highly dependent on the confinement due to transverse reinforcement and cover thickness. The turning point of failure according to Fib Bulletin 10 (2000) is given in figure 1.5 (d), after passing this point pull-out failure is likely to occur as described in figure 1.3.

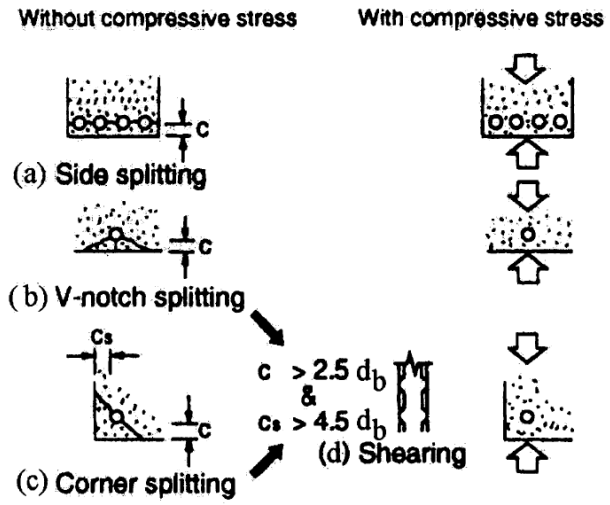

Figure 1.5: Modes of splitting failure.

Another aspect that has significant influence on the failure mode is the transverse pressure. Many design rules for bond anchorage disregard this pressure for matters of simplicity. More information of the calculation methods of the standards can be found in part II of the literature survey. However, the transverse pressure could have positive influence on the ultimate failure strength. Hoop stresses (and radial cracks) will be reduced or eliminated resulting in a confined rebar.

1.2. Bond mechanics for macroscopically uncracked concrete

Analytical research was performed to describe the stresses and relative displacement for a rebar embedded in concrete. For the macroscopically uncracked stage, the concrete can be modelled by considering a continuum. This could be the case for heavy confining transverse reinforcement and relatively large cover in proportion to the rebar diameter. Pull-out is caused by shearing- off of the concrete between the lugs and radial cracks are absent.

The differential equations for a single bar embedded in concrete are summarized below (Fib Bulletin 10, 2000). However, the bar is assumed as axial symmetric and the radial dimension is neglected owing the fact no splitting cracks are considered.

Reinforcing bar equilibrium: $$A_s \frac{d\sigma_s}{dx} = -\sum_0 \tau(s) \quad (1)$$

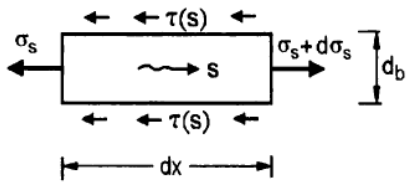

Figure 1.6: Stresses acting on a small length (dx) of a rebar.

Where A_s is the bar section, $\sum_0$ is rebar circumference, σ_s is steel stress and $\tau(s)$ is bond stress as a function of relative slip s. The relative slip is the displacement of the rebar with respect to concrete.

Strain- displacement relation: $$\varepsilon_s - \varepsilon_c = -\frac{ds}{dx} = -s' \quad (2)$$

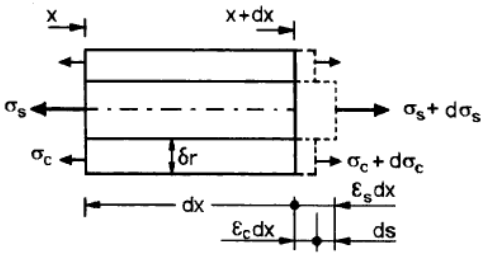

Figure 1.7: stresses and strains in the rebar and concrete.

Where ε_s is steel strain, ε_c is concrete strain.

Reinforced- concrete equilibrium: $$A_c \frac{d\sigma_{cm}}{dx} = -A_s \frac{d\sigma_s}{dx} \quad (3)$$

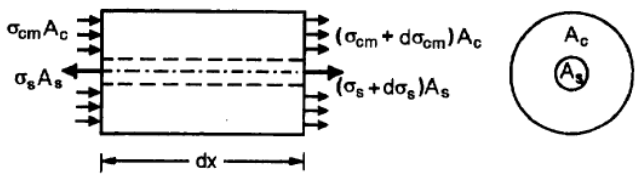

Figure 1.8: Forces acting on a reinforced- concrete element.

Where A_c is concrete cross- section and σ_{cm} is mean stress on concrete section A_c.

Stress- strain relationship for steel and concrete:

$$\sigma_s = \hat{\sigma}_s(\varepsilon_s) \qquad \sigma_c = \hat{\sigma}_c(\varepsilon_c) \qquad \text{(4 and 5)}$$

The local bond stress- slip relationship:

$$\tau = \hat{\tau}[s(x)] \qquad (6)$$

Experimental research has proven that equation (6) is non- linear. Consequently, several studies have proposed empirical expressions to describe the bonds stress- slip relationship. The expression proposed by Ciampi, Eligehausen, Bertero and Popov (1981) is adopted by Model Code 1990 as standard for the development of design rules:

$$\tau_{b0} = \tau_{b\max}\left(s/s_1\right)^{\alpha} \qquad for\ 0 \le s \le s_1 \qquad (7)$$

Where α represents the rate parameter for nonlinear behaviour in the first stage. Followed by a plateau $\tau = \tau_1 = \tau_{b\max}$ for $s_1 \le s \le s_2$, for $s \ge s_2$ the bond stress decreases linearly to the ultimate frictional bond resistance τ_3 at point s_3. It is assumed that the value s_3 is equal to the clear distance between the lugs of the deformed bars.

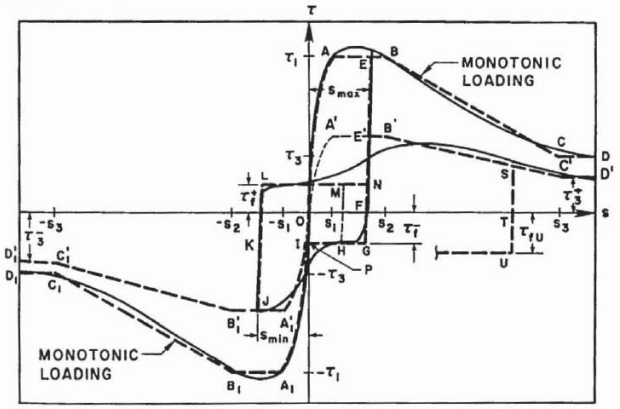

Figure 1.9: Proposed analytical model for local bond Stress- slip relationship (Ciampi et al.,1981).

The bond stress at the interface from Ciampi et al. (1981) is assumed uniform distributed over the length of the bar. In practice, the stresses and strains in rebars and the surrounding concrete are variable over the anchorage length x. Although, the interface steel- concrete can be considered as nonlinear. Several studies performed an analytical solution to describe the displacement of the rebar during pull-out. For a nonlinear interface, equation (3) no longer suffices, an additional coefficient is necessary. According to Edwards and Picard (1972) the factor can be defined as:

$$\psi = \frac{\int_{Ac} \sigma(x,r)dA_c}{A_c\sigma_c} \qquad (8)$$

Assuming ψ is dependent of x, equation (3) can be rewritten to:

$$\psi \cdot A_c \frac{d\sigma_{cm}}{dx} = -A_s \frac{d\sigma_s}{dx} \qquad (9)$$

Hereafter, the derivative of (2), taking into account (4,5 and 9) is (Russo et al, 1990):

$$\frac{d^2 s}{dx^2} - \chi \hat{\tau}[s(x)] = 0 \qquad (10)$$

With: $\chi = (1+\xi)\frac{\sum_0}{A_s E_s}$ and $\xi = \frac{\frac{E_s}{E_c} \cdot \frac{A_s}{A_c}}{\psi}$ (11 and 12)

Hence, the following equation (7) has been utilized, and the first integral of equation (10) is:

$$\frac{ds}{dx} = \pm\sqrt{2(\gamma \cdot s^{1+\alpha} + C)} \qquad (13)$$

With $\gamma = \chi \cdot \frac{\tau_1}{(1+\alpha)\cdot s_1^{\alpha}}$ (14)

And C is the integration constant. Then integration is performed by Russo et al (1990) with an implicit solution for $0 < s \le \left|\frac{C}{\gamma}\right|^{1/(1+\alpha)}$:

$$x = B - \frac{1}{\sqrt{2C}} \sum_{k=0}^{\infty} \left(k^{-0,5}\right) \cdot \left(\frac{\gamma}{C}\right)^k \frac{s^{1+k(1+\alpha)}}{1+k(1+\alpha)} \qquad (15)$$

If the integration constant C is zero, the solution of differential equation (13) can be written in a closed form:

$$s = \left[\pm\frac{1-\alpha}{2} \cdot \sqrt{2\gamma} \cdot (x-B)\right]^{\frac{2}{1-\alpha}} \qquad (16)$$

The equation (15) gives slip and strain distributions for the concrete- steel interaction in tension. The distribution could have the following form (figure 1.10):

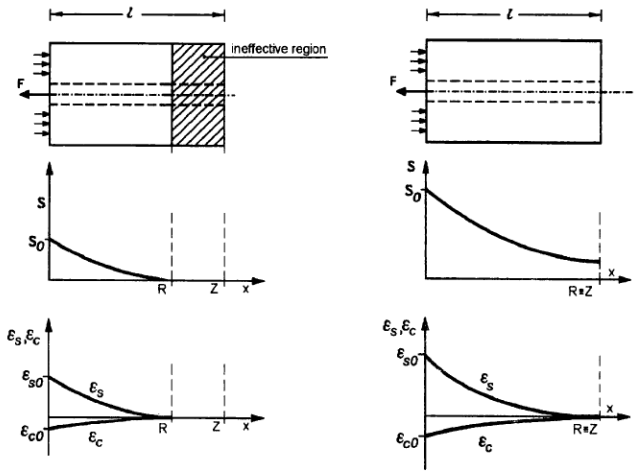

Figure 1.10: Typical slip and strain distribution for long- member (left) and short member (right) behaviour in tension. (Russo et al, 1990).

Russo et al. extended the previous research with the addition of an inelastic steel stress. Therefore, only minor changes have to be applied to the derived expression (15). The young's modulus should be adjusted for steel in the inelastic stage. The E_s should be replaced for E_{sh}, the hardening modulus after passing the ultimate steel stress.

1.3. Bond mechanics for transversely- cracked concrete

The concrete section in paragraph 1.2 is modelled as an elastic material. However, due to the tension force applied on the rebar, the stresses in the concrete could exceed the ultimate tensile stress. The schematization of figure 1.8 is not valid for this situation, because concrete is usually loaded in tension instead of compression. In order to model the cracks in concrete, the schematization is adjusted to figure 1.11 (symmetric structure).

The analytical derivation of paragraph 1.2 also applies to the model of cracked concrete. Only cracks have to be taken into account in the analytical solution. Russo and Romano (1992) extended previous research for transversely cracked concrete. Slip and strain distribution according to the analytical solution is revealed in figure 1.11. In comparison with figure 1.9, both strains of concrete and steel have in the positive sign. The behaviour of concrete in tension is different from its behaviour in compression, resulting in deviating stresses and strains.

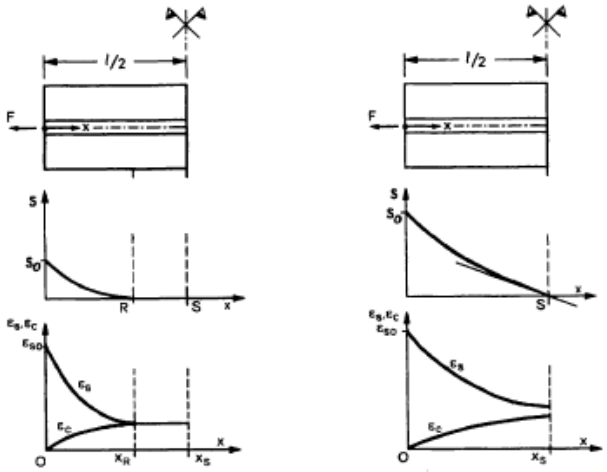

Figure 1.11: Typical slip and strain distribution for long- member (left) and short member (right) behaviour in tension. (Russo and Romano, 1992).

The solution for long members is provided by (16) in paragraph 1.2 with a minus sign. The slip of the loaded end, s_0 is given by (Russo and Romano, 1992).

$$s_0 = \left(\frac{\varepsilon_{s0}^2}{2\gamma} \right)^{\frac{1}{1+\alpha}} \tag{1}$$

And the abscissa of the point with s = 0 and ds/dx =0 is:

$$x_R = \frac{2}{1-\alpha} \left[\varepsilon_{s0} \left(\frac{1}{2\gamma} \right)^{\frac{1}{1-\alpha}} \right]^{\frac{1-\alpha}{1+\alpha}} \tag{2}$$

This analytical solution for the transversely cracked concrete member subjected to tension is compared to experimental research of Dörr (1978). As revealed in figure 1.12, the bond stress – slip relationship is located close to the results of the experimental tension test.

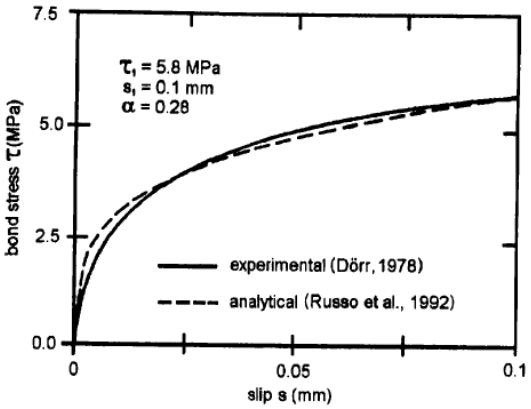

Figure 1.12: Comparison between analytical and experimental bond stress- slip relationship (Russo and Romano, 1992).

1.4. Bond mechanics of lap splices

The analytical solutions performed by Russo et all (1990) and Russo, Romano (1991, 1992) and other research are based on one anchorage length of rebar. Eligehausen (1979) performed research to lap splices in Heft 301. Equilibrium can be considered with the following equations and figure 1.13.

$$\tau_1(x) \cdot u \cdot dx = d\sigma_{e1}(x) \cdot F_e \tag{1}$$

$$\frac{d\sigma_{e1}(x)}{dx} = \frac{4}{d_e} \cdot \tau_1(x) \tag{2}$$

$$\frac{d\sigma_{e2}(x)}{dx} = \frac{4}{d_e} \cdot \tau_2(x) \tag{3}$$

$$d\sigma_b(x) = -\frac{F_e}{F_b}(d\sigma_{e1}(x) + d\sigma_{e2}(x)) \tag{4}$$

$$\frac{d\sigma_b(x)}{dx} = -\mu \cdot \frac{4}{d_e}(\tau_1(x) + \tau_2(x)) \tag{5}$$

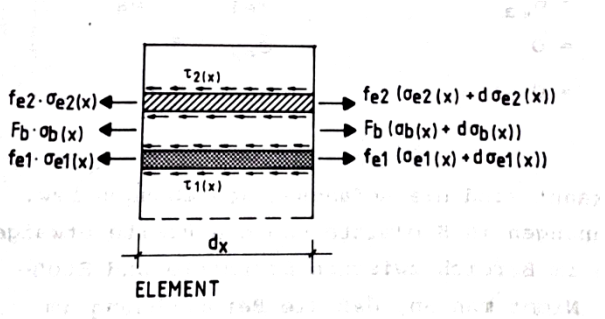

Figure 1.13: Stresses and forces in lap splices.

The bond strength τ(x) is dependent on the slip s(x):

$$\frac{\tau(x)}{\beta_w} = f(s(x)) = b_0 + b_1 s(x)^{b2} \tag{6}$$

The slip can be derived from the shifts between steel and concrete by differentiating:

$$s(x) = s_0 + \int_0^x \varepsilon_e dx \cdot \int_0^x \varepsilon_b dx \tag{7}$$

Hereafter, differentiating with respect to x gives:

$$\frac{ds_1}{dx} = \frac{\sigma_{e1}}{E_e} - \frac{\sigma_b}{E_b} \tag{8}$$

$$\frac{ds_2}{dx} = \frac{\sigma_{e2}}{E_e} - \frac{\sigma_b}{E_b} \tag{9}$$

Consequently, both equations (8) and (9) can be differentiated to x, taken into consideration equation (2) to (5) and $n=E_e/E_b$.

$$\frac{d^2 s_1(x)}{dx^2} = \frac{4}{d_e} \cdot \frac{1}{E_e} \left((1 + n \cdot \mu) \tau_1(x) + n \cdot \mu \cdot \tau_2(x) \right) \tag{10}$$

$$\frac{d^2 s_1(x)}{dx^2} = \frac{4}{d_e} \cdot \frac{1}{E_e} \left(n \cdot \mu \cdot \tau_1(x) + (1 + n \cdot \mu) \cdot \tau_2(x) \right) \tag{11}$$

Finally, τ_1 and τ_2 can be replaced by respectively $f(s_1(x))$ and $f(s_2(x))$

The principle of stresses and slip in a lap splice is revealed in figure 1.14. Dependent on the length of the lap splice, transverse cracks occur and affect the bond stress, slip and steel stress.

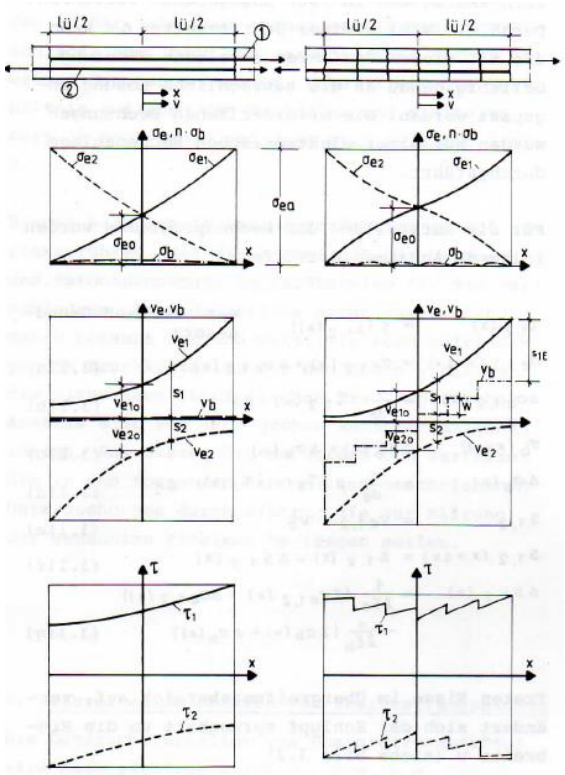

Figure 1.14: Distribution of stresses, displacement and bond stress in a lap splice (Eligehausen, 1979).

Experimental research by Goto (1971) provides the crack distribution of a long specimen. This cracking pattern induces an altered bond stress distribution as described by Eligehausen (1979).

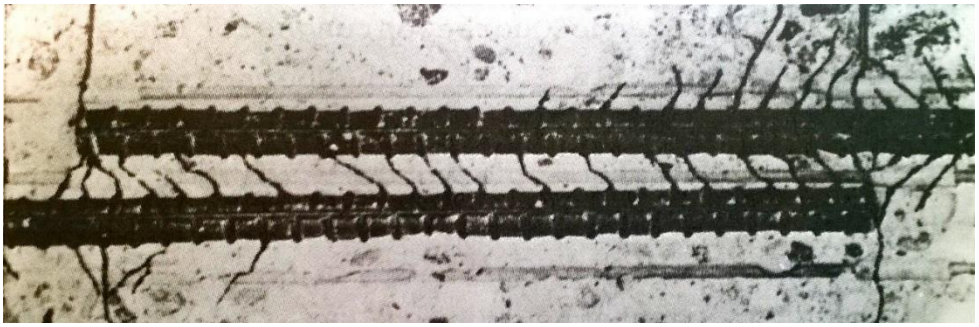

Figure 1.15: Transverse cracks in a noncontact lap splice (Goto, 1971).

1.5. Splitting of concrete cover

Due to the wedging action of the lugs, radial compressive stresses are induced in the concrete cover. Perpendicular to these stresses tensile stresses are induced (σ of figure 1.16) that could cause cracking in the zone cr. These cracks are highly dependent on the lug angles. The wedging action of large lug angles produces a relatively high stress perpendicular to the bar and a lower radial stress. Subsequently, σ is relatively low, for small lug angles it is conversely.

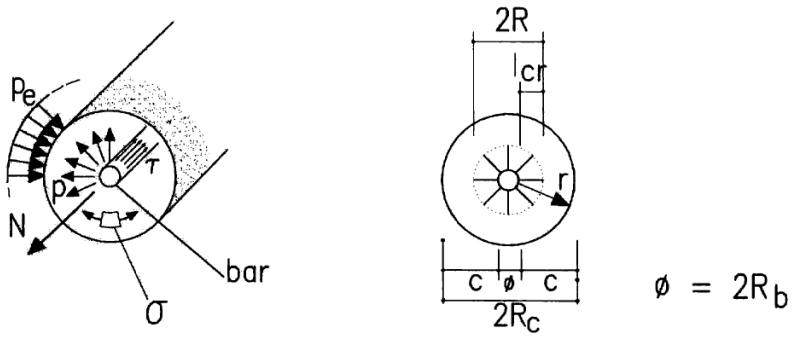

Figure 1.16: Hydraulic pressure of pull out of rebar.

An analytical study to the tensile stresses (hoop stresses) is performed by Tepfers (1973). With the consideration of the failure modes of figure 1.5, stresses around the rebar can be derived in the uncracked and cracked stage. Lug angles larger than 45 degrees are disregarded; the considered effect is produced by face angles of approximately 30 to 40 degrees.

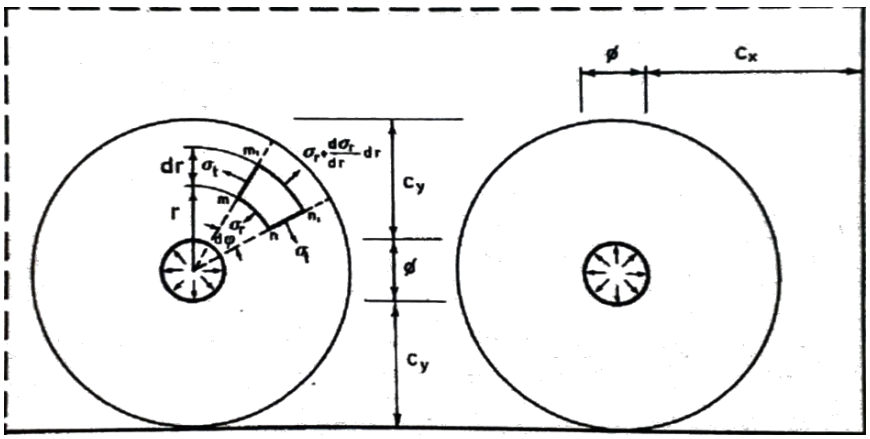

Figure 1.17: Section through a tension lap splice with the stress distribution around a rebar (Tepfers, 1973).

Based on figure 1.17 the following equilibrium equation can be set up:

$$\sigma_r \cdot rd \cdot \varphi + \sigma_t \cdot d\,rd \cdot \varphi - \left(\sigma_r + \frac{d\sigma_r \cdot dr}{dr} \right)(r + dr)d\varphi = 0 \qquad (1)$$

Neglecting small quantities of higher order gives:

$$\sigma_t - \sigma_r - r\frac{d\sigma_r}{dr} = 0 \qquad (2)$$

Hereafter, two unknowns remain, a second equation is necessary to obtain parameters around the lap splices. By considering the deformation of the cylinder two expressions can be formed:

$$\sigma_t = \frac{E}{1-v^2}\left(\frac{du}{dr} + v\frac{u}{r}\right) \quad \text{and} \quad \sigma_t = \frac{E}{1-v^2}\left(\frac{u}{r} + v\frac{du}{dr}\right) \qquad (3 \text{ and } 4)$$

"The deformation of the cylinder is symmetrical with respect to the axis and consists of a radial displacement of all points in the wall of the cylinder. This displacement is constant in the circumferential direction but varies along the radius, i.e. it is a function of the radius only. If u denotes the radial displacement of a cylindrical surface of radius r the expressions for the stresses in terms of the strains are expressions (3 and 4)" (Tepfers, 1973)

Then substituting both equations in (2) for determining the displacement u:

$$\frac{d^2u}{dr^2} + \frac{1}{r}\frac{du}{dr} - \frac{u}{r^2} = 0 \qquad (5)$$

The necessary constant in the expression can be determined since the normal stresses are known at the inner and outer cylinder:

$$\sigma_r = \frac{(\phi/2)^2 \tau \tan\alpha}{(c_y + \phi/2)^2 - (\phi/2)^2} \cdot \left(1 - \frac{(c_y + \phi/2)^2}{r^2}\right) \qquad (6)$$

$$\sigma_t = \frac{(\phi/2)^2 \tau \tan\alpha}{(c_y + \phi/2)^2 - (\phi/2)^2} \cdot \left(1 + \frac{(c_y + \phi/2)^2}{r^2}\right) \qquad (7)$$

Where α is the lug angle face; furthermore, σ_r is always a compressive stress and σ_t is always a tensile stress. The tensile stress is at the maximum value at the inner surface of the cylinder:

$$\frac{\sigma_{t(\max)}}{\tau \tan\alpha} = \frac{(c_y + \phi/2)^2 + (\phi/2)^2}{(c_y + \phi/2)^2 - (\phi/2)^2} \qquad (8)$$

This expression can be used to reveal the hoop stresses around a rebar (figure 1.17). The concrete cover is of influence to prevent splitting failure, the tensile stress decreases along the thickness of c_y. However, the concrete is assumed as linear elastic in this analysis.

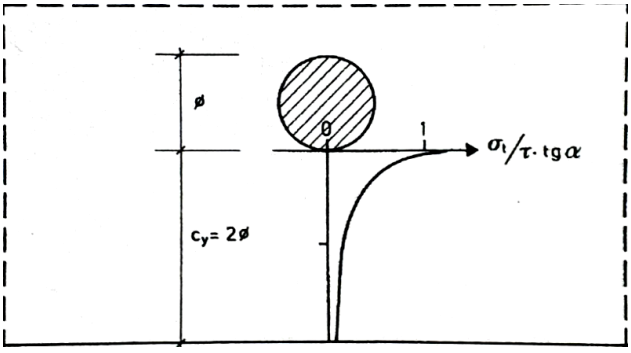

Figure 1.18: Variation of the tensile stress in the concrete cover (Tepfers, 1973).

The analytical solution for the tensile stresses around a pulled- out rebar is supported by numerical research performed by Eligehausen (1979). Three failure mechanisms are considered to obtain the stress distribution of the numerical analysis.

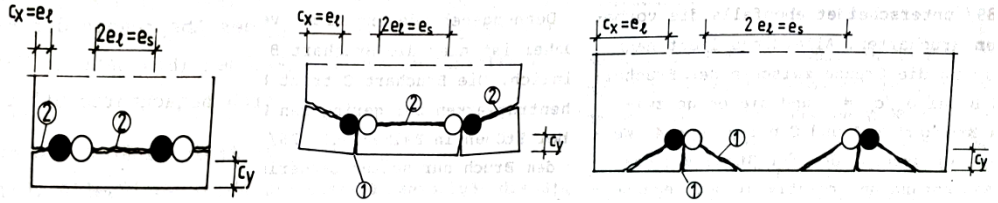

Figure 1.19: Possible mechanisms for splitting failure A,B,C (Eligehausen,1979).

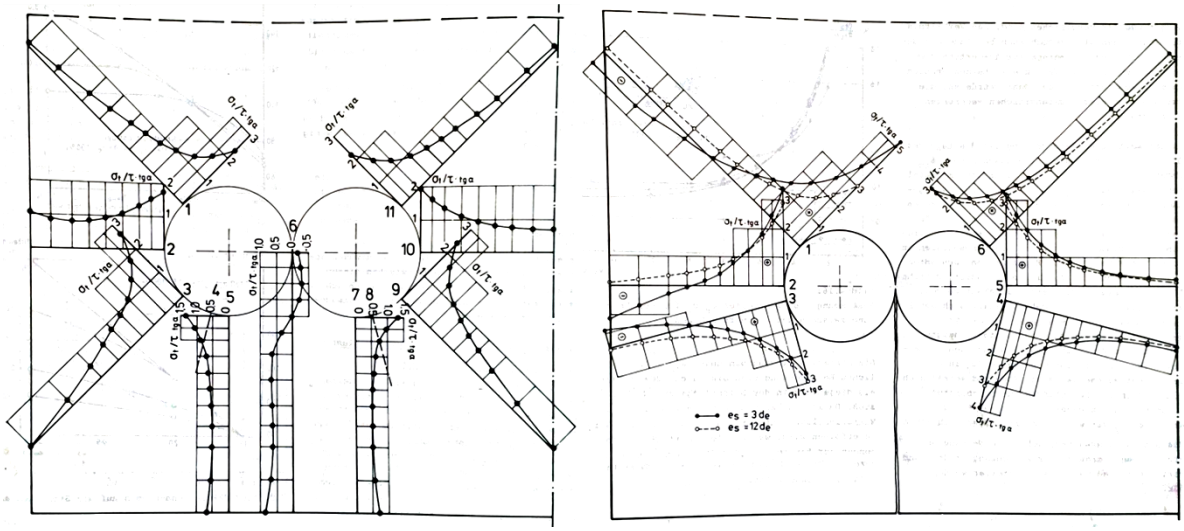

Figure 1.20: FEM analysis performed by Eligehausen (1979) for respectively A and B,C.

The values of the stresses cannot be compared due to variable specimen characteristics. However, the distribution is schematically equivalent to the analytical solution. Furthermore, the mode of failure depends on the boundary conditions and specimen characteristics (e.g. casting position, transverse pressure and reinforcement, cover thickness, concrete and steel strength). These have significant influence on the stress distribution.

The above discussed research of Tepfers (1973) is extended for partly cracked concrete. The tensile stresses (radial stresses) close to the rebar are significant, cracks immediately occur when loading a deformed rebar in tension. For splitting failure, the crack will penetrate through the cover. The minimum thickness of the cover c_y, at which the crack can no longer remain an internal one, can be derived analytically.

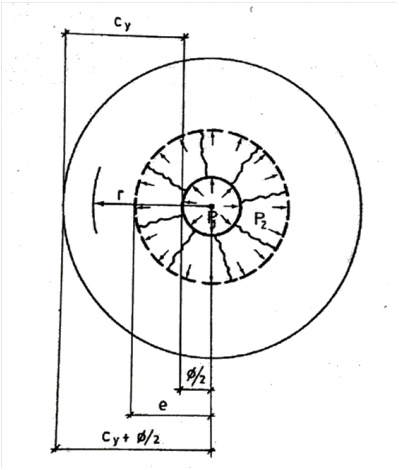

Figure 1.21: Confined rebar with internal radial and longitudinal cracks (Tepfers, 1973).

The radial stresses in figure 1.18 are provided by the wedging action of the lugs, since the chemical adhesion between concrete and steel is already broken. Subsequently, the pressure on a cracked ring should be reduced compared to an uncracked ring. This reduction is dependent on the depth of the internal cracks.

$$p_1 \cdot \pi \cdot \phi = p_2 \cdot \pi \cdot 2e \rightarrow \qquad p_2 = \frac{\phi}{2e} \cdot p_2 \qquad \rightarrow \qquad p_2 = \frac{\phi}{2e} \cdot \tau \tan\alpha \tag{9}$$

Hereafter, the circumferential stress distribution in the unckracked ring with an inner radius e can be written according to (10).

$$\sigma_t = \frac{e^2 (\phi/2e) \tau \tan\alpha}{(c_y + \phi/2)^2 - e^2} \cdot \left(1 + \frac{(c_y + \phi/2)^2}{r^2} \right) \tag{10}$$

And again the maximum stress at the inner surface of the uncracked part:

$$\frac{\sigma_{t(\max)}}{\tau \tan\alpha} = \frac{\phi}{2e} \cdot \frac{(c_y + \phi/2)^2 + e^2}{(c_y + \phi/2)^2 - e^2} \tag{11}$$

However, in this case e is the only unknown variable since the concrete is cracked ($\sigma_{t(\max)} = \sigma_{cu}$).

$$\frac{\tau \tan\alpha}{\sigma_{cu}} = \frac{2e}{\phi} \cdot \frac{(c_y + \phi/2)^2 - e^2}{(c_y + \phi/2)^2 + e^2} \tag{12}$$

This equation of the bond force capacity can be expressed in a graph as a function of the longitudinal crack penetration e in the concrete cover (figure 1.22). From the graph can be read the maximum bond force for a certain e, this e can be calculated. Therefore, equation (13) can be differentiated with respect to e.

$$\frac{d\left(\frac{\tau \tan\alpha}{\sigma_{cu}} \right)}{de} = \frac{2}{\phi\left((c_y + \phi/2)^2 + e^2 \right)} \cdot \left[\frac{(c_y + \phi/2)^2 - 3e^2 - 2e^2}{(c_y + \phi/2)^2 + e^2} \cdot (c_y + \phi/2)^2 + e^2 \right] \tag{13}$$

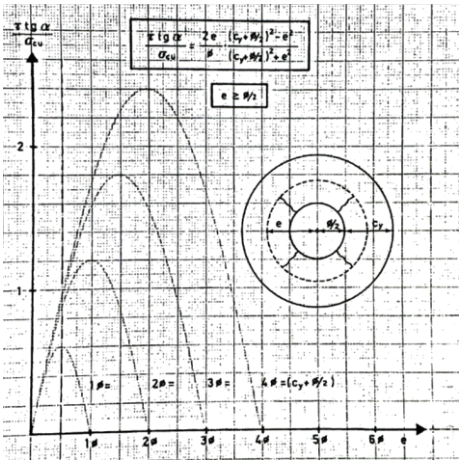

Figure 1.22: Bond force capacity as a function of the crack penetration e.

Putting the differential coefficient equal to zero:

$$e^4 + 4\left(c_y + \frac{\phi}{2}\right)^2 \cdot e^2 - \left(c_y + \frac{\phi}{2}\right)^4 = 0 \qquad (14)$$

Only obtain the real root e within the limits for which the bond force capacity of the concrete ring is a maximum.

$$e = 0{,}486\left(c_y + \frac{\phi}{2}\right) \qquad (16)$$

Assumed is the optimum crack depth: $e - \frac{\phi}{2} = 0{,}486\left(c_y + \frac{\phi}{2}\right) - \frac{\phi}{2} = 0{,}486c_y - 0{,}257\phi$

$$c_y = 0{,}529\phi \qquad (17)$$

This value is the minimum thickness, at which the crack is not able to remain an internal one, splitting failure is governing. Function (16) can be implemented in (11) to predict the tensile (hoop) stress in a certain structural element.

$$\sigma_{t(\max)} = \sigma_{cu} = \frac{1{,}664\phi \cdot \tau \tan\alpha}{\left(c_y + \frac{\phi}{2}\right)} \qquad (18)$$

Perhaps, more interesting is the required cover thickness to prevent splitting failure. Assume a bond stress of 5 N/mm^2, a rebar diameter 12 mm, lug angle of 45 degree and concrete class C20/25. The remaining unknown is the cover, which should be:

$$2{,}2 = \frac{1{,}664 \cdot 12 \cdot 5 \tan 45}{\left(c_y + 6\right)} \qquad \Rightarrow \qquad c_y = 39{,}4mm$$

Note: transverse reinforcement and pressure is not taken into account in this analytical expression. Therefore, this value is not valid in practical situations; specimen characteristics and boundary conditions have positive influence on crack penetration through the cover.

1.6. Lap vs Anchorage length

Most of the research was performed on the anchorage of rebars in concrete. However, are the results transferable to lap splices? With the aid of simple reasoning a first argument can be formed to make distinguish between both. Anchorages are mostly situated at the outside of a moment envelope and theoretically does not anchor any force. However, anchorages at supports may partly be within the moment envelope and may have to anchor considerable force. Furthermore, the support pressure and stirrups have positive influence for the confinement. Conversely, lap splices are situated within the moment envelop and anchor full bar force. The chosen splice length determines the bond stress gradient (Tepfers, 2006).

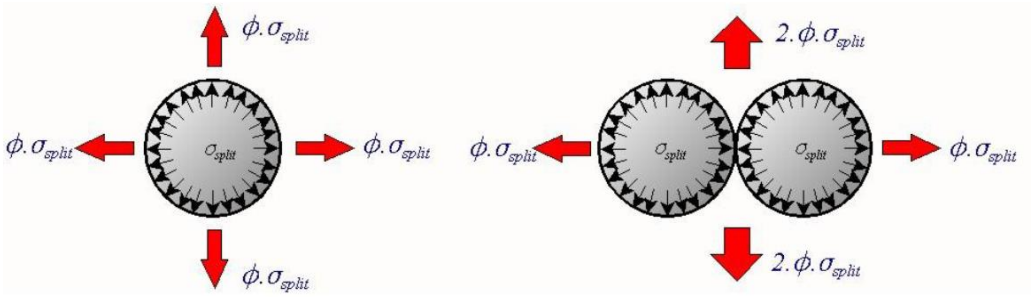

Figure 1.23: Hydraulic pressure for anchorage length and lap splices (Cairns, 2013).

Another argument to make distinction between both is derived from bond mechanics. The hydraulic pressure discussed in paragraph 1.5 affects the stress distribution around lap splices. Therefore, the bursting action of two loaded rebars is significantly higher than one rebar (figure 1.23). As a result, splitting failure is more likely to occur; consequently, the ultimate strength is lower.

1.7. Lap splices in bending

Hitherto, anchorage lengths and lap splices are loaded in tension. In practice, lap splices are applied in structural elements subjected to bending. If transverse reinforcement is applied, a lap splice loaded in tension (or compression) is a good approximation of the real situation. Hence, when the stirrups are absent, the failure mechanism is not comparable to a member loaded in tension. In addition to enhancing the confinement, stirrups have an additional function. The transverse reinforcement retains the longitudinal rebar to split the cover from the cross- section (figure 1.24). However, in practice this failure mechanism is not common.

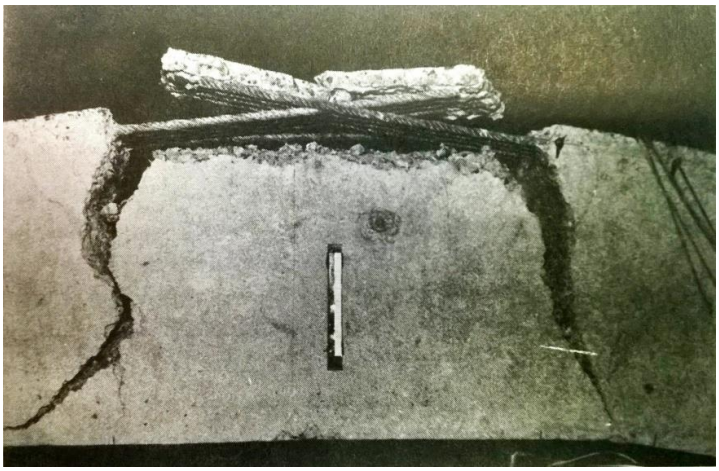

Figure 1.24: Failure mechanism for lap splices in bending when stirrups are absent (Eligehausen, 1979).

2. Experiments

2.1. Experimental setups

Many experimental researches were performed on the co-operation of deformed reinforcing bars and concrete. In general these methods can be subdivided as follows:

- Simple, less time consuming and relatively cheap tests; e.g. pull-out test on tubes or cylinders. However, the representation of reality is inadequate and difficult to extrapolate to beams or slabs. For instance, the transverse pressure should be taken into account since the influence provides a significant better result. For simple pull-out test, this is not taken into account.
- Test which represent the actual conditions are mostly more expensive and time consuming; e.g. four point bending tests. Large test setups and specimens are required to perform the experimental analysis.

The three most common experimental setups are pull-out test, four point bending and pull-out bending. As an example, experimental researches are highlighted to discuss the principle of these setups. First the simplest setup, the pull-out test, performed by among others Abrahms (1917). Other pull-out tests are based on the same principle as depicted in figure 2.1. A concrete block with a rebar is placed in the setup and measurement is placed at the loaded or/and unloaded end of the rebar. To ensure pull-out without imperfections a spherical bearing block is placed to balance the concrete block. Other equipment is available, for instance a suspended or hinged concrete block. The induction of moments due to imperfections is not permitted.

A drawback for this setup is the representation for a structural element. However, bond behaviour between steel and concrete can be investigated. In case of a lap splices, this setup is not adequate, the setup should be extended. A long concrete member with a lap splice is necessary to take transverse cracking into account. The concrete specimen of this setup is loaded in compression. Furthermore, lap splices are not axissymmetrically, as a result moment equilibrium is induced during testing.

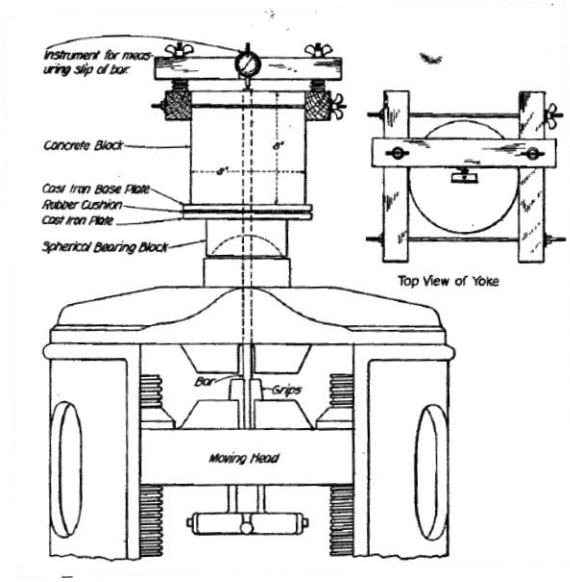

Figure 2.1: Pull-out test (Abrahms, 1917)

A more representive setup for lap splices is the four point bending test. The lap splices are subjected to a constant bending moment, the splice fails in splitting or pull-out failure depending on the boundary conditions and specimen characteristics For instance, Ragi Ali (2007) performed experimental

research to lap splices in the fibre reinforced concrete with the following setup (figure 2.2). Due to the large dimensions of the specimen (length of 4,2 m), these tests are time consuming and expensive. Inverse analysis makes it possible to construct a force- slip diagram for these experimental results.

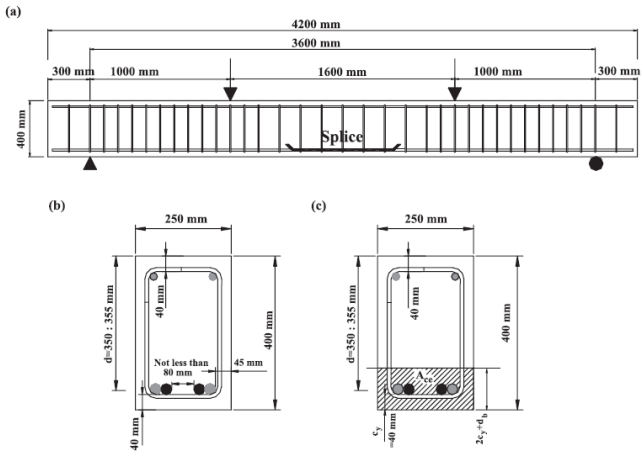

Figure 2.2: Four point bending test (Ragi Aly, 2007).

If stirrups are applied in the concrete section, pull-out failure is likely to occur. Transverse cracks due to the bending moment occur, radial cracks are absent in this loading situation. Further increasing of the mid- span deflection could result in radial cracking. The failure mode of figure 1.23 is impossible due to transverse reinforcement.

Figure 2.3: Experimental setup by Abdel-Kareen et al (2013) comparable to Ragi Aly (2007).

A combination of both previous setups is also possible; this is a pull-out bending setup as revealed in figure 2.4 (Pepe et al, 2012). In this case, no inverse analysis is required to provide a force- slip relationship. The mid- span opening allows placement of measurement for the loaded end slip. Another positive aspect is the transverse pressure and reinforcement, which is taken into account. The forces and stresses are more comparable to a reinforced structural element.

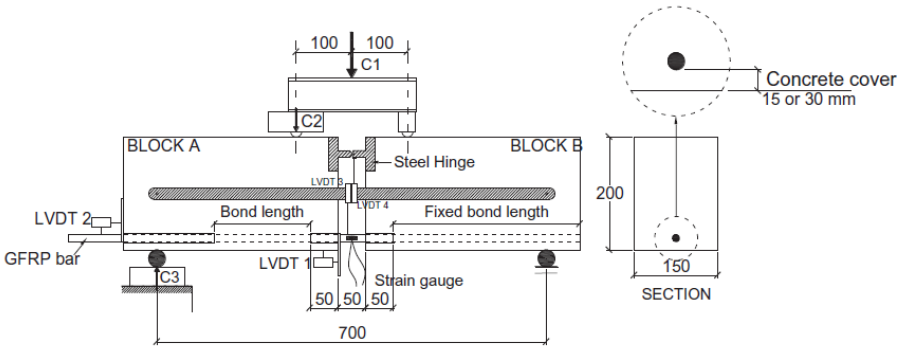

Figure 2.4: Pull- out bending setup (Pepe et al, 2012).

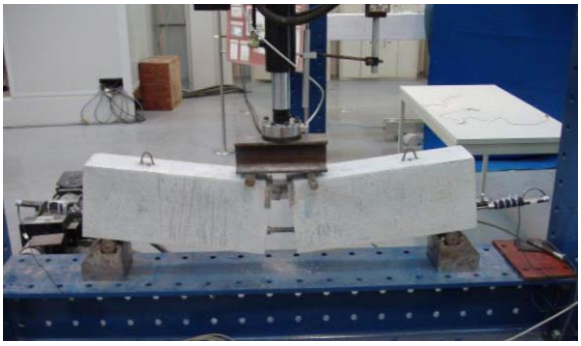

Figure 2.5: Experimental setup by Moreno et al (2006) comparable to Pepe et al (2012).

However, for lap splices subjected to a constant bending moment, this setup could cause some issues. The splice cannot be placed in the middle of the span due to the opening. Therefore, this specimen is more appropriate as an investigation for the anchorage (development) length of rebars.

2.2. Experimental research

The databases of VBC, Stuttgart and ACI (see part II for more information about these experimental databases) consist experimental researches to anchorage length and lap splices. Although, typical bond stress- slip relationships will be discussed to get a better understanding of the behaviour of reinforced concrete. Will the local bond- slip relationship according to Tassios (1979) be confirmed by other experimental results?

As discussed before, distinguish of pull-out and splitting failure is important for the bond stress- slip relationship. Two researches are highlighted Eligehausen et al. (1983) and Tepfers and Lorenzis (2006) to describe both failure mechanisms.

Note: do not consider the absolute values of the experimental results. The boundary conditions and specimen characteristics of both researches do not correspond. The intention of this comparison is to consider the behaviour of the failure mechanisms with reference to the bond stress- slip relationship.

First the relationship for pull-out failure. The possible failure modes are already discussed in paragraph 1.1. Globally, the bond stress- slip can be described by figure 2.6 (Eligehausen, 1983). The shape of the curve corresponds with Tassios (1979). The first branch until the ultimate bond stress failure is the chemical adhesion and the bearing capacity of the lug. Due to the confinement, the residual capacity is significant, no major decline in strength after passing the ultimate bond stress. The crushed granulates still provide bearing capacity and shearing resistance in collaboration with the lugs (aggregate interlocking effect). After a certain displacement, the granulates are extremely shattered, resulting in a significant lower bearing and shearing capacity. In case of shearing of mode (a), both concrete surfaces are smoothed due to shearing after aggregate interlocking. This results in lower friction, thus less residual bond stress.

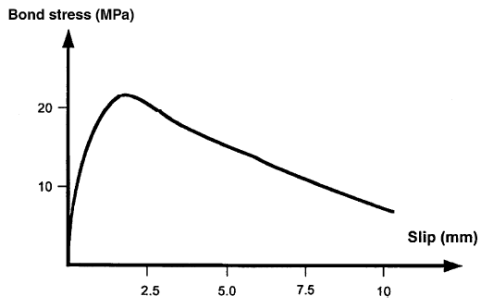

Figure 2.6: Typical bond stress- slip relationship of pull-out failure.

The experiments are performed as follows. In order to achieve the necessary confinement for pull-out failure, the specimen was casted as shown in figure 2.7. Transverse confining pressure is applied to simulate the dead load on a structural element. Furthermore, longitudinal and transverse reinforcement is applied to simulate the stirrups. Both prevent the intention of macroscopic cracks and subsequently splitting failure.

The results of the performed experimental series are revealed in figure 2.7. As shown, the shape of the curves are comparable, they are only shifted from each other with a relative small deviation.

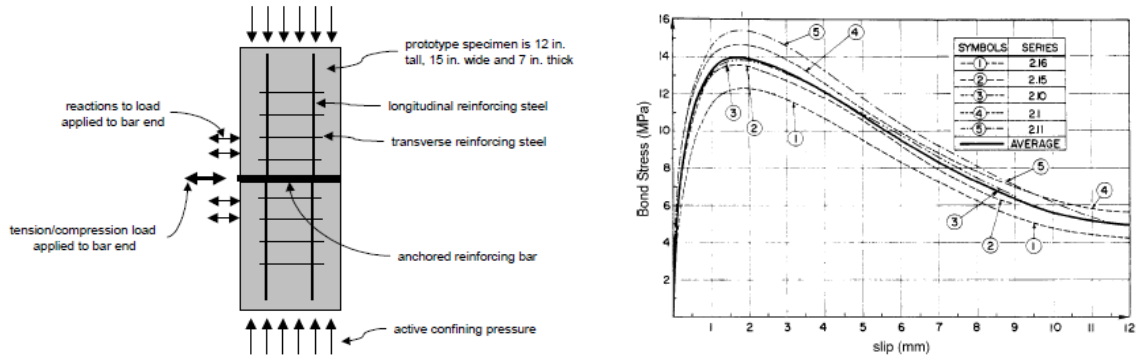

Figure 2.7: Specimen for pull-out experiments and the corresponding bond stress- slip graph (Eligehausen et al, 1983).

Conversely, Tepfers et al (2006) focused on splitting failure. The tests were performed with a pull-out setup, which is comparable to Abrahms (1917). As revealed in figure 2.8 the bond stress- slip relationship is different form Eligehausen (1983). The first branch of the graph is the chemical adhesion and bearing capacity of the lugs. Hereafter, splitting cracks will occur due to tangential stresses caused by the lugs (figure 2.8, left).

As a result, the transverse pressure on the rebar decreased enormously, the residual capacity after splitting is low. This failure mode is brittle compared to pull-out failure. Therefore, this mode should be avoided in practice by prescribing a minimum cover and amount of stirrups. Furthermore, the shape of the bond stress- slip relationship is indeed comparable to Tassios (1979). The ultimate strength is slightly lower; the main difference is the residual strength. Depending on the boundary conditions and material characteristics, the residual strength decreases enormously.

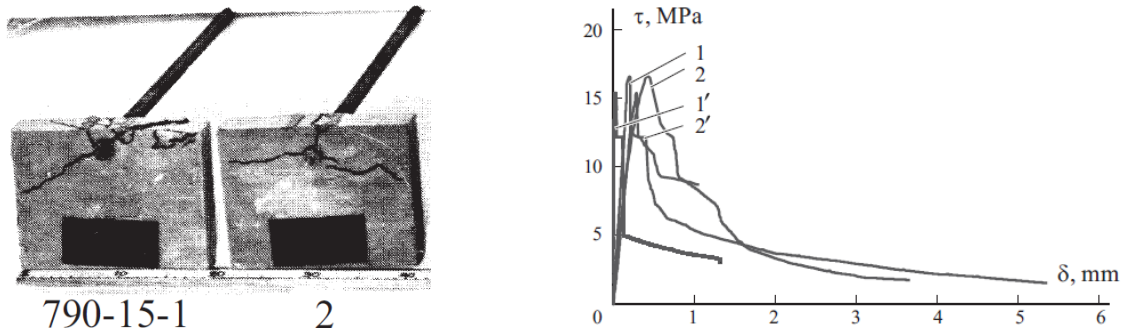

Figure 2.8: Specimen for pull- out experiments and the corresponding bond stress- slip graph (Tepfers/ Lorenzis, 2006)
1-1' and 2-2' are free and loaded ends respectively for both specimens.

3. Numerical

In addition to analytical and experimental research, a number of researches are performed with numerical analysis. However, the numerical studies which represents the actual situation accurate is rare. As concluded by Fib bulletin 10 (2000), any bond problem seems to be a special case. Several models are necessary to capture different mechanisms which characterize bond in the different limit states. However, FE modelling is capable to simulate bond behaviour and might be helpful in composing calculation methods for new materials, e.g. high strength concrete, epoxy coated reinforcement, bar rusting and size effect. Several FEM models will be discussed hereafter to provide an overview of the possibilities in bond modelling.

3.1. Layer model

Bond induced effects occur mostly in the concrete zone close to the rebar. Therefore, the concrete specimen can be subdivided into two regions. Both regions have different behaviour; the inner (slip) layer is tweaked in such a way that the bond stress- slip relationship is comparable to a realistic situation. A drawback for this model is that the failure mechanism is not taken into account. It is counterfeiting the bond- slip behaviour from experimental results.

For instance, Cox and Herrmann (1992 and 1994) developed a 2D plasticity model as revealed in figure 3.2. The bar- concrete interface is modelled with a bond layer instead of lugs (figure 3.1). On the basis of experimental results, information is provided as input for this bond layer, e.g. stress distribution, stiffness of the steel- concrete interface, friction, etc.

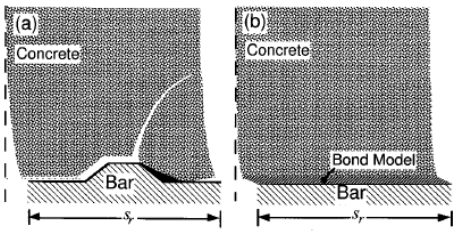

Figure 3.1: Idealized deformation of the bond zone for actual (a) and layer (b) model (Cox and Herrmann, 1994).

Several experimental results are successfully fitted with the 2D model. For instance Eligehausen et al. (1983) developed a FE model which shows good agreement with the bond stress- slip relationship.

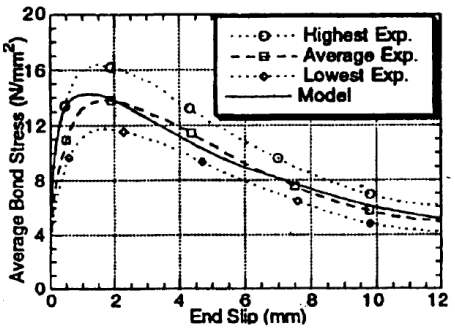

Figure 3.2: Model proposed by Cox and Herrmann (1992) compared to Eligehausen et al. (1983).

When the boundary conditions and material characteristics of the test specimen changes (e.g. anchorage length, bar diameter, concrete class), the mechanism changes and the bond layer should be adjusted to represent the actual stress distribution. One universal FE model is not valid; the parameters may be obtained from the calculation method proposed by Cox and Herrmann (1992 and 1994).

3.2. Interaction between surfaces

Several models for bond- slip relationship for reinforced concrete are proposed in literature. Casanova et al. (2012) highlighted the most common possibilities in figure 3.3. Namely spring, joint/interface and embedded elements. However, the model should be able to describe adhesive bonding, debonding and friction. Therefore, these elements are not appropriate; combining two of these methods should give a better result (Van der Aa, 2014). Therefore, Abaqus offers the method of surface based contact formulation to model these three stages combined in the research of Van der Aa (2014).

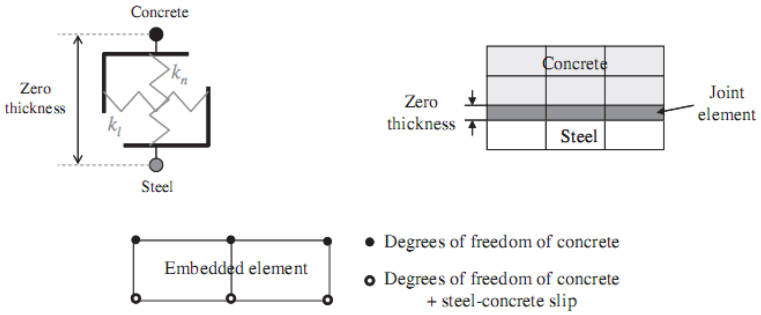

Figure 3.3: Possible bond elements (Casanova et al., 2012).

A similar method is applied by Tavares et al. (2014) for pull-out of a rebar. To represent the bearing and friction capacity of the lugs, the friction coefficient is nonlinear as a function of the displacement. "According to Lundgren et al (2002), it can be consider the problem as being controlled by friction approximately, although the bond process in ribbed bars was made by mechanical engagement" (Tavares et al, 2014). This friction coefficient can be defined over a certain sliding surface, see figure 3.4. By implementing this various friction coefficient in the model, the numerical results can be compared with experimental results (figure 3.5).

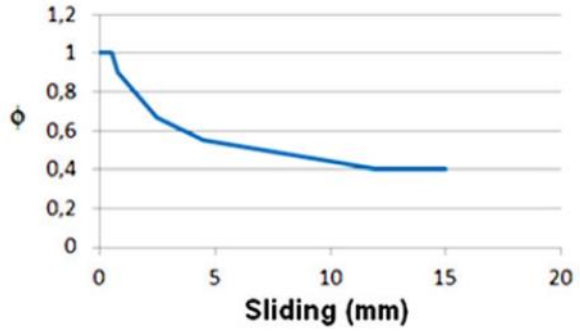

Figure 3.4: Friction coefficient variation as a sliding function based on Lundgren et al (2002).

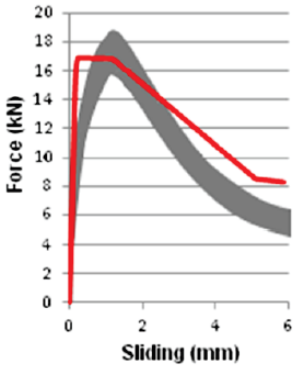

Figure 3.5: The comparison of numerical (red) and experimental results.

3.3. Damage model

In addition to interface, contact and embedded elements, pull-out can be modelled with the nonlinear behaviour of the surrounding concrete (Pijaudier et al., 1991). No properties are necessary to define the bond between both surfaces. The nonlinear response of concrete in tension, compression and shear should be implemented as a material property to model damage (cracking, crushing and shearing). Comparison with experimental results provides accurate results (figure 3.6), the stress distribution in the specimen is comparable. However, an additional parameter β should be introduced since interaction between surfaces is absent. The internal friction and aggregate interlock have to be taken into account to have a residual strength after crushing, cracking and shearing off of concrete.

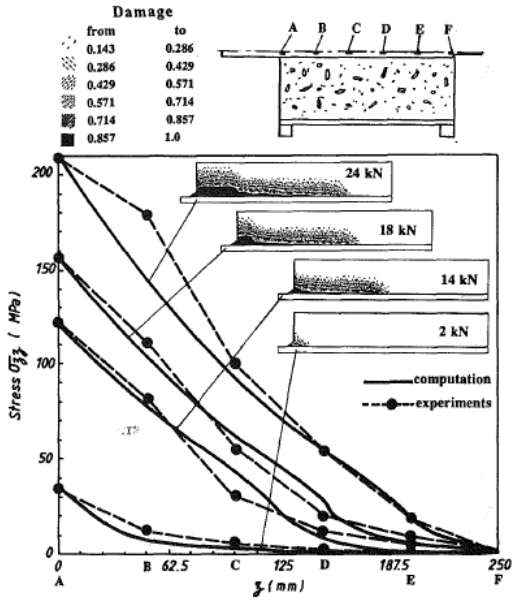

Figure 3.6: Comparison of the steel stress over the length of the model with experimental results.

3.4. Detailed model

The previous discussed FE models do not represent the actual geometry, or the concrete, or the steel bar is modelled in a non-realistic manner. Lettow and Eligehausen (2003) performed numerical and experimental research to a detailed model (figure 3.7), which represent the actual situation.

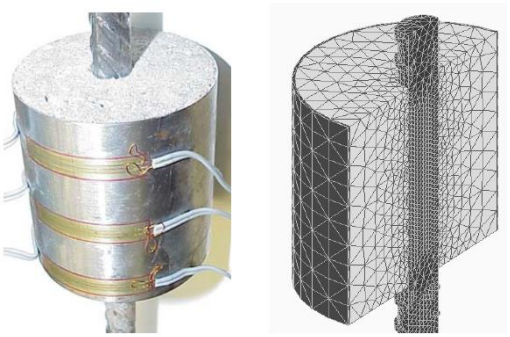

Figure 3.7: Test specimen and detailed FE model to obtain the bond stress- slip relationship.

The results of both experimental and numerical tests are revealed in figure 3.8. Ultimate bond strength shows good agreements; however, the stiffness is overestimated for the FE model. Conversely, hoop stresses as a function of the slip provide no satisfactory agreement. This finite element model is not appropriate for analyses of rebar pull-out for large displacements.

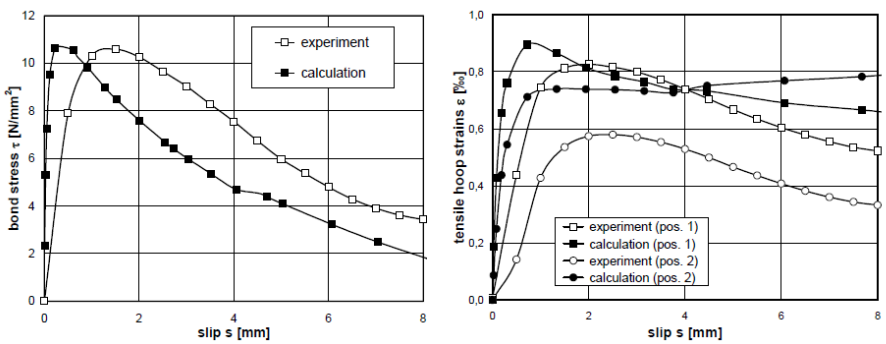

Figure 3.8: Comparison of the experiment and the numerical simulation for bond stress and hoop stress.

III. Backgrounds to Standards

4. NEN 6720: article 9.6

The latest Dutch Standard for concrete structures is the NEN 6720, where article 9.6 describes the calculation rules for anchorage length of reinforcing bars. The proposed method is very straightforward; with the following formula the basic anchorage length can be determined:

$$l_{vo} = \alpha_1 \phi_k \frac{f_s}{\sqrt{f'_b}} \qquad (1)$$

With:

$\alpha_1 = 0{,}4\left(1 - 0{,}1\frac{c}{\phi_k}\right) \geq 0{,}24$ for deformed bars

$\alpha_1 = 0{,}8\left(1 - 0{,}1\frac{c}{\phi_k}\right) \geq 0{,}48$ for plain bars

ϕ_k = diameter of the rebar

c = cover of the rebar

f_s and f'_b = values based on the concrete strength class

Remarkable is the fact that no distinction has been made between anchorage length and lap splice in the calculation method. Although, a factor (table 50, NEN 6720) should be taken into account for bundled bars. Another factor which is of importance is the casting position dependency. The above calculated l_{vo} is valid for lower rebars, for upper rebars the value l_{vo} has to be multiplied by a factor 1,25 due to the assumption of good or bad bond conditions. However, what is the origin of these formulas and values?

4.1. CUR 23

The first calculation method regarding anchorage length in the Netherlands was published in CUR 23. This is an experimental research to anchorage of rebars in a concrete section. Starting point in the CUR 23 is an analytical investigation of stresses in and around a deformed bar.

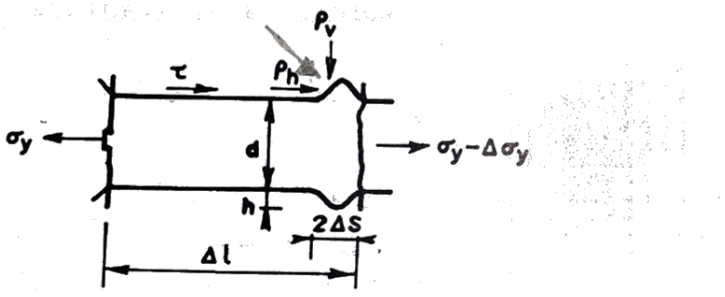

Figure 4.1a: Stresses in deformed bars embedded in a concrete section.

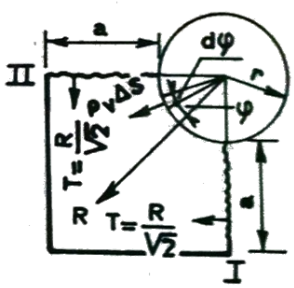

Figure 4.1b: Section of 4.1a.

An approximation of figure 4.1a is:

$$\Delta\sigma_y \cdot \tfrac{1}{4}\pi d^2 = \tau \pi d(\Delta l - 2\Delta s) + \rho_h \pi d\, h \qquad (2)$$

In words this equation describes: The transfer of force between steel and concrete over length Δl is equal to the average shear force multiplied by the mantle surface plus the normal stress introduced by the lugs of the bar. This equation can be rewritten to express the horizontal in vertical stresses and replace the following variables; $\rho_h = \alpha\rho_v$; $h = \beta\Delta l$; $\Delta s = \gamma\Delta l$;

$$\Delta\sigma_y \cdot {}^{1}\!/_{4}\pi d^2 = \tau\pi d\Delta l(1-2\gamma) + \alpha\beta\rho_v \pi\, d\, \Delta l \quad \text{Or} \quad \frac{\Delta\sigma_y}{\Delta l} = \frac{4\tau}{d}(1-2\gamma) + \frac{4}{d}\alpha\beta\rho_v \tag{3}$$

Conversely, stresses in the radial direction are important due to splitting of the concrete cover, which results in failure of the cross section. This radial force R can be obtained from figure 4.1b and the following differential equation.

$$R = \int_{-\frac{\pi}{4}}^{+\frac{\pi}{4}} \rho_v \cdot \Delta s \cdot r \cdot \cos\varphi\, d\varphi = \rho_v r\gamma\Delta l \int_{-\frac{\pi}{4}}^{+\frac{\pi}{4}} \cos\varphi\, d\varphi = \rho_v r\gamma\Delta l\sqrt{2} \tag{4}$$

Perpendicular to this force, the stress σ_t is present (force T in figure 4.1b). This is a tension stress that could cause splitting of the concrete cover.

$$\frac{R}{\sqrt{2}} = \rho_v r\gamma\Delta l = \sigma_t a\delta\Delta l \quad \rightarrow \quad \rho_v = \frac{\sigma_t a\delta}{r\gamma} = \sigma_t\lambda\frac{a}{d} \tag{5}$$

Substitute this expression into (3):

$$\frac{\Delta\sigma_y}{\Delta l} = \frac{4\tau}{d}(1-2\gamma) + \frac{4}{d}\alpha\beta_v\lambda\frac{a}{d}\sigma_t \tag{6}$$

This results in the approximation:

$$\sigma_{y\max} = \frac{4l}{d}\left[\tau(1-2\gamma) + \alpha\beta_v\lambda\frac{a}{d}\sigma_t\right] = \frac{4l}{d}\left[\eta\tau + \nu\frac{a}{d}\sigma_t\right] = \frac{4l}{d}\cdot\tau_1 \tag{7}$$

This is in line with previous studies of anchorage of rebar, the relation of $\sigma_{y\max}$ and $\frac{l}{d}$ is linear.

The bond stress obtained from the analytical solution in CUR 23 should have the form:

$$\tau_1 = \frac{\sigma_{y\max}}{4\frac{l}{d}} = \left(A + B\frac{a}{d}\right)\sigma_t + C \qquad [\text{kg/cm}^2] \qquad \text{Or rewritten:} \tag{8}$$

$$\tau_1 = A'\sigma_t\frac{a}{d} + B'\sigma_t + C'\frac{a}{d} + D' \qquad [\text{kg/cm}^2] \tag{9}$$

Where the values A', B', C' and D' are dependent on steel quality and position of the bar (upper or lower). However, is this formula in accordance with experimental data? Therefore, experimental tests were performed to check the analytical solution and to find reasonable values for the variables.

A short summary of the test specimen, setup and results will be given, for more information reference is made to CUR 23. The experimental pull-out tests were performed with the setup shown in figure 4.2.

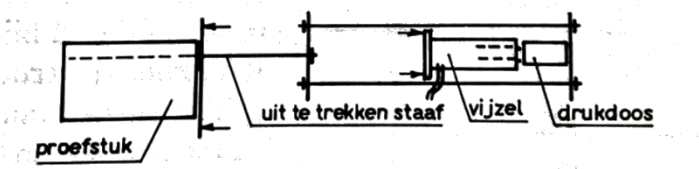

Figure 4.2: Test setup of the experimental research performed by CUR 23

And the properties of the specimens are listed in the table below:

Variable	
Concrete σ_{k28}	170- 410 (N/mm^2)
Type rebar	H- bond/ Kam/ Ribbed/ Tor and Torwa steel
Diameter	10,18-20, 25-26 (mm)
l/d	14,21,28,35
Number of specimens	107

Table 4.1: Summary of the test specimens

Due to the variety of the specimens, the output for the values A', B', C' and D' is ambiguous. Every type of rebar contains a mean value as input for the derived expression (9). However, is the overall mean value applicable for a general deformed bar? The mean values, which are based on the experimental results, are:

For lower rebar:

$$\tau_1 = 0{,}0161 \cdot \frac{a}{d} \cdot \sigma_{k28} + 0{,}095 \cdot \sigma_{k28} + 3{,}16 \cdot \frac{a}{d} + 15{,}79 \qquad [kg/cm^2] \qquad (10)$$

For upper rebar:

$$\tau_1 = 0{,}0202 \cdot \frac{a}{d} \cdot \sigma_{k28} + 0{,}122 \cdot \sigma_{k28} + 3{,}97 \cdot \frac{a}{d} - 6{,}62 \qquad [kg/cm^2] \qquad (11)$$

Statistical research has proven that the deviation of equation (10) and (11) is within the 4 and 7% compared to the experimental results of the individual bars. The formulas for the determination of the bond stress τ_1 are based on the mean value, not a design value. Therefore, CUR 23 recommend a safety factor of $\gamma = 1{,}7$ for the bond stress in structural elements.

Remarkable in the experimental research of CUR 23; no specimens with lap splices were tested. As a result the origin of the values of Table 50 (NEN 6720) for bundled bars is unknown.

A comparison can be made between the NEN 6720 and CUR 23. Hitherto, few similarities are visible in both calculation methods. Nevertheless, the NEN 6720 is derived from this research. In the course of time (from 1963 to 1995), adjustments were made in the Dutch standard. A subsequent old Dutch standard is necessary to provide a better understanding of the development of the calculation methods.

4.2. CUR 94-13

The CUR 94-13 describes the transition of the standard VB 1974/1984 to VBC (NEN 6720). The calculation rule for the bond stress in VB 74/84 is:

$$f_d = \left(1{,}86 + 0.316\frac{c}{\phi}\right) f_b - 0{,}15 \tag{12}$$

This is followed by the anchorage length of a rebar:

$$l_d = \frac{1}{4}\frac{f_a}{f_d}\phi \tag{13}$$

The origin of expression (13) is obvious; it is similar to the analytical solution in 4.1. Conversely, formula (12) does not correspond. Although the general form of expression (8) is comparable. Throughout the years, the concrete material has evolved and the experience with concrete structures is enlarged. This could be the reason of slight changes in properties of concrete and corresponding design rules. The Cur 94-13 has compared VB 74/84 and VBC in a graph with the concrete strength on the x-axis and l_d/ϕ on the y- axis (figure 4.3), hereinafter more about this comparison. First the transition of Cur 23 to VB 74/84, therefore the graph of the calculation rules according to Cur 23 is added. As can be seen, the shape of the graph of both standards is similar, only they are shifted from each other. The Cur 23 design rules are on the unsafe side compared to VB 74/84.

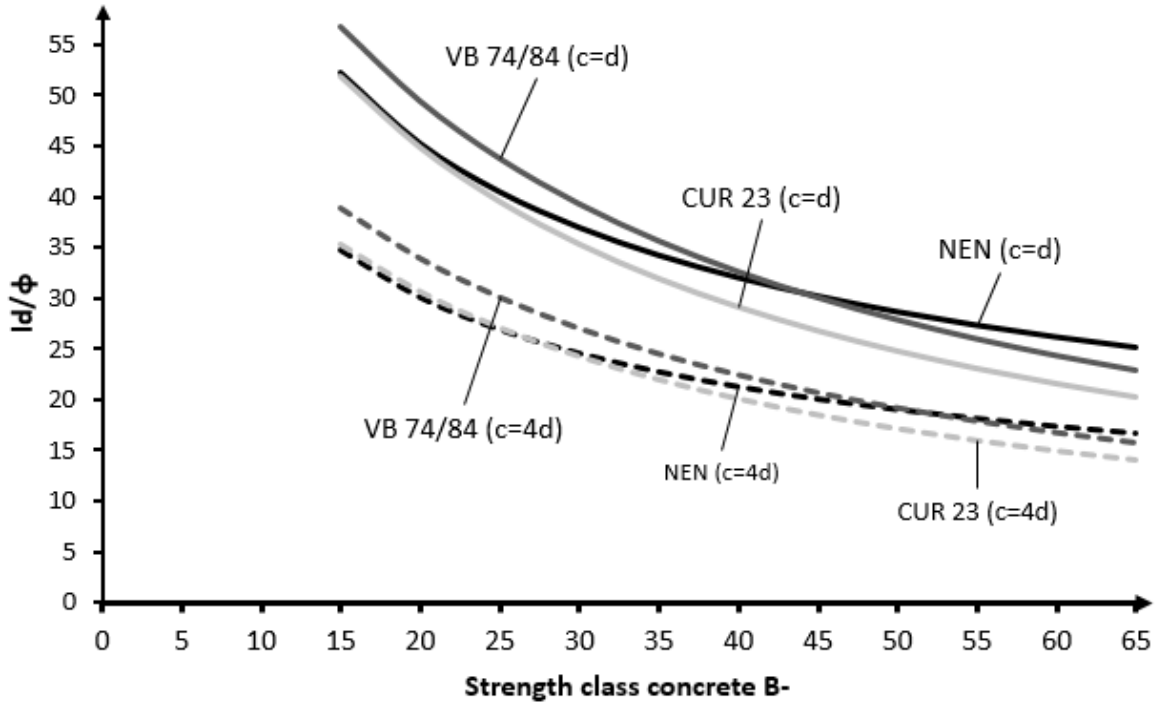

Figure 4.3: Comparison of the design rules for lap splices of three old Dutch standards

The successor of VB 74/84 is the NEN, which gives a more simple approximation formula:

$$\frac{l_{vo}}{\phi} = 0{,}4\left(1 - 0{,}1\frac{c}{\phi}\right)\frac{f_s}{\sqrt{f'_b}} \tag{14}$$

Figure 4.3 reveals the comparison with the previous standards. Remarkable is the different shape of the graph, indeed the new design rules of VBC are not based on studies. It is an approach of VB 74/84, which fit the experimental results. However, the anchorage length for lower concrete classes corresponds to CUR 23 and the lower steepness results in a safe value for the higher concrete classes.

5. NEN- EN 1992-1-1: article 8.4/8.7

Since 2010, the Eurocode 2 is introduced in the Netherlands as a replacement of NEN 6720.The change compared to the old standard is significant, there is no relation anymore with the experimental data of Cur 23. The calculation method according to NEN-EN 1992-1-1 will be summarized shortly.

First, the bond strength can be calculated with the following formula:

$$f_{bd} = 2{,}25 \cdot \eta_1 \cdot \eta_2 \cdot f_{ctd} \tag{1}$$

With:

$\eta_1 = 1{,}0$		for good bond conditions.
$= 0{,}7$		for bad bond conditions.
$\eta_2 = 1{,}0$		for $\phi \leq 32mm$
$= (132 - \phi)/100$		for $\phi \geq 32mm$
f_{ctd}		is design value of tensile strength of concrete

Hereafter, the basic anchorage strength can be calculated with the assumption of an uniform distributed bond stress.

$$l_{b,rqd} = \left(\frac{\phi}{4}\right)\left(\frac{\sigma_{sd}}{f_{bd}}\right) \tag{2}$$

With:

ϕ		diameter of steel rebar
σ_{sd}		design value of steel stress

Then the formula for lap splice can be filled in:

$$l_{bd} = \alpha_1\alpha_2\alpha_3\alpha_5\alpha_6 \cdot l_{b,rqd} \tag{3}$$

With: α_n are variables based on structural conditions (confinement of transverse reinforcement, transverse pressure, concrete cover, shape of rebar, casting position and percentage of lapped bars [table 8.2 and 8.3 NEN-EN 1992-1-1])

A comparison with the calculation method of NEN 6720 allows little similarities. The main difference is distinguished between splice length and anchorage length. A separate formula for anchorage length and splice length is implemented. The formula for anchorage length is:

$$l_{bd} = \alpha_1\alpha_2\alpha_3\alpha_4\alpha_5 \cdot l_{b,rqd} \tag{4}$$

On second thoughts, the calculation method for lap splice is also based on a factor (α) which is based on experimental results as well. However, further research should give more information of the background of these experimental specimens and setup. Are the lap splices taken into account in these researches?

5.1. Model code 1990

Backgrounds of the NEN-EN 1992-1-1 can be found in the Model code 1990. Despite the fact that the model code 2010, a revised version of Model code 1990, was published November 2013. A comparison between MC 90 and EC2 reveals that both calculation methods correspond exactly with the exception of the factor α_6. This factor represents percentage of the lapped bars relative to the cross section. This factor in MC 90 is significantly higher than the prescribed value in NEN-EN 1992-1-1. Assume a cross section with lap splices, all these laps are positioned on a small area, within the area of 0,65 l_0 (figure 5.1).

According to MC90, α_6 should be 2,0 in expression (3). In words, the splice length would be more than 1,6 times larger compared to a uniform distribution of the lap splices over a certain length. This factor could cause a significant higher overlap length. This value is adjusted in EC 2, α_6 should be 1,5 for the same conditions. However, the influence of closely located lap splices remains in this calculation method.

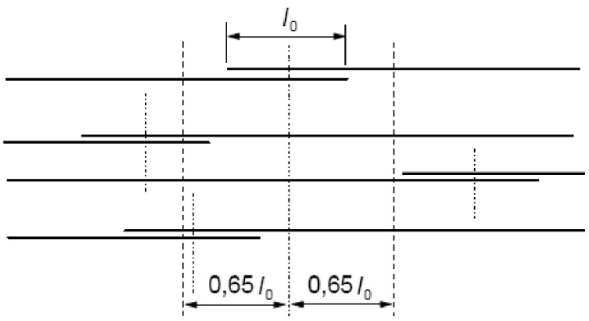

Figure 5.1: percentage lapped bars according to figure 8.8 EC2

Hitherto, the origin of the discussed formulas is underexposed. The calculation method is formed from an experimental database which is composed by fib Task Group 4.5 "Bond models". The expressions of EC2 are fitted to this experimental data in a manner that it provides a safe result for every input. More additional information about this database in comparison with design rules will be given in the next paragraph and in chapter 9.

5.2. Model code 2010

The MC10 proposes significant changes in the calculation method. First, a local bond- slip relationship is assumed to describe the failure behaviour of a deformed bar in concrete. This graph is not unambiguous due to the diversity of failure mechanism. The behaviour of deformed bars in concrete is already discussed in part I of this literature survey. Therefore, the bond stress- slip relationship of figure 5.2 is obvious, which can be described by the following equations:

$$\tau_{b0} = \tau_{b\max}\left(s/s_1\right)^{\alpha} \qquad for\ \ 0 \le s \le s_1 \qquad (5)$$

$$\tau_{b0} = \tau_{b\max} \qquad for\ \ s_1 \le s \le s_2 \qquad (6)$$

$$\tau_{b0} = \tau_{b\max} - \frac{\left(\tau_{b\max} - \tau_{bf}\right)\left(s - s_2\right)}{\left(s_3 - s_2\right)} \qquad for\ \ s_2 \le s \le s_3 \qquad (7)$$

$$\tau_{b0} = \tau_{bf} \qquad for\ \ s_3 \le s \qquad (8)$$

The confinement due to stirrups and transverse pressure is ofimportance for the failure mechanism. For both dashed lines, the transverse pressure is absent; this could result in splitting of the concrete cover. The compressive stress is capable to eliminate (partly) the radial tensile force around the deformed bar. Splitting of the cover is not governing. As a result, the rebar will be pulled-out due to cracking and crushing of the concrete close to the steel. The influence of stirrups is also significant; the reason for this is comparable to the transverse pressure. The stirrups around the rebar will capture a part of the tensile stresses in the radial direction.

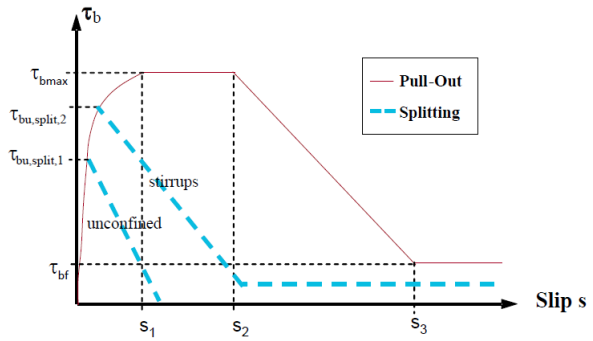

Figure 5.2: Analytical bond stress- slip relationship from Model Code 2010 figure 6.1-1.

Hitherto, the behaviour is analytically considered. Though, the design rules of MC10 are based on the experimental database Stuttgart 2005. Relevant experimental researches of lap splices from 1956 to 2000 are collected to provide an overview of data regarding anchorage of rebars. From these tests, an expression is derived (10) for the mean strength value:

$$f_{stm} = 54\left(\frac{f_{cm}}{25}\right)^{0,25}\left(\frac{25}{\phi}\right)^{0,2}\left(\frac{l_{cr}}{\phi}\right)^{0,55}\left[\left(\frac{c_{\min}}{\phi}\right)^{0,25}\left(\frac{c_{\max}}{c_{\min}}\right)^{0,1} + k_m K_{tr}\right] \le f_y \le 10\sqrt{f_c}\,\frac{l_0}{\phi} \qquad (9)$$

With:

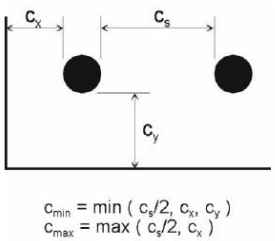

Figure 5.3: Values for c according to MC 10

f_{stm} = Steel stress (N/mm^2)

f_{cm} = Concrete cylinder compressive strength (N/mm^2)

ϕ = Diameter rebar (mm)

l_0 = Splice or anchorage length (mm)

$c_{\max}$ *and* $c_{\min}$ are defined in figure 5.3

k_m = represents the efficiency of confinement

K_{tr} = Value based on confining reinforcement

$$= \frac{n_t A_{st}}{n_b \phi s_t} \le 0{,}05$$

Equation (10) can be summarized in a graph to visualize the results of the tests, which is done by Cairns (2013). Therefore, a number of assumptions are necessary to provide a relationship between bar stress and bond length. The concrete strength is 32 N/mm^2, bar diameter 20 mm, minimum cover of 20 mm 40 mm clear spacing and no transverse reinforcement, see figure 5.4.

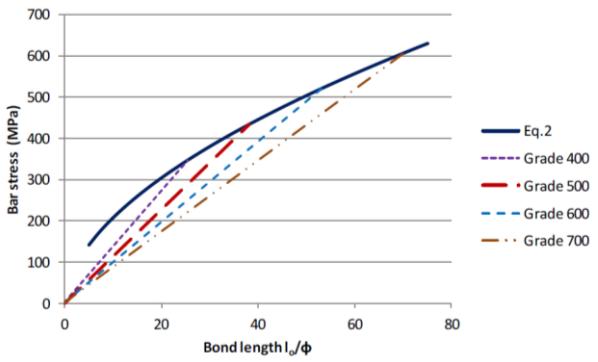

Figure 5.4: Relationship bar stress – bond length according to the mean value expression (10) from MC10

Based on the experimental database, the design rules have been formed. The basic bond strength, which is considered as an average stress, can be calculated with:

$$f_{bd,0} = \eta_1 \eta_2 \eta_3 \eta_4 \frac{\sqrt{\left(\frac{f_{ck}}{25}\right)}}{\gamma_{cb}} \qquad (10)$$

With: η_1 = Coefficient for bar surface, 1,75 for ribbed bars, 1,4 for epoxy coated and 0,9 for plain bars.
η_2 = Coefficient for casting position, 1,0 for good bond conditions, 0,7 for all other cases.
η_3 = 1,0 for $\phi \leq 25$ and $\left(\frac{25}{\phi}\right)^{0,3}$ for $\phi \geq 25$
η_4 = Coefficient for yield strength 1,0 for B500

However, the basic bond stress is not a design value, the design bond strength is:

$$f_{bd} = (\alpha_2 + \alpha_3) f_{bd,0} - 2p_{tr.} < 2{,}0\, f_{bd,0} - 0{,}4 p_{tr} < (1{,}5/\gamma_{cb}) \cdot \sqrt{f_{ck}} \qquad (11)$$

With: α_2 = Influence of passive confinement of the cover.
α_3 = Influence transverse reinforcement.
p_{tr} = Mean compression stress perpendicular to the potential splitting failure surface at ultimate limit state

(In order to come to these values, the formulas in MC10; 6.1.3.3 are required. Due to the complexity and for matters of simplicity reference is made to MC10. A conservative assumption for α_2 and α_3 is 1,0 and p_{tr} is 0 when no stresses perpendicular to the splitting surface are present.)

Hereafter, the lap length in tension can be calculated straightforward with the following formula.

$$l_b = \alpha_4 \frac{\phi \cdot f_{yd}}{4 \cdot f_{bd}} \geq l_{b,\min} \qquad (12)$$

With: α_4 = Coefficient based on the calculated stress in the reinforcement. If this does not exceed 50% of the characteristic strength, this factor is 0,7, or no more than 34%, α_4=1,0.

Expression (13) is formed with due consideration of the distinction between laps and anchorage length. The formula for anchorage length differs, not the ultimate steel stress should be filled in, but the design value of the steel stress. The origin of the distinction is unkown (Cairns, 2013). “It is not clear how the distinction between strength of laps and anchorages became established in Design Codes, and there appeared to be two possibilities.” These possibilities are already discussed in the paragraph Laps vs Anchorages in part I of the literature survey.

6. DIN 1045-1: article 12,5/12.6

The calculation method for the anchorage length of DIN 1045 is almost similar to NEN- EN 1992-1-1. The main cause of this similarity is that both standards are derived from Fib Model Code 1990. Therefore, only this standard will be summarized shortly to expose the differences.

First, the formula for ultimate bond stress of DIN 1045 is similar to EC2, only minor changes are present in the formulation:

$$f_{bd} = 2{,}25 \cdot \frac{f_{ctk;0,05}}{\gamma_c} \qquad (1)$$

This formula only applies for rebar diameter < 32 mm and for bad bond conditions 0,7 f_{bd} .

Hereafter, the anchorage length can be calculated with the familiar formula for uniform distributed bond stress over the length of the rebar. The major difference is the input of the steel stress. DIN 1045 prescribes the ultimate steel stress; this is in contrast with EC2, where a reduction of the stress is allowed. For instance, the splice is not located in the centre of a moment envelope.

$$l_{b,rqd} = \left(\frac{d}{4}\right)\left(\frac{f_{yd}}{f_{bd}}\right) \qquad (2)$$

Subsequently, the design anchorage length can be calculated. In comparison with EC2, the coefficient α is captured in α_a instead of 6 separate coefficients in (4, NEN- EN 1992-1-1). Remarkable in (3) is the reduction in anchorage length due to the excessive size, which is comparable to the reduction of steel stress. The remaining difference between EC2 and DIN 1045 is the coefficient α.

$$l_{b,net} = \alpha_a \cdot l_b \left(\frac{A_{s,erf}}{A_{s,vorh}}\right) \qquad (3)$$

The subdivision of the factor is applied to take the influence of transverse reinforcement and transverse pressure into account. Both provide a positive effect on the reduction of anchorage length. Due to these missing parameters, the DIN 1045 is on the safe side compared to EC2.

Finally, the lap splice can be calculated with the following formula:

$$l_{b,net} = \alpha_1 \cdot l_{b,net} \qquad (4)$$

The coefficient α describes the same aspect as α_6, the percentage of lapped bars. Hence, the principle for determining the coefficient α according to [Table NA.8.3 DIN 1045] and [table 8.3 NEN-EN 1992-1-1] is comparable, although minor differences exist in both tables.

7. BS 8110: article 3.12.8

The calculation rules of the British standard regarding anchorage length are very straightforward. The main parameter for these design rules is the bond stress. First the ultimate anchorage bond stress can be calculated with:

$$f_{bu} = \beta\sqrt{f_{cu}} \qquad (1)$$

With f_{cu} is the ultimate compressive stress and β a coefficient dependent on figure 7.1. These values include a partial safety factor (y_m) of 1,4.

Bar type	β	
	Bars in tension	Bars in compression
Plain bars	0.28	0.35
Type 1: deformed bars	0.40	0.50
Type 2: deformed bars	0.50	0.63
Fabric (see **3.12.8.5**)	0.65	0.81

Figure 7.1: Values for bond coefficient β

Subsequently, the design anchorage bond stress can be calculated with the following formula:

$$f_b = \frac{F_s}{\pi \cdot \varphi_e \cdot l} \qquad (2)$$

With:
F_s = force in the bar or group of bars
f_b = bond stress
φ_e = effective bar diameter
l = anchorage length

In case of tension lap splices an additional factor is implemented. The value of these factors depends on the following provisions according to BS 8110:

- Where a lap occurs at the top of a section as cast and the minimum cover is less than twice the size of the lapped reinforcement, the lap length should be increased by 1,4.
- Where a lap occurs at the corner of a section and the minimum cover to either face is less than twice the size of the lapped reinforcement, or where the clear distance between adjacent laps is less than 75 mm or six times the size of the lapped reinforcement, whichever is greater, the lap length should be increased by a factor 1,4.
- In case where both conditions apply, the lap length should be increased by a factor of 2,0.

A more simple method to determine the lap splice is by using table 3.27 - Ultimate anchorage bond lengths and lap lengths as multiples of bar size in BS 8110. No calculation rules are necessary; the values can be read from the table.

Hitherto, the origin of the BS 8110 for lap splices is unknown. This method is not derived from the model code, the values β are likely based on a fitted line on experimental data.

8. ACI 318: article 12.2 and 12.15

In comparison with the previous discussed standard, the ACI is based on a database which is composed by the ACI committee. This database is independent of the database from the Model Code. The design rule for the anchorage (development) length is:

$$l_d = \left(\frac{f_y}{1{,}1\sqrt{f'_c}} \cdot \frac{\psi_t \psi_e \psi_s \lambda}{\left(\frac{c_b + K_{tr}}{d_b} \right)} \right) d_b \qquad (1)$$

With:

ψ_t = Coefficient depending on casting position.
Where horizontal reinforcement is placed such that more than 300 mm of fresh concrete is cast below the splice, factor is 1,3, for other situations 1,0.

ψ_e = 1,0 for uncoated reinforcement.

ψ_s = 0,8 for no. 19 and smaller bars.

λ = 1,0 for normal weight concrete.

The term $\frac{c_b + K_{tr}}{d_b}$ shall not be taken greater than 2,5, for values above 2,5 pull-out failure is expected. Increase in cover or transverse reinforcement does not result in a higher anchorage capacity anymore. Furthermore, the parameter $K_{tr} = \frac{A_{tr} f_{yt}}{10sn}$ depends on transverse reinforcement, for matters of simplicity K_{tr} can be taken as 0, which is a safe approximation. No transverse reinforcement is applied in this case, resulting in a lower strength in the ultimate limit state.

However, the development length is not applicable to tension lap splices. Therefore, l_d should be multiplied by a factor dependent on the following table. If the splice is class A, the factor is 1,0 and 1,3 for class B.

$\frac{A_s \text{ provided}^*}{A_s \text{ required}}$	Maximum percent of A_s spliced within required lap length	
	50	100
Equal to or greater than 2	Class A	Class B
Less than 2	Class B	Class B

* Ratio of area of reinforcement provided to area of reinforcement required by analysis at splice locations.

Figure 8.1: Tension lap splices dependent on class.

8.1. ACI committee report 408R

Several design rules are proposed for the development length in the ACI 318. These calculation rules are fitted to the experimental results of the ACI database. However, what is the most realistic expression to describe the development length of a rebar? More information about the ACI database can be found in chapter 9.

Orangun, Jirsa and Breen

A regression analysis performed by Orangun, Jirsa and Breen (1977) from experimental beam testing with and without confining reinforcement. The expression for development length was the basis of the first appeared ACI 318-95 standard. The expression is:

$$\frac{A_b f_s}{\sqrt{f'_c}} = 3\pi l_d \left(c_{\min} + 0{,}4 d_b\right) + 200 A_b + \frac{\pi l_d A_{tr}}{500 s n} \cdot f_{yt} \qquad (2)$$

In case of no transverse reinforcement, the last term disappears.

Darwin et al.

A sequel to this expression is a reanalysed research of the data performed by Darwin et al (1996). Therefore, two expressions are created to improve the accuracy compared to the mean value of the test results.

No confined transverse reinforcement: $$\frac{A_b f_s}{f'^{\,0{,}25}_c} = \left[63 l_d \left(c_{\min} + 0{,}5 d_b\right) + 2130 A_b\right] \left(0{,}1 \frac{c_{\max}}{c_{\min}} + 0{,}9\right) \qquad (3)$$

In case of transverse reinforcement, two additional terms are necessary to get the best-fit equation:

$$+ 2226 t_r t_d \frac{N A_{tr}}{n} + 66 \qquad (4)$$

(Due to the fact, this formula is only an intermediate step, the variables will not be discussed expanded. However, more information can be found in ACI Committee 408 report).

Zuo and Darwin

The previous work is extended by Zuo and Darwin (2000) by increasing the database and adding test specimen containing high- strength concrete. This analysis supported the earlier observations that $f'^{\,0{,}25}_c$ realistically represents the contribution of concrete strength to bond strength for bars without transverse reinforcement.

No transverse reinforcement: $$\frac{A_b f_s}{f'^{\,0{,}25}_c} = \left[59{,}8 l_d \left(c_{\min} + 0{,}5 d_b\right) + 2350 A_b\right] \left(0{,}1 \frac{c_{\max}}{c_{\min}} + 0{,}9\right) \qquad (5)$$

With transverse reinforcement: $$+ \left(31{,}14 t_r t_d \frac{N A_{tr}}{n} + 4\right) \sqrt{f'_c} \qquad (6)$$

With: $t_r = 9{,}6 R_r + 0{,}28$ and $t_d = 0{,}78 d_b + 0{,}22$

ACI Committee 408

The Committee 408 (2003) only applies minor changes to equation (5) and (6), the form corresponds.

$$\frac{A_b f_s}{f'^{\,0{,}25}_c} = \left[59{,}9 l_d \left(c_{\min} + 0{,}5 d_b\right) + 2400 A_b\right] \left(0{,}1 \frac{c_{\max}}{c_{\min}} + 0{,}9\right) + \left(30{,}88 t_r t_d \frac{N A_{tr}}{n} + 3\right) \sqrt{f'_c} \qquad (7)$$

However, which equation predicts the results of ACI database with the smallest accuracy? This can be investigated by plotting the test/ prediction ratio against the compressive strength.

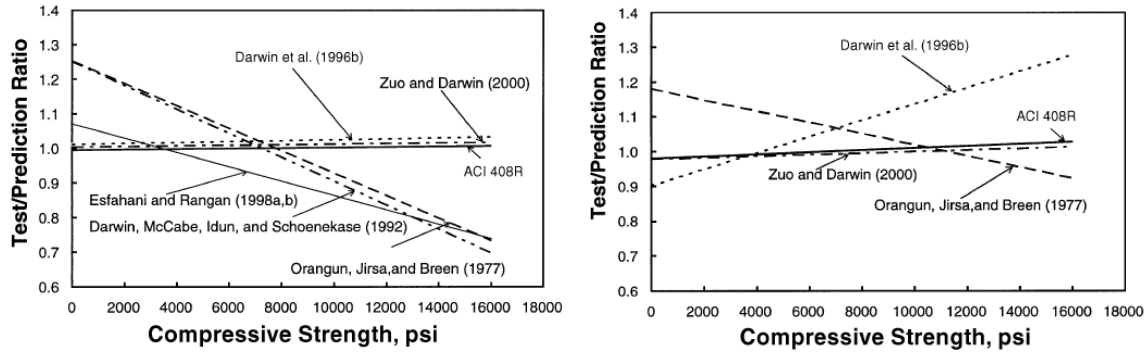

Figure 8.2: Test prediction ratios for six descriptive equations for not confined bars and confined bars respectively

ACI 418

The design rules described in the ACI 418 are derived from Oragun, Jirsa and Breen (1977). This is remarkable due to the results in figure 8.2. Conversely, the equations provided by ACI 408R, Zuo and Darwin (2000) and Darwin et al (1996) are more accurate, however no safety factors are included in these formulas. Equation (2) overestimates the failure value until a concrete strength of 8000 psi (55N/mm^2) without transverse reinforcement and 10000 psi (69 N/mm^2) with transverse reinforcement. It is not permitted to use this formula for high strength concrete structural elements.

Equation (2) in this form not comparable to the design rules from ACI 418; therefore the equation should be rewritten. Solving equation (2) for the ration of the development length l_d to the bar diameter d_b and replacing (c_{min}+0,4d_b) with (c_{min}+0,5d_b) gives:

$$\frac{l_d}{d_b} = \frac{f_s - 200}{12\left(\frac{c + K_{tr}}{d_b}\right)\sqrt{f'_c}} \qquad \text{with:} \qquad K_{tr} = \frac{A_{tr} f_{yt}}{1500sn} \tag{8}$$

Subsequently, equation 8 can be simplified by removing the 200 in the formula. Hereafter, the constant (1/12) will be changed into (3/40) to take the removed constant into account.

$$\frac{l_d}{d_b} = \frac{3}{40}\frac{f_s \alpha\beta\gamma\lambda}{\left(\frac{c + K_{tr}}{d_b}\right)\sqrt{f'_c}} \tag{9}$$

With α is reinforcement factor, β is coating factor, γ is reinforcement size factor and λ is factor for lightweight. In comparison with the last published standard ACI 318, minor changes were applied.

9. Comparison

9.1. Parameters of the databases

Hitherto, the calculation methods of several standards are investigated. Experimental research is the common thread in order to form the formulas. As discussed in part II, several parameters have significant influence on the pull-out/ splitting behaviour of reinforced elements. The database of ACI and Stuttgart are composed without any restrictions for these parameters. For instance, high strength concrete, high strength steel, large rebar diameter and large cover are included in these databases. To get a better insight in the structure of the databases, the experimental data is divided into five groups to filter the parameters for both ACI and Stuttgart database. Note, that all the selected experimental data is based on good bond conditions.

The "standard" group:	d_s = (0-20) mm
	c_y = (0-36) mm
	f_{yd} = (350-550) N/mm^2
	f_{cm} = (0-40) N/mm^2
Large diameter rebar group:	d_s = (20- →) mm
Large cover group:	c_y = (36- →) mm
High strength steel group:	f_{yd} = (500- →) N/mm^2
High strength concrete group:	f_{cm} = (40- →) N/mm^2

The results of these groups are plotted in figure 9.1. The black/grey points are data from the ACI and the coloured points are data from Stuttgart. The data of Stuttgart reveals no regularity in the influence of parameters. All the points are mixed up and no clusters can be recognized. Conversely, the ACI database (black/grey) is more structured when subdividing the experimental data. Practically no HSS, HSC and LDB are present in the database (when using the "standard" group as starting point), these will be ignored. Two groups remain and these give an expected result. The "standard" group (black) prescribes a larger anchorage length compared to the large cover group (grey).

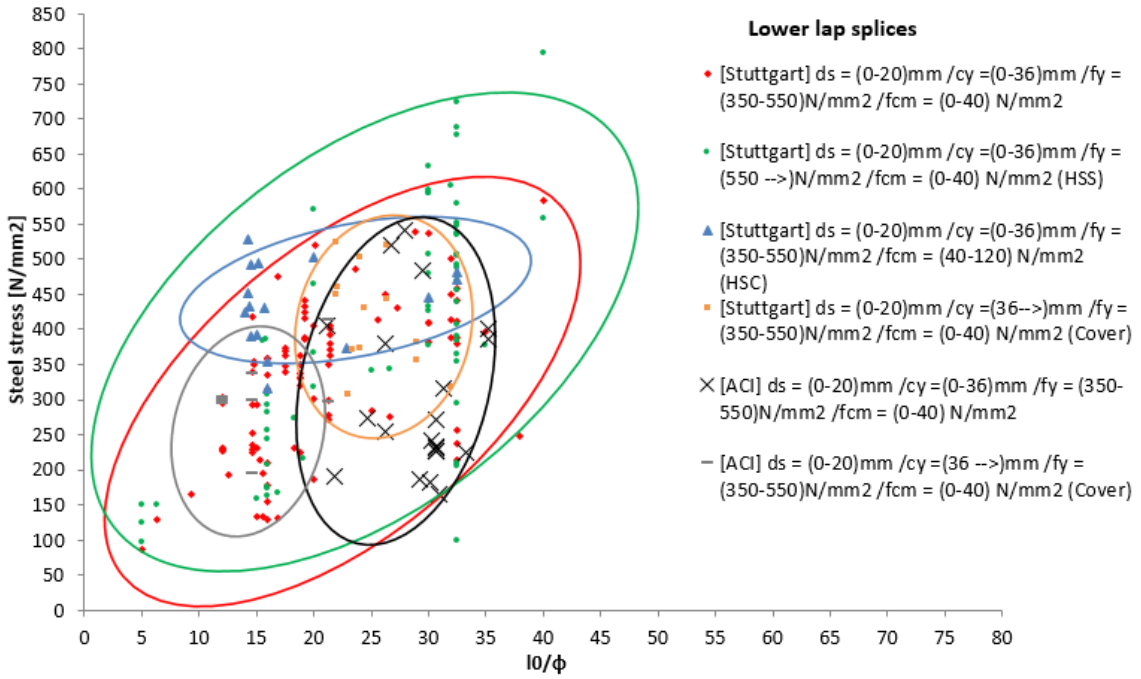

Figure 9.1: Steel stress with respect to the rebar diameter for anchorage length.

9.2. Results of the standards

Once getting a better understanding of the composition of the database, the previous discussed standards can be compared. However, a starting point is necessary for the comparison of several standards. Owing the fact a number of calculation methods take the effect of transverse reinforcement and pressure into account. The following structural element is assumed:

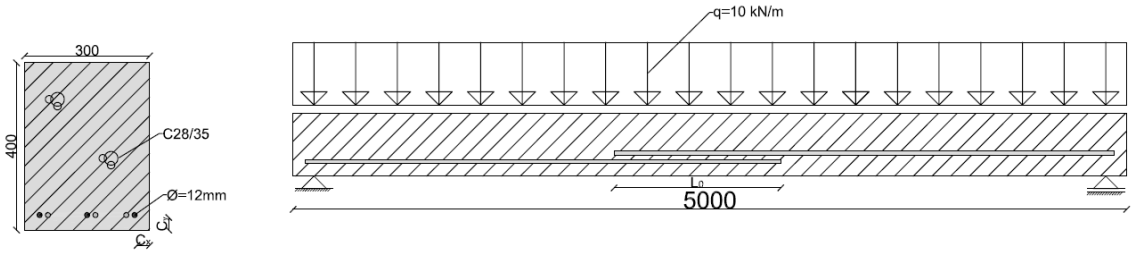

Figure 9.2: The assumed structural element for the comparison of several standards.

Hereafter, the required lap splice can be calculated as multiples of the bar size. Increasing the steel stress gives a linear or bi- linear graph (figure 9.3). The test results and the mean value of the experimental data of Stuttgart can be plotted in the same graph. Two graphs can be formed for both bad and good bond conditions. Most of the available experimental data is based on good bond conditions. The data for bad bond conditions (figure 9.4) gives less insight in the conformity of the coefficient which applies for the bad bond conditions.

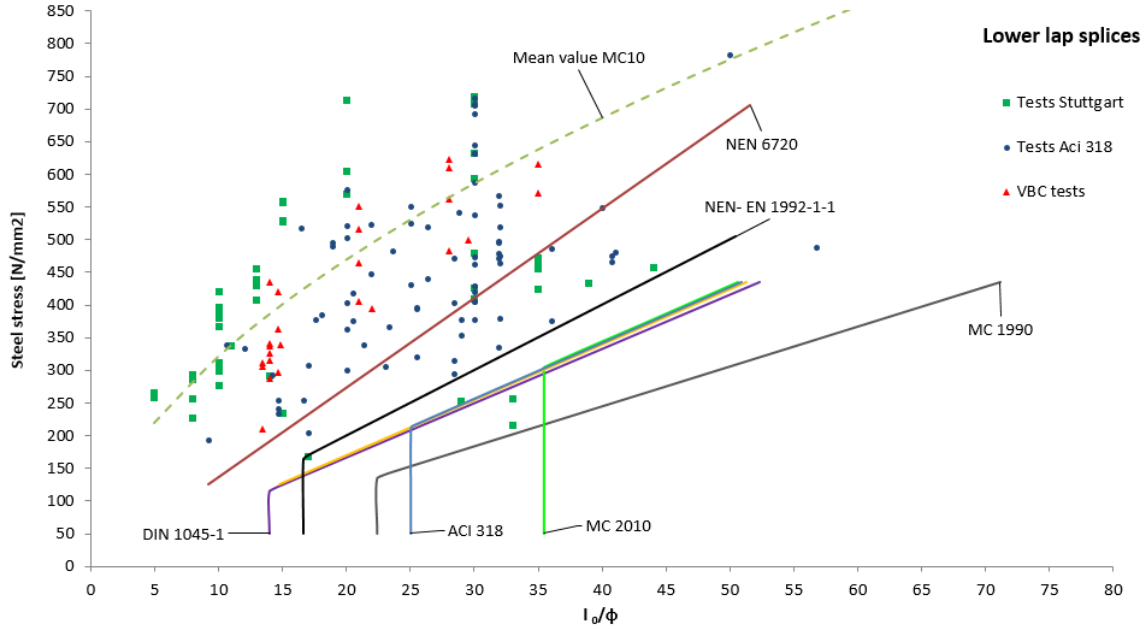

Figure 9.3: Steel stress as a function of the lap splice as multiple of the rebar diameter for good bond conditions.

The experimental data is selected in a way that corresponds roughly with the assumed structural element of figure 9.2. This ensures to make a comparison. The first remarkable aspect is the deviation of the experimental data. Especially tests from the Stuttgart database have a large deviation. Conversely, the mean value is comparable to the experimental test performed by VBC. In contrast, ACI experimental data seems to have a lower average. However, the number of lower strength values are governing for the final composition of the calculation methods. Based on the available databases, NEN 6720 appears to be on the unsafe side. The other standards are much more conservative and appear to provide a safe outcome. Nevertheless, a number of tests provide extremely low ultimate failure strength.

The same graph can be formed for bad bond conditions, the vast majority of the standards use a factor 0,7 or equivalent for the bond stress. The origin of this coefficient is indistinct; also figure 9.4 provides no better understanding. The available tests from the three databases are not sufficient in order to construct a formula. Only VBC and ACI database provide some experimental results.

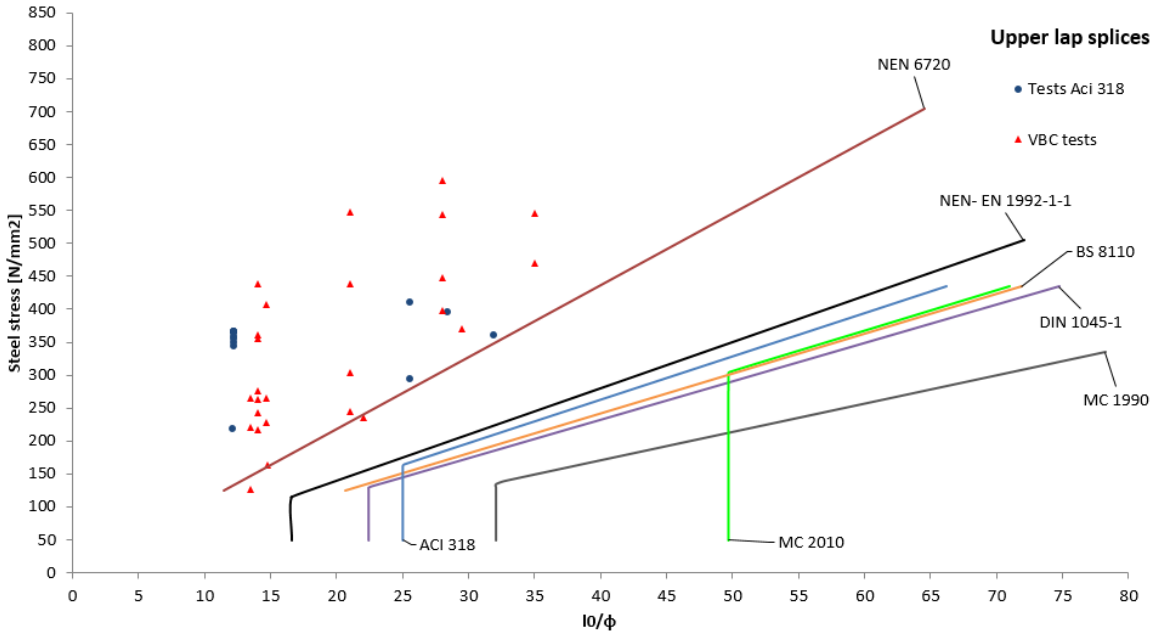

Figure 9.4: Steel stress as a function of the lap splice as multiple of the rebar diameter for bad bond conditions.

Nevertheless, the origin of the coefficient is obvious. For lower bars it is expected that the bar has a better embedment in comparison with upper bars due to the vertical pressure of the dead weight of the poured concrete. Good bond assumes less voids and significant confinement with respect to bad bond conditions and as a result brittle failure is more likely. Abrupt failure is undesirable; the coefficient for bad bond ensures a calculation method which is a safe assumption.

For instance, NEN-EN 1992-1-1 prescribes the following (figure 9.5) boundary conditions and material characteristics for the distinction between bond conditions. (a) provide good bond conditions due to an improved anchorage of bended rebar and (b) has good bond conditions due to the limited height of the bar or plate (the granulates are evenly distributed). For thicker elements (c) and (d), the hatched zone gives bad bond conditions. Heavier granulates will sink and perhaps some voids remain. This could result in a lower ultimate strength.

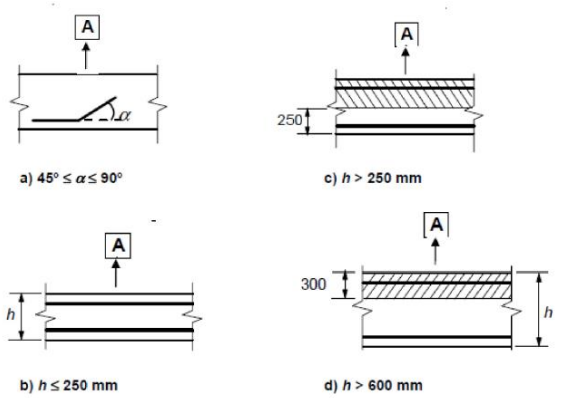

Figure 9.5: Prescribed boundary conditions for good and bad bond conditions according to NEN-EN 1992-1-1.

In addition to the comparison for splice length dependent on steel stress, bond stress is a point of discussion. The same structural element is considered. However, the concrete cover is variable and the lap splice constant. The ultimate bond stress is highly dependent on the mode of failure (paragraph 1.5). Therefore, standards prescribe a minimum concrete cover to avoid splitting failure (next to the minimum based on durability). As can be seen in figure 9.6, some standards prescribe a constant bond stress from a certain cover thickness. For a small cover thickness, many standards prescribe an unsafe bond stress. Therefore, the minimum concrete cover is introduced in these standards. Furthermore, the differences between several standards mutually are comparable to previous comparison.

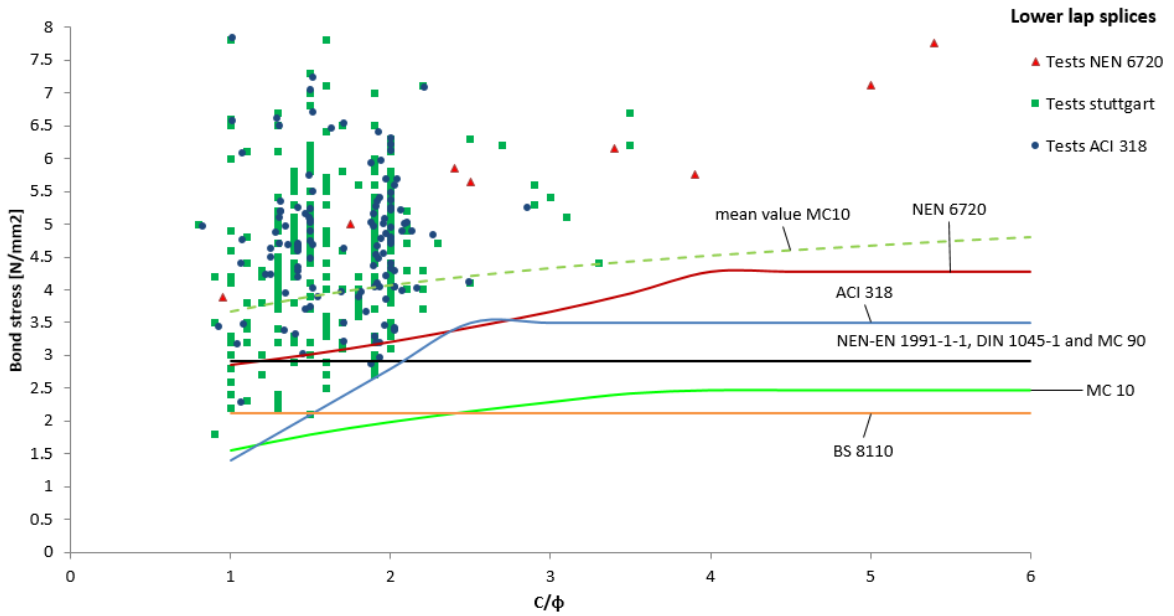

Figure 9.6: Bond stress as a function of the cover thickness as multiples of the bar size for good bond conditions

For bad bond conditions, the lack of experimental results is an issue too. Therefore, no clarity can be given on the background of the chosen coefficient of 0,7 or equivalent. (Figure 9.7)

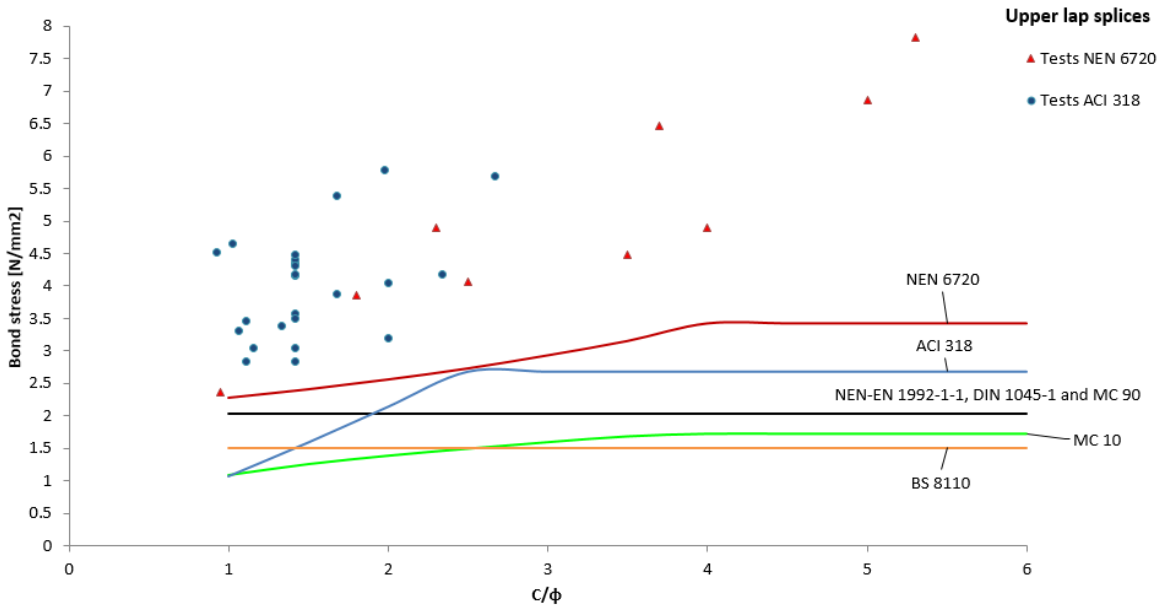

Figure 9.7: Bond stress as a function of the cover thickness as multiples of the bar size for bad bond conditions

IV. Conclusion

The overall conclusion can be subdivided into two parts, the analytical, experimental and numerical research; and backgrounds to standards. Both have other purposes, research is performed to gain insight in the actual behaviour during failure and background of standards is essential to obtain a safe value from simple design rules fitted on experimental data.

Concerning analytical research, models are presented to describe pull-out behaviour and stress distribution of anchorage length and lap splice. Essential for structural applications is the bond stress-slip relationship in order to configure design rules. For instance, the expression proposed by Ciampi et al (1981), which is adopted by Model Code 1990 as standard for the development of design rules. In addition to analytical models, experimental research is required to investigate the influence of several boundary conditions and material characteristics (transverse pressure, concrete cover, concrete class, rebar geometry, steel strength and transverse reinforcement) and the deviation in results due to material dispersion. In addition to experiments, numerical research can be useful. However, currently it is not possible to capture several mechanisms in one universal model. Multiple models are necessary to characterize bond in different limit states (Fib Bulletin 10, 2000). Combining models could be a solution; whether it is necessary to elaborate one single system in the future?

However, the purpose for this research of anchorage length and lap splice is derived from the changes of design rules in the Netherlands. Is there an explanation for the significant larger prescribed values in the new standard (NEN-EN 1990-1-1)? Over the past decades, the number of experimental researches have been increased, with the consequence of expanding variation in results (Stuttgart database). Hereby, the safe lower limit for design rules should change to meet the experimental databases. The database of CUR23, which is the foundation for NEN 6720, is not involved in Eurocode 2 and thus these experiments are disregarded. The foundation of Eurocode 2 is mainly derived from DIN 1045-1 (Germany) and the corresponding database (Stuttgart), many formulas for the design rules are comparable. The same applies to the section concerning lap splices and anchorage length. However, the origin of the formulas is unknown, the background documentation is not available. Based on Stuttgart and ACI databases, the values prescribed by Eurocode 2 are necessary. Conversely, the conditions for all experimental data is inconsistent due to diversity in research. Presumably, consistent boundary conditions and material characteristics for large- scale test should result in a smaller variation.

References

ABDEL-KAREEM, A.H., ABOUSAFA,H., EL-HADIDI, O.S., *Effect of Transverse Reinforcement on the Behavior of Tension Lap slice in High- Strength Reinforced concrete Beams,* International Journal of Civil, Architectural Science and Engineering 7 (12), 2013.

ABRAHMS, D.A., *Tests of Bond between concrete and steel,* Bulletin no. 71, University of Illinois, 1913.

ACI COMMITEE 318, *Building Code Requirements for Structural Concrete,* ACI 318, 2005.

ACI COMMITTEE 408, *Bond and Development of Straight Reinforcing Bars in Tension*, ACI 408R, 2003.

ACI 408, *Bond test database; may be obtained from:*
http://fibtg45.dii.unile.it/files%20scaricabili/Database%2010-2001.xls

BRITISCH STANDARD, *Structural use of concrete, BS 8110-1, 1997.*

BRUGGELING, A.S.J., DE BRUIJN, W.A., *Theorie en praktijk van het gewapend beton, deel 1,* Den Bosch, 1986.

CAIRNS, J., *Bond and anchorage of embedded steel reinforcement of the fib model code 2010,* Heriot- Watt University, School of Built Environment, Edinburgh, UK, 2013.

CAIRNS, J., *Design of concrete structures using fusion bonded epoxy coated reinforcement,* Proc. Inst. Of Civil Engineers: Structures & Buildings, 1992.

CEB-FIB MODEL CODE 90, *Design code*, Comite Euro- International du Beton, Lausanne, Switzerland, 1993.

CEB TASK GROUP BOND MODELS, *Bulletin 10 Bond of reinforcement in concrete,* State of art report, Lausanne, Switzerland, 2000.

CIAMPI, V., ELIGEHAUSEN, R., BERTERO, V., POPOV, E., *Analytical Model for Deformed Bar Bond under Generalized Excitations*, University of California, Berkeley, USA, 1981.

COX, J.V., HERRMANN, L.R., *Confinement- stress dependent bond behaviour,* Riga Technical University, Riga, Latvia,1992.

HERRMANN, L.R., COX, J.V., *Development of Plasticity bond model for steel reinforcement,* Mechanics of cohesive- frictional materials 3, 1994

CUR RAPPORT 23, *Onderzoek naar de samenwerking van geprofileerd staal met beton*, commissie voor de uitvoering van research ingesteld door de betonvereniging, Den Haag, 1963.

CUR RAPPORT 94-13, *Achtergronden bij de VBC 1990,*CUR, Gouda, 1994.

DARWIN, D., THOLEN, M.L.,IDUN, E.K., ZUO, J., *Splice Strength of High Relative Rib Area Reinforcing Bars,* ACI Structrual Journal 93 (10), 1996.

DEUTHCHE NORM, *Plain, reinforced and prestressed concrete structures,* DIN 1045-1, 2001.

DÖRR, K., *Bond behaviour of ribbed reinforcement under transversal pressure,* Symposium on nonlinear behaviour of reinforced concrete spatial structures, Düsseldorf, Germany, 1978.

EDWARDS, A., PICARD, A., *Theory of cracking in concrete members,* ACI journal 67 (7), 1972.

ELIGEHAUSEN, R., *Übergreifungsstöße zugbeanspruchter Rippenstäbe mit geraden Stabenden, Deutcher Ausschuss für Stahlbeton*, Heft 301, Stuttgart, Germany, 1979.

ELIGEHAUSEN, R., POPOV, E. P. , BERTORO, V. V., *Local bond stress-slip relationships of deformed bars under generalized excitations*", Report 82/23, Earthquake Engineering Research Centre, university of California, Berkeley, 1983.

ERTZIBENGOA, D., MATTHYS, S., TAERWE, L., *Bond behaviour of flat stainless steel rebars in concrete,* Rilem, Ghent University, Department of Structural Engineering, Ghent, Belgium, 2012.

EUROCODE 2, *Ontwerp en berekening van betonconstructies,* NEN-EN 1992-1-1, 2011.

FIB MODEL CODE 2010, *Bulletin 65,* Ernst & Sohn, Berlin, Germany, 2013.

FIB TIG4.5, *Bond test database; may be obtained from:*
http://fibtg45.dii.unile.it/files%20scaricabili/Database_splicetest%20Stuttgart%20sept%202005.xls

GOTO, Y., *Cracks formed in concrete around deformed tension bars,* ACI journal 68 (26), 1971.

LETTOW, S., ELIGEHAUSEN, R., *The Simulation of Bond between Concrete and Reinforcement in Nonlinear Three-dimensional Finite Element Analysis, IWB*, University of Stuttgart, Stuttgart, Germany, 2003.

LUNDGREN, K.; GUSTAVSON, R.; MAGNUSSON, J., *Finite element modelling as a tool to understand the bond mechanisms*. Budapest. 2002.

MORENO, C., BASTOS, A.S., *Experimental and numerical evaluation of bond properties between reinforcement and concrete,* 5th International Conference on Mechanics and Materials in Design, Porto, Portugal, 2006.

NEN 6720, *Technische grondslagen voor bouwconstructies,* TGB 1990 - Voorschriften beton constructieve eisen en rekenmethoden (VBC), 1995.

ORANGUN, C.O., JIRSA, J.O., BREEN, J.E., *A Reevaluation of Test Data on Development length and Splices,* ACI Structural Journal 74 (11), 1977.

PEPE, M., MAZAHERIPOUR, J., BARROS, J., SENA-CRUZ, J., MARTINELLI, E., *Numerical calibration of bond law for GFRP bars embedded in steel fibre- reinforced self- compacting concrete,* Composites: Part B, 2013.

PIJAUDIER- CHABOT, G., MAZARS, J., PULLIKOWSKI, J., *Steel- concrete bond analysis with nonlocal continuous damage, ASCE* J. Struct. Eng. 117 (3), 1991

RAGI ALY, *Stress along tensile lap- spliced fibre reinforced polymer reinforcing bars in concrete,* Can. J. Civ. Eng. 34, 2007.

RUSSO, G., ZINGONE, G., ROMANO, F., *Analytical solution for bond- slip of reinforcing bars in R.C. joints,* ASCE, Journal of Structural Engineering 116(2), 1990.

RUSSO, G., ROMANO, F., *Cracking Response of RC Members Subjected to Uniaxial Tension,* ASCE, Journal Structural Engineering 118 (9), 1992.

TASSIOS, T.P., *Properties of bond between concrete and steel under load cycles idealizing seismic actions,* CEB Bulletin No. 131, Rome, Italy, 1979.

TAVARES, A.J. BARBOSA, M.P., BITTENCOURT, T.N., LORRAIN, M., *Bond steel- concrete; simulation analysis of the pull- out test using the program ATENA,* Bracon structures and materials journal 7 (1), 2014.

TEPFERS, R., *A theory of bond applied to overlapped tensile reinforcement splices for deformed bars,* Chalmers University of Technology, division of concrete structures, Göteborg, Sweden, 1973.

TEPFERS, R., DE LORENZIS., *Bond of FRP reinforcement in concrete,* Mechanics of Composite Materials 39 (4), 2003.

TEPFERS, R., *Should the anchorage length and overlap splice length for reinforcement be the same in codes?* Presentation fib Task Group 4.5 "Bond models", 2006.

VAN DER AA., *Biaxial stresses in steel fibre reinforced concrete*, Eindhoven, 2013.

ZUO, J., DARWIN, D., *Splice Strength of Conventional and High Relative Rib Area Bars in Normal and High- Strength Concrete,* ACI Structural Journal 97 (65), 2000.